UNIVERSITÉ DE SHERBROOKE

Faculté de Génie

Département de génie chimique et de génie biotechnologique

Conception de catalyseur pour la carboxylation du diméthyle éther assistée par calculs DFT

`

Thèse de doctorat

Spécialité : génie chimique

Jean-François LACROIX

Jury :   Jean-Michel Lavoie Pr. (directeur)

Armand Soldera Pr. (co-directeur)

Esteban Chornet Pr.

Ludovic Pinard Pr.

Pierre Proulx Pr.

 J. Peter Jones (President du jury)

Sherbrooke (Québec) Canada   Septembre 2014

This work is dedicated to humanity.

Résumé combiné

Au cours de ce projet, la faisabilité de l'insertion du CO_2 dans une fonction éther aliphatique à été démontrée pour la première fois. Cette découverte à été effectuée suite à la résolution cinétique et thermodynamique de la décarboxylation du diméthyle carbonate (DMC) en diméthyle éther (DME) et CO_2 à la surface d'un catalyseur faujasite échangé avec du zinc(II) (Zn-FAU). Un profile réversible typique aux carbonates a été observé, soit que le CO_2 est relâché à plus haute température et inséré aux plus basses températures. La structure de l'état de transition entre le DMC et DME a ensuite été résolue en corrélant des calculs en modélisation moléculaire aux mesures thermodynamiques effectuées entre le DMC et Zn-FAU. La méthode de calcul développée lors de l'analyse mécanistique a ensuite été appliquée à l'évaluation théorique de plusieurs structures catalytiques, ce qui a permis d'identifier les paramètres structurels des catalyseurs qui sont favorables à la réaction de carboxylation du DME.

Combined abstract

In this study, the feasibility of the insertion of CO_2 in an aliphatic ether function was demonstrated for the first time. This finding results from a thermodynamic and kinetic study on dimethyl carbonate (DMC) decarboxylation into dimethyl ether (DME) and CO_2 at the surface of a zinc(II) exchanged faujasite catalyst. The typical reversible profile of carbonates synthesis chemistry was observed, higher temperature being favorable to CO_2 release and lower temperature being favorable to CO_2 insertion. A structural resolution of the rate determining transition structure between DMC and DME was then achieved by correlating molecular modelling calculations to the thermodynamic measurements on DMC decarboxylation. The calculation method developed during the mechanistical analysis was further applied to theoretical catalyst activity screening, which allowed determining structural catalytic sites parameters that favor DME carboxylation over DMC decarboxylation.

Mots clés: CO_2, Dimethyl ether, Dimethyl carbonate, Carboxylation, Decarboxylation, DFT

Acknowledgements

In a first instance, I would like to thank Enerkem for hosting, supporting and supervising this work. There is no other group with which I had such a good affinity; we both share an entire dedication of our expertise at building a more sustainable world.

A special mention is also given to Pr. Jean-Michel Lavoie and Pr. Armand Soldera from Sherbrooke University. The possibility of such an association between the academic and industrial world is the results of their dedication at providing the best education as possible to their students.

It is also important to mention Laurene Petitjean. As good I could be with molecules and numbers, as bad I am at writing. No matter how long was my documents and busy she was, she always took the time to look back at my writing.

TABLE DES MATIÈRES

Liste des figures

1.   Base littéraire et définition du projet de recherche

2.   A thermodynamic resolution of Dimethyl Carbonate decarboxylation and the first example of its reversibility: Dimethyl Ether carboxylation

3.   Dimethyl Carbonate decarboxylation: Structural resolution of the rate-determining step

4.   Insight into metal exchanged faujasite catalytic site properties that favor DME carboxylation over DMC decarboxylation

Liste des tableaux

1. Base littéraire et définition du projet de recherche

1.1 Introduction

Les hydrocarbures fossiles, soit le charbon, le gaz naturel et le pétrole représentent actuellement près de 80,9% des sources d'énergie primaire répondant à la demande énergétique mondiale, lorsque combinés.[1] Le contenu énergétique de ces composés carbonés est extrait par des procédés oxydatifs, la plus commune étant la combustion. Malgré l'efficacité économique de ces sources d'énergie, leur utilisation massive a des répercussions sur l'état environnemental de la planète. En effet, le CO_2, la forme de carbone ayant le degré d'oxydation le plus élevé, est la composante principale du gaz résiduel produit par tout procédé oxydatif visant à extraire l'énergie des hydrocarbures. Ainsi, l'utilisation de ressources non renouvelables, tels les hydrocarbures d'origine pétrolière, est accompagnée par un rejet annuel de près de 30 000 Mt de CO_2 dans l'atmosphère, quantité qui croît proportionnellement à l'augmentation de la population de la planète.

Une telle accumulation de CO_2 dans l'atmosphère est désormais reconnue pour avoir des conséquences climatiques majeures, qui s'observent entre autres par une intensification des périodes de sécheresse et des tempêtes tropicales.[2] De plus, une augmentation du niveau des océans, également associée à l'augmentation de la concentration atmosphérique en CO_2, se traduit par de nombreuses inondations résultant en une perte de superficie habitable pour les espèces terrestres, au profit des océans. Ces derniers absorbent à eux seuls près de 30% du CO_2 atmosphérique, absorbtion qui repose sur l'équilibre entre le dioxyde de carbone et l'acide carbonique et qui résulte en une diminution du pH ainsi qu'une dissolution des coraux. L'effet de la diminution du pH sur l'écosystème sous marin est encore incertain, mais une dissolution des précipités carbonates est décrite comme ayant un effet indéniable sur les organismes calcifiés, qui sont à la base de la chaîne alimentaire marine[3]. Par ailleurs, la modification de la composition de l'atmosphère est également à l'origine de variations climatiques.[4-5] La terre reçoit en permanence des radiations solaires, qui sont soit absorbées, soit reflétées par l'atmosphère. La balance des radiations absorbées et reflétées est donc inévitablement affectée par un changement de composition de l'atmosphère. Ainsi, une

augmentation de la concentration de CO_2 dans l'atmosphère provoque une augmentation de l'absorption des radiations solaire, résultant en une augmentation globale d'absorption d'énergie solaire par la planète. Une augmentation de l'absorption d'énergie par la planète résulte en une hausse de température.[6]

En réponse au profil de consommation énergétique de la société et au déséquilibre engendré par le rejet de CO_2 dans l'atmosphère, l'écosystème tente de retrouver l'équilibre en augmentant l'absorption d'énergie en provenance du soleil. En effet, un retour à l'équilibre de la planète n'est qu'une éventualité due aux procédés biologiques de réduction chimique du CO_2, procédés qui convertissent le surplus d'énergie absorbé par la planète en énergie chimique.[7] Ainsi, suivant une hypothèse où toute émission de CO_2 serait complètement arrêtée, un retour à l'équilibre de l'écosystème ne serait qu'une question de temps. Toutefois, à l'encontre de cette dernière hypothèse, les émissions de CO_2 ne cessent de croitre, entrainant une crainte de plus en plus prononcée au sein de la population.

Le désir sociétaire de réduire voir couper complètement les émissions de CO_2 est fort et représente l'un des enjeux les plus importants pour la communauté scientifique moderne. Le défi relatif à la réduction des émissions de CO_2 consiste d'abord à optimiser la consommation d'hydrocarbures de manière à minimiser les émissions de gaz résiduel, puis de rechercher et inventer des procédés de transformation industriellement pertinent de ces gaz résiduels.
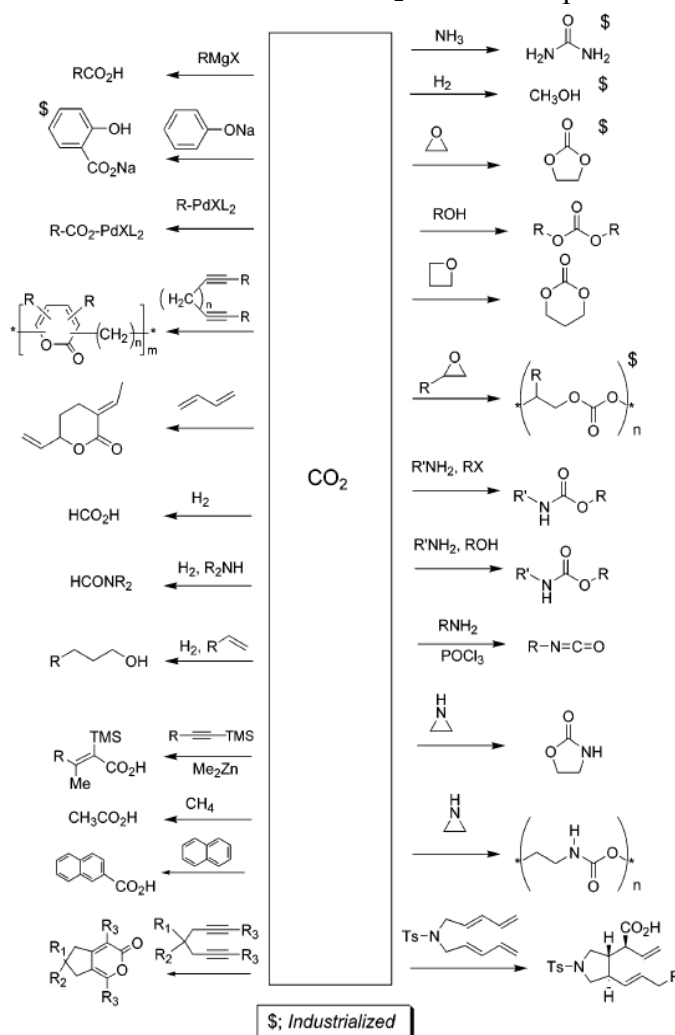
Figure 1.1 : Réaction et produits connus de valorisation du CO_2

Les produits accessibles lorsque le CO_2 est employé comme source de carbone ont été revus en 2007 par *Sakakura & al* (**Figure 1.1**).[8] Malgré le fait que plusieurs réactions de transformation du CO_2 soient connues, il n'y a que les synthèses d'urée, du méthanol et de carbonates cycliques ou polycarbonates qui aient été industrialisées.

La production industrielle d'urée requiert deux moles d'ammoniac par mole de CO_2 et fonctionne généralement à 200°C et sous une pression dépassant les 2000 psi. Pour ce qui est de l'hydrogénation du CO_2 en méthanol, la perte d'une mole d'hydrogène par mol de méthanol formé est une pénalité concrétisée par la coproduction d'H_2O. La synthèse industrielle de carbonates nécessite quant à elle l'utilisation d'époxydes, réactifs de haute valeur.

Ainsi, les procédés établis de transformation du CO_2 sont encore chimiquement et économiquement très limités. Des percées fondamentales et technologiques sont donc intensivement recherchées par les institutions académiques et privées, afin de répondre au besoin urgent de la société d'établir des procédés de transformation massive du CO_2 en produits à valeur ajouté.

1.1 Définition et objectifs du projet de recherche

Suite au développement d'un procédé industriel de synthèse de méthanol à partir de biomasse hétérogène, notre groupe s'intéresse désormais à la synthèse du diméthyle carbonate (DMC), étant une opportunité de valorisation du CO_2. En effet, l'approche actuelle de synthèse directe du DMC est la carboxylation du méthanol (**Equation 1.1**). Ainsi, en plus de l'accessibilité aux réactifs, le potentiel économique d'un tel procédé se montre fort attrayant quant à la réalisation de travaux de recherche et développement. Le contenu en oxygène du DMC rend cette substance très intéressante en tant qu'additif à l'essence, cette dernière devant respecter une teneur en oxygène imposée par le traité ''Clean Air Act''.[9] De plus, le DMC se dégrade facilement et rapidement dans l'environnement, faisant en sorte que son utilisation en tant que solvant soit valorisée étant une alternative aux solvants de source fossiles. Par ailleurs, la réactivité chimique du diméthyle carbonate permet également son utilisation comme agent méthylant, avec un éventuel potentiel pour le remplacement de réactifs nocifs

tels les halogénures de méthyle, le sulfate de diméthyle et le phosgène, réactifs nocifs et actuellement utilisés dans l'industrie.[10]

$$2\text{MeOH} + \text{CO}_2 \rightleftharpoons \underset{\underset{\text{CH}_3}{|}\ \ \underset{\text{CH}_3}{|}}{\text{O} \overset{\overset{\text{O}}{\|}}{\text{C}} \text{O}} + \text{H}_2\text{O} \qquad \textbf{(1.1)}$$
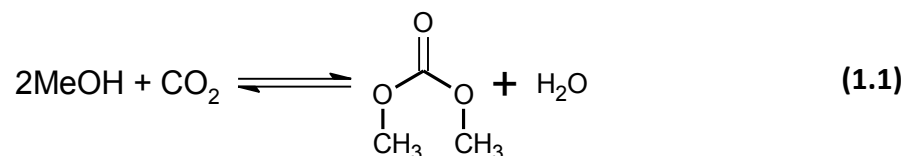
La carboxylation du méthanol est décrite comme étant un équilibre chimique, exothermique et non spontané.[11] La co-formation d'eau avec le DMC lors de la carboxylation du MeOH, est une limitation majeure devant être résolue afin d'amener cette transformation à une plus grande échelle. En réponse à cette contrainte, le diméthyle éther (DME), produit de la déshydratation du méthanol, est ici étudié pour la première fois en tant que co-réactif avec le CO_2 pour produire le DMC. Puisque la carboxylation du DME n'a jamais été rapportée de manière officielle antérieurement, la chimie entourant cette réaction est étudiée dans ses fondements en vue de développer un procédé catalytique hétérogène en phase gazeuse. Ainsi, l'objectif du projet consiste à déterminer la faisabilité de la carboxylation du DME, à en comprendre le fonctionnement puis à définir les facteurs catalytiques qui lui sont favorable (**Equation 1.2**).

$$\text{H}_3\text{C} \diagdown_{\text{O}} \diagup \text{CH}_3 + \text{CO}_2 \overset{?}{\rightleftharpoons} \underset{\underset{\text{CH}_3}{|}\ \ \underset{\text{CH}_3}{|}}{\text{O} \overset{\overset{\text{O}}{\|}}{\text{C}} \text{O}} \qquad \textbf{(1.2)}$$
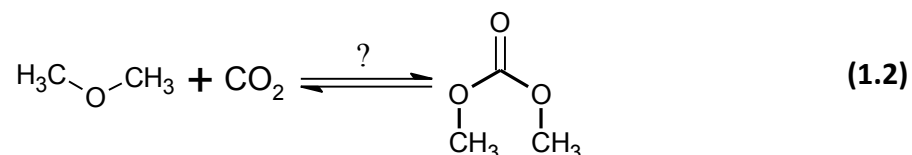
En réponse à cette problématique, une structure catalytique qui peu à la fois promouvoir la réaction directe et inverse à été conçue. C'est ensuite à l'aide de calculs théoriques de modélisation moléculaire que le point d'équilibre entre les réactifs et les produits a été élucidé. La méthode de calcul a ensuite été appliquée à la compréhension des facteurs catalytiques qui sont favorable à la carboxylation du DME.

Concrètement, les objectifs du projet de recherche consistent à :

- Concevoir et construire un banc d'essai permettant de tester l'activité de catalyseurs pour des réactions en phase gazeuse

- Développer une méthode de calcul permettant d'élucider les intermédiaires réactionnel entre le DMC et le DME
- Synthétiser et caractériser des catalyseurs pour application à l'insertion du CO_2 dans le DME
- Tester les catalyseurs sur le banc d'essai préalablement construit
- Extraire expérimentalement des données cinétiques et thermodynamiques des réactions de carboxylation du DME et de décarboxylation du DMC
- Définir les propriétés du site catalytique qui sont favorables à la carboxylation du DME

À la lumière de ce travail, des bases fondamentales nécessaires au développement d'une nouvelle voie de synthèse du DMC en phase gazeuse sans coproduction d'eau ont été établies, avec pleine compréhension mécanistique de la réaction.

1.2 Contribution scientifique

Ce projet possède les bases quant au développement d'une nouvelle voie de synthèse du diméthyle carbonate à partir du CO_2. Cette nouvelle voie synthétique a été conçue en réponse aux limitations imposées aux voies synthétiques déjà connues, avec emphase sur la compréhension mécanistique afin de faciliter les développements futures.

À ce jour, il est reconnu que la chimie entourant les carbonates et le CO_2 sont des processus réversibles. Que ce soit la production d'ion bicarbonate par catalyse biologique où la production de polycarbonates et carbonates cycliques par catalyse chimique, la réversibilité de ces transformations a été démontrée.

Par contre, malgré les nombreux travaux ayant été effectués sur ce sujet, la chimie entourant les carbonates aliphatiques est beaucoup moins connue. Un consensus à propos d'un équilibre chimique a été établi et accepté relativement à la réaction de carboxylation du méthanol, en raison de l'impact négatif de la coproduction d'eau avec le DMC. Cependant, au mieux de notre connaissance, la décarboxylation du DMC en présence d'eau de manière à produire du méthanol n'a jamais été étudiée expérimentalement. D'un autre coté, la décarboxylation intramoléculaire et à sec du DMC en DME est une réaction bien connue.

Ironiquement dans ce cas, c'est la réaction directe, la carboxylation du DME qui n'est pas connue.

C'est donc sur ces propos que les contributions scientifiques de ce projet ont été établies. Nos travaux visent d'abord à établir les points d'équilibre de manière très spécifique, ensuite de déterminer les conditions chimiques et expérimentales pouvant permettre d'effectuer les réactions soit dans une direction, soit dans l'autre.

Afin d'obtenir ces données, il est nécessaire de développer des méthodes de calculs théoriques qui correspondent très étroitement aux données expérimentales, ainsi que de concevoir et synthétiser des catalyseurs dont l'activité chimique sera évaluée pour des réactions chimiques de transformation du CO_2 sans précédent. Les méthodes de calculs qui seront développées pourraient présenter une avancée des connaissances relatives à la chimie des carbonates, alors que les catalyseurs synthétisés et testés avanceront la connaissance dans le domaine de la catalyse industrielle.

L'apport ultime de ce projet réside en son potentiel à fournir les bases nécessaires au développement d'un procédé industriel de transformation du CO_2 en produits à forte demande. Ces travaux ont pour objectif de minimiser l'impact environnemental du mode de consommation énergétique de la société actuelle, mode de consommation auquel de nombreux et sévères déséquilibres climatiques sont associés.

1.3   État de l'art, approches synthétiques du DMC à partir du CO_2

Les efforts actuels concernant le développement d'un procédé de synthèse du DMC à partir du CO_2 et du méthanol peuvent être classés selon trois différentes approches synthétiques, résumées schématiquement à la **Figure 1.2**.
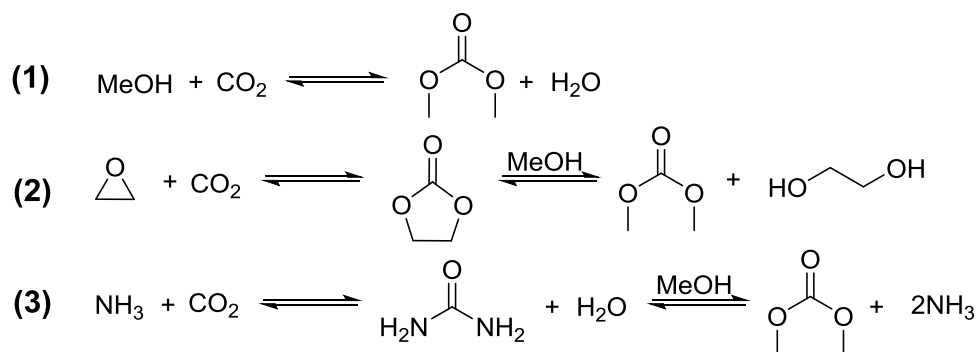
Figure 1.2 : Résumé des approches synthétiques du DMC se basant sur l'utilisation du CO₂

La première voie (1) consiste à effectuer directement la carboxylation du méthanol. Malgré le fait que cette méthode possède le meilleur potentiel économique, il s'agit de l'approche qui nécessite encore le plus de recherche avant d'atteindre un niveau permettant la mise à l'échelle industrielle. La seconde méthode (2) consiste à insérer par cycloaddition une molécule de CO_2 dans une fonction époxyde produisant soit des carbonates cycliques, soit des polycarbonates, réactions déjà à ce jour établie à l'échelle industrielle. Le DMC peut ensuite être obtenu par transestérification du carbonate cyclique avec du méthanol. Cette technologie, également mature à l'échelle industrielle mène toutefois à la production d'un 1,2-diol comme coproduit. Ce chemin réactionnel n'est cependant pas établi selon une boucle catalytique puisqu'il débute avec un époxyde et termine avec un 1,2-diol. La troisième voie (3), consiste d'abord à former de l'urée à partir du CO_2 et de l'ammoniac, pour ensuite effectuer une méthanolyse du correspondant diamide. Malgré le fait que d'excellents rendements aient été obtenus par cette dernière voie de synthèse, cette réaction n'est toujours pas appliquée industriellement et est encore en développement.

1.3.1 Carboxylation du méthanol

Les premiers rapports scientifiques concernant la préparation du diméthyle carbonate à partir de dérivés du CO_2 dates du milieu des années 1950 et avaient pour objectif d'obtenir une forme deutérée du DMC.[12] Dès lors, la méthode employée consistait à effectuer la méthylation de carbonate d'argent en présence d'un excès d'halogénure de méthyle-D_3. Déjà à cette

époque, il a été observé que la température influençait fortement le déroulement de cette réaction. Lorsque la réaction était effectuée à 60°C, le diméthyle carbonate était obtenu à 98%, alors que si la température de réaction était augmentée a 90°C, le carbonate de métal se décomposait en relâchant du CO_2.

C'est au cours des années 1980 que le DMC a commencé à être étudié dans l'optique d'utiliser le CO_2 comme matériau de construction pour des produits de consommation.[13-14] Encore à ce moment, les recherches consistaient à méthyler un carbonate inorganique, principalement le carbonate de potassium, toujours en utilisant des halogénures de méthyle et en absence de catalyseur. La formation d'éthers dérivés des halogénures d'alkyles utilisés lors des réactions avait été observée et expliquée selon un chemin réactionnel impliquant une décarboxylation à l'alkoxyde, suivi d'une alkylation par l'halogénure d'alkyle. L'ajout de catalyseurs de type organnostannyl a ensuite permis d'obtenir des rendements en dialkyle carbonate qui dépassaient la barre des 80%.

Ce n'est que dans le milieu des années 1990, avec les recherches du professeur *Juraj Kizlink* de *l'université technique slovaque,* que les travaux concernant la synthèse du DMC à partir du CO_2 ont pris une tournure à caractère industriel et en visant la réintégration du CO_2 dans des produits commerciaux. C'est alors que la carboxylation catalytique du méthanol (**Équation 1.3**) s'est révélée faisable.[15-17] Les rendements obtenus par *Kizlink & al* étaient de 60-220 mol% de produit, tel que calculé par rapport a leur catalyseurs qui étaient a base d'étain ou de titane. Les rendements pouvaient être augmentés à 330 mol% en ajoutant à la réaction des agents desséchant tel des acétals et ortho ester. Ainsi, il avait déjà été établi dès le début que cette réaction est un équilibre chimique hautement favorable aux réactifs, dont l'enlèvement in situ de l'eau favorise le déplacement de l'équilibre vers les produits. Des résultats similaires à ceux de *Kizlink & al* ont été obtenus durant la même période par *Wagner & al* pour lesquels une conversion en méthanol de 2,2% a été atteinte sans agent desséchant et 4,3% en présence d'acétals, en utilisant SnO_2 comme catalyseur.[18]

$$2CH_3OH + CO_2 \xrightarrow[\text{(acetals, ortho ester)}]{\text{Cat}} \quad + H_2O \qquad \textbf{(1.3)}$$
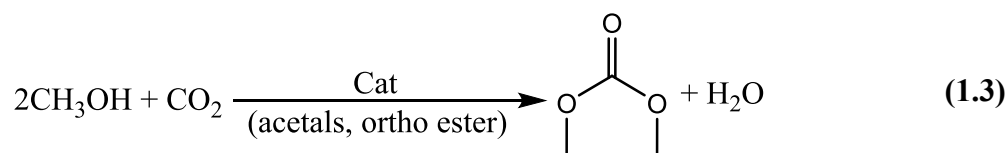
En raison de l'influence positive de l'addition d'ortho ester tel qu'observé lors des travaux antérieurs de carboxylation du méthanol, c'est en 1998 que *Sakakura & al* ont publié une étude sur la carboxylation du trimethyl ortho acétate (**Équation 1.4**).[19] Il s'agit du premier effort consistant à élaborer une voie de synthèse du DMC via l'insertion du CO_2 dans un dérivé déshydraté du méthanol. Trois formes déshydratées du méthanol y ont été mentionnées, soit le diméthyle éther (DME), des acétals et des ortho esters dont leur réactivité vers une insertion du CO_2 augmente dans l'ordre mentionné. *Sakakura & al* qui se sont orientés vers l'utilisation de l'intermédiaire déshydraté le plus réactif, l'ortho ester, ont démontré que lorsque la réaction est effectuée sous conditions supercritiques du CO_2, des conversions allant jusqu'à 75% pouvait être obtenues en utilisant des catalyseurs à base de methoxide d'étain ou de titane. Par contre, les réactions ont été effectuées en utilisant des autoclaves et avec une durée de réaction allant jusqu'à 72h pour l'obtention des meilleurs résultats. À la suite de leurs travaux utilisant des ortho ester, *Sakakura & al* ont montré que des rendements de 88% pouvait être obtenus à partir d'acétals de dimethoxides, sous 2000 atm et également qu'après 72h de réaction.[20]

Ortho ester , R = OCH_3
Acetal, R = CH_3 R $+$ CO_2 $\xrightarrow{\text{Cat}}$ R $+$ (1.4)
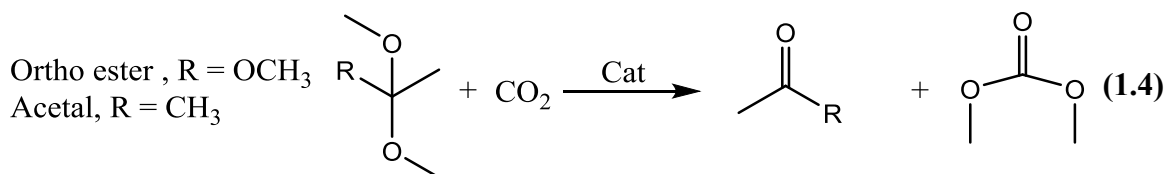
Peu après les travaux de *Sakakura & al*, la carboxylation de carbonates inorganique en présence de DME comme agent desséchant a été étudiée en autoclave par un groupe japonais dirigé par *Shikada Tsutomu*.[21] Les tests de *Tsutomu & al* consistaient à faire réagir le DME en présence d'un excès de 10 mol% de CO_2 et d'une quantité catalytique de sels tels des carbonates alcalins et d'iodure de méthyle. Pour une réaction d'une durée de 2h, des rendements de l'ordre de 14% en DMC ont été rapportés, sans désactivation du catalyseur. Lorsque le temps de réaction était augmenté à 5h, plus de 17% de DMC a été obtenu. La carboxylation d'un mélange de DME et MeOH utilisant CuI, MgO et H-ZSM5 comme catalyseur a également été rapportée avec un rendement de 28.58% par *Yiling & al*.[22]

Des études de compréhension mécanistique sur la carboxylation directe du méthanol en présence d'un catalyseur de méthoxyde d'étain ont été effectuées vers la fin des années 90.

Sakakura & al ont d'abord étudié par RMN et DRX le premier intermédiaire se formant à la surface de leur catalyseur après interaction avec le CO_2.[23] Ils ont été en mesure de caractériser un intermédiaire méthoxycarbonate d'étain CH_3OCO_2-Sn, où le CO_2 s'est inséré dans la liaison CH_3O-Sn. C'est ensuite à partir de cet intermédiaire que le DMC peut être produit par réaction avec le méthanol, mais également accompagné par la formation d'un oxyde d'étain. L'intermédiaire isolé et caractérisé de méthoxycarbonate, s'est montré stable uniquement à basse température, le CO_2 étant relâché à température et pression normales.

À la suite des nombreuses études de carboxylation directe du méthanol ou de ses dérivées déshydratés en présence de catalyseur d'oxyde ou de méthoxide d'étain, *Keiichi Tomishige* a découvert l'activité carboxylative de l'oxyde de Zirconium.[24-28] En testant en autoclaves les propriétés catalytiques de matériaux acido-basiques, *Tomishige & al* ont obtenu une conversion de 0.15% du méthanol en DMC en présence de ZrO_2, sans modification structurale du catalyseur au cours de la réaction. Cette avancée aura révolutionnée le design de catalyseur pour la carboxylation du méthanol, puisqu'il y a été établi que pour la réaction de carboxylation, les structures catalytiques doivent présenter à la fois une force acide et basique.

C'est d'abord *Tomishige & al* qui ont travaillé à optimiser l'utilisation de l'oxyde de zirconium comme support catalytique pour la réaction de carboxylation du méthanol. Les premiers progrès ont été obtenus en incorporant H_3PO_4 au ZrO_2, permettant d'obtenir une conversion de 0.47% du méthanol, amélioration attribuée à une augmentation de la force d'acide Bronsted du catalyseur. Il a également été observé que l'incorporation de CeO_2 au ZrO_2 augmentait la conversion du méthanol en DMC à 0.42%, et qu'en ajoutant un agent desséchant (2,2-dimethoxypropane), la conversion augmentait à 3.59%.[29-30]

À la suite de cette amélioration de la structure catalytique à base de ZrO_2, *Tomishige & al* ont entrepris une étude mécanistique à l'aide d'analyse DRIFT in situ, afin de comprendre le site actif du catalyseur H_3PO_4/ZrO_2. Ainsi, il a d'abord été observé que le méthanol est déprotoné par un site hydroxyde, produisant des méthoxyde de zirconium et de l'eau. À ce stade, deux types de méthoxydes ont été identifiés, soit terminaux et pontés. De ces deux types de méthoxydes, il a été noté que l'insertion du CO_2 formant un méthoxycarbonate de zirconium se produit uniquement avec les sites méthoxyde terminal, laissant le signal du méthoxy ponté intact après interaction avec le CO_2. La complétion du cycle catalytique au DMC se produit ensuite hypothétiquement par interaction entre la seconde molécule de

méthanol et un site acide, soit de Lewis soit de Brønsted, de manière à promouvoir la méthylation du bicarbonate par le méthanol, résultant au DMC et à la régénération du site initial (**Figure 1.3**). Les sites hydroxydes pontés, à l'origine des méthoxydes pontés, ont été décrits comme ayant une importance particulière lors de la dernière étape d'activation du méthanol. L'incorporation de H_3PO_4 dans la structure de ZrO_2 forme préférentiellement des sites d'hydroxydes pontés et avec une force acide supérieure, ce a quoi est attribué l'augmentation d'activité due à l'incorporation de H_3PO_4 à ZrO_2. L'étape limitant lors de la carboxylation du méthanol est le bris de la liaison C-O du méthanol lors de la méthylation du bicarbonate, ce qui est activé sur des sites catalytique acide.
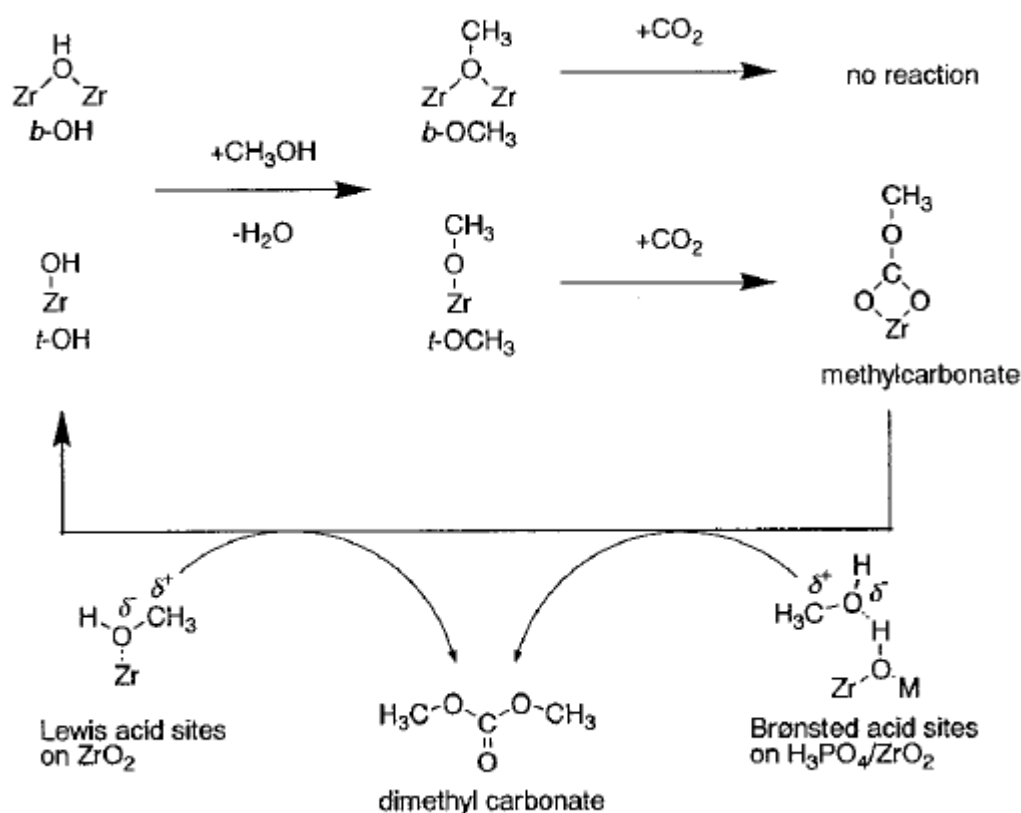
Figure 1.3 : Mécanisme proposé pour la réaction de carboxylation du méthanol à la surface de ZrO_2 (M = P, Zr)

En parallèle aux travaux de *Tomishige & al*, *Alexis T. Bell & al* ont effectués une étude mécanistique par analyses IR et Raman *in situ* sur la réaction de carboxylation du méthanol à la surface de ZrO_2. *Bell & al* sont arrivés aux mêmes conclusions que *Tomishige & al*, soit que

le méthanol est d'abord déprotoné sur un site basique, générant un méthoxyde de métal dans lequel s'insère le CO_2, suivi de l'étape limitante de méthylation du méthoxycarbonate promu par un site acide.[31-32]

Suite à la découverte de l'influence positive de l'amplification de la force acide de support acido-basique, ainsi qu'une compréhension mécanistique détaillée de la réaction, l'activité de nombreuses structures catalytiques composées d'oxydes mixtes dopées avec des acides a été rapportée. L'activité d'une série de catalyseurs composés d'oxydes mixtes dopés avec des acides ou d'acides échangés avec un métal est résumée dans le **Tableau 1.1**.

Tableau 1.1 : Résumé de l'activité des catalyseurs à caractère acide pour la carboxylation du méthanol

Catalyseur/Réacteur	Conditions	Yield DMC %	Ref
1.43 mol% $H_3PW_{12}O_{40}/ZrO_2$ autoclave	373 K, 580 psi, 3.5h	2.02	[33]
1.43 wt% $H_3PW_{12}O_{40}/Ce_{0.6}Zr_{0.4}O_2$ autoclave	443 K, 870 psi, 3h	0.14	[34]
15 wt% $H_3PW_{12}O_{40}/Ce_{0.1}Ti_{0.9}O_2$ autoclave	443 K, 725,2 psi, 12h	2.51	[35]
P/V = 0.2 H_3PO_4/V_2O_5 micro réacteur à lit fixe	413 K, 87 psi, en continu	1.80	[36]
$Co_{1.5}PW_{12}O_{40}$ micro réacteur à lit fixe	473 K, 14.7 psi, en continu Produit secondaire : DMM, MF	6.57	[37]
5% Rh/ZSM-5 micro réacteur à lit fixe	400K, 14.7 psi, en continu Produit secondaire : DME	24.9	[38]

La raison pour laquelle la catalyse acide a connu un tel succès pour ce qui a trait à la carboxylation du méthanol au cours de la dernière décennie, découle de la possibilité de générer significativement in situ des méthyllium CH_3^+. Les études de synthèse du DMC orientées vers l'utilisation de catalyseurs basiques tel le méthoxyde de potassium ont nécessité l'addition d'iodure de méthyle afin de compléter la réaction au DMC.[39] Cependant, cette nécessité est uniquement présente lors de réaction dont leur fonctionnement procède selon le schéma réactionnel décrit à la **Figure 1.3**.

C'est en 2009 après près d'une décennie d'évaluations catalytiques de structures acido-basiques que *Meng & al* de l'université *Sun Yat-Sen*, ont suggéré une nouvelle voie synthétique du DMC (**Figure 1.4**).[40-43] Ils ont suggéré qu'à la surface de support de carbone imprégné au cuivre et au nickel, le CO_2 est scindé générant une forme adsorbée du monoxyde de carbone. Il est ensuite mentionné que cet intermédiaire est carbonylé selon un mécanisme similaire à celui de la carbonylation oxydative du méthanol en DMC.[44-45] Cette voie synthétique n'a cependant pas été étudiée *in situ* et a été présumée en fonction des produits secondaires de la réaction soit le CO, le CH_4 et le DME.

Les catalyseurs composés de cuivre et de nickel supporté sur des structures de carbones développés par *Meng & al* ont permis d'obtenir 10.1% de conversion du méthanol avec 90.2% de sélectivité en DMC. La composition exacte du catalyseur ayant donné le meilleur rendement est 20% massique CuONiO/graphite avec un ratio Cu/Ni de 2. Les conditions opératoires optimales identifiées à partir de leur système gazeux et en continu impliquent une température de 373 K, une pression de 175 PSI et un ratio $MeOH/CO_2$ de 2. Cependant, la synthèse de leur type de catalyseur se fait en plusieurs étapes, limitant son application à une échelle industrielle. C'est pour cette raison que ces travaux ont ensuite mené a plusieurs tentatives de préparer plus simplement des structures catalytiques similaires. Les rendements obtenus avec différentes méthode de synthèse de leur catalyseur ont été inférieurs.[46-49]
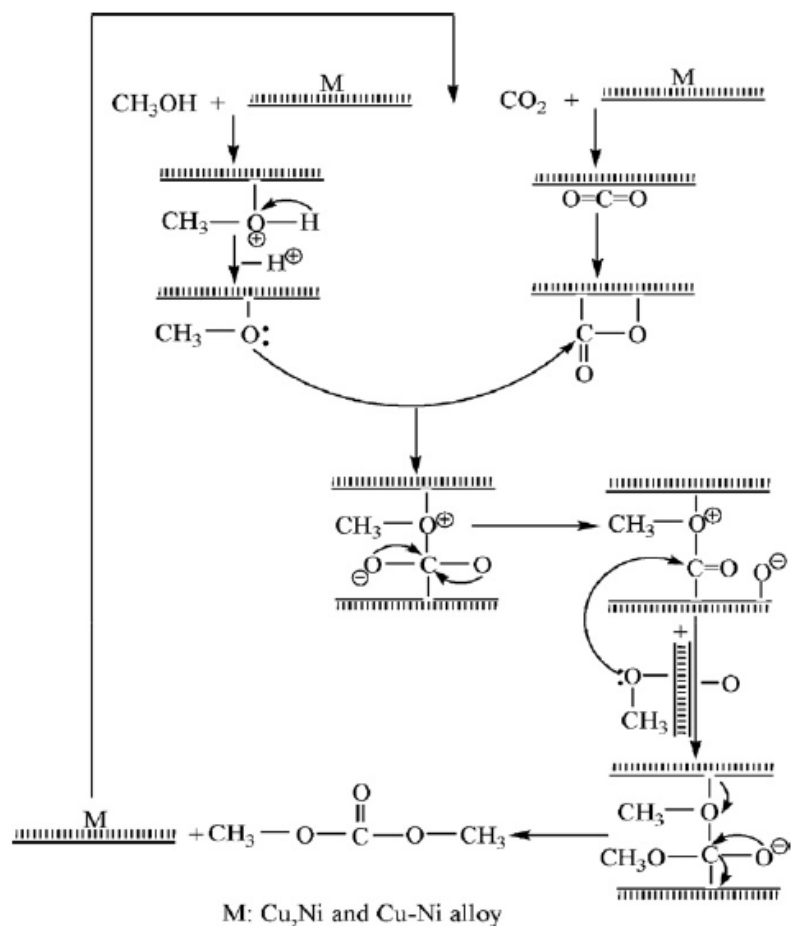
Figure 1.4 : Mécanisme de réaction à la surface de CuNi/Graphite proposé par *Meng & al*

Ainsi, un nouveau type de catalyseurs non acide a été récemment découvert avec une activité sans précédent pour la carboxylation du méthanol. Son fonctionnement exact n'est toujours pas démontré, mais il est suggéré qu'une désoxygénation du CO_2 se produit en simultanée avec une carbonylation oxydative du méthanol.

Pour résumer, la carboxylation directe du méthanol est une réaction exothermique non spontanée et qui fonctionne selon un équilibre chimique hautement favorable vers les réactifs. Les meilleurs résultats concernant la synthèse du DMC en autoclave à partir du méthanol et du CO_2 ont été obtenus en présence d'agent desséchant ou en utilisant des formes déshydratées du méthanol comme réactif. Quant au procédé en continu, à l'exception de *Khalid Almusaiteer* qui a affirmé obtenir 40% de conversion et 60% de sélectivité en DMC en utilisant un catalyseur composé de 5% de rhodium sur la zéolite ZSM-5, l'état actuel des efforts de carboxylation directe du méthanol en continu se situe tout juste à la barre des 10% de

rendement en DMC. L'accumulation d'eau dans les catalyseurs limite cependant leur activité à de courtes périodes. De plus, les meilleurs catalyseurs ayant été identifiés pour une réaction en phase gazeuse et en continu sont de composition et préparation complexe, faisant en sorte que leur application industrielle soit encore loin d'une maturité industrielle.

1.3.2 *Voies de synthèses alternatives du DMC*

Les voies alternatives de synthèse du DMC, basées sur des réactions déjà établies industriellement du CO_2, sont données aux **Figure 1.5 et 1.6**.
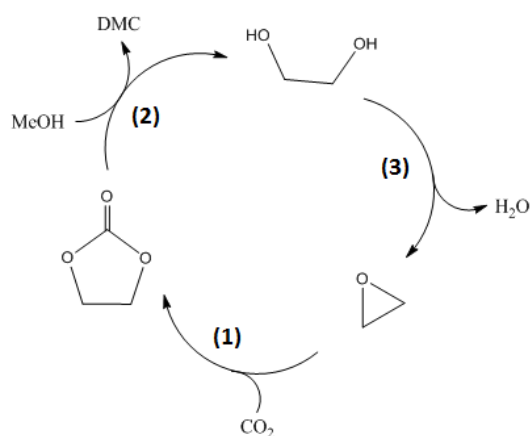
Figure 1.5 : Utilisation de l'oxyde d'éthylène pour la synthèse du DMC

On retrouve à la **Figure 1.5** un cycle fermé de production du DMC, qui nécessite la formation de trois intermédiaires. Le cycle débute avec l'oxyde d'éthylène, à partir duquel l'éthylène carbonate est produit par cycloaddition du CO_2. C'est ensuite par transesterification de l'éthylène carbonate avec le méthanol que le DMC est produit, accompagné de l'éthylène glycol comme coproduit. L'insertion du CO_2 dans l'oxyde de propylène produisant le propylène carbonate, est un procédé commercialisé depuis les années 1950 et peu être obtenu avec 99% de rendement et 99% de sélectivité.[50-51] Cependant, l'insertion du CO_2 dans un époxyde est industriellement accessible seulement en catalyse homogène. La seconde réaction de cette séquence réactionnelle est la transesterification de l'éthylène carbonate. La distillation réactive est généralement la méthode de transformation par excellence pour cette étape, permettant d'obtenir des rendements de 100% en présence de base tel NaOH ou K_2CO_3.

Un plan commercial de production de carbonates cyclique, de diméthyl carbonate ainsi que du 1,2-diol associé se retrouve entre autres dans le parc industriel de *Dongying* en Chine, où la compagnie *Shandong Wells Chemicals Co* a une capacité de production de 60 kTon/an de propylène carbonate, 50 kTon/an de DMC et 40 kTon/an de propylène glycol.

La seule réaction n'étant pas industriellement mature de la séquence présentée à la **Figure 1.5** est la déshydratation d'un 1,2-diol en époxyde. Récemment, des travaux visant la déshydratation du propylène glycol en oxyde de propylène en phase gazeuse ont démontré la faisabilité de cette réaction. La meilleure activité obtenue est de 44% de conversion et 70% de sélectivité au propylène oxyde, avec un catalyseur composé de 3mmol·g^{-1} de potassium sur la silice. La formation d'acétaldéhyde est la réaction concurrente principale à la surface de cette dernière structure catalytique.[52] Une méthode alternative pouvant permettre d'obtenir l'oxyde d'éthylène à partir de l'éthylène glycol consiste à dériver le glycol en halohydrins ou composé analogue, puis de le traiter en milieu basique. Cette méthode n'a cependant pas été établie de manière catalytique et produit des sels quantitativement par rapport à la conversion des réactifs.
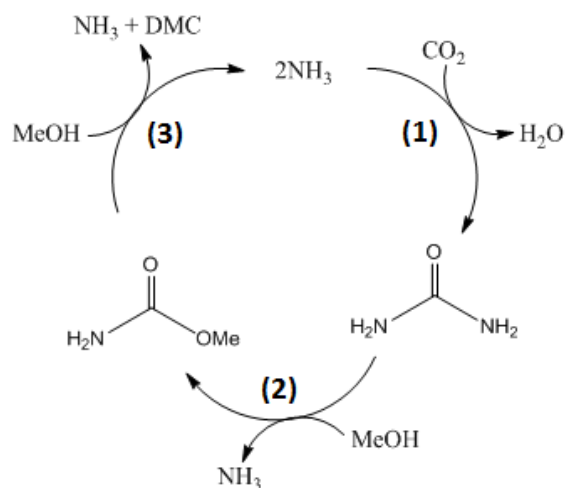
Figure 1.6 : Voie de synthèse du DMC utilisant l'urée

Finalement, la seconde voie alternative majeure de synthèse du DMC consiste à effectuer la méthanolyse de l'urée (**Figure 1.6**), dont la production industrielle à partir de l'ammoniac et du CO$_2$ est actuellement en exploitation. Cette seconde voie de synthèse fait

l'objet d'un projet mené en parallèle par un autre membre de notre groupe et ne sera donc pas discutée lors de cette étude. Il s'agit néanmoins d'une voie de synthèse du DMC très prometteuse, lorsque couplée a un plan de production d'urée.

1.4 Fondements de la carboxylation du diméthyle éther

En raison du fort désavantage thermodynamique engendré par l'accumulation d'eau lors de l'équilibre chimique de la réaction de carboxylation directe du méthanol, il a été stipulé que le diméthyle éther, forme déshydratée du méthanol, devrait être un réactif plus approprié que le méthanol pour la synthèse directe du DMC. En effet, la synthèse du DMC à partir du diméthyle éther est une réaction avec une économie d'atomes de 100% donc sans coproduction de produits secondaires (**Équation 1.2**). Par ailleurs, en appui à cette précédente hypothèse, la décomposition du DMC en DME et CO_2 a été démontrée. En appui sur les nombreux exemples de réversibilité quant à la synthèse des carbonates, il est ici postulé que la décarboxylation du DMC est également réversible.[53-54]

(2)
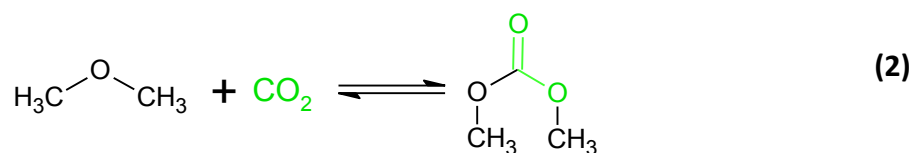
Cette réaction, qui se résume en l'insertion du CO_2 dans une fonction éther, n'a jamais été rapportée avec des éthers aliphatiques, seulement avec des éthers cycliques. Dans un premier temps, il a été stipulé que le DME doit être activé à la surface de la structure catalytique de manière à générer un groupement méthoxy adjacent à un groupement méthyllium, tel qu'illustré dans l'analyse rétrosynthétique donnée à la **Figure 1.7**.
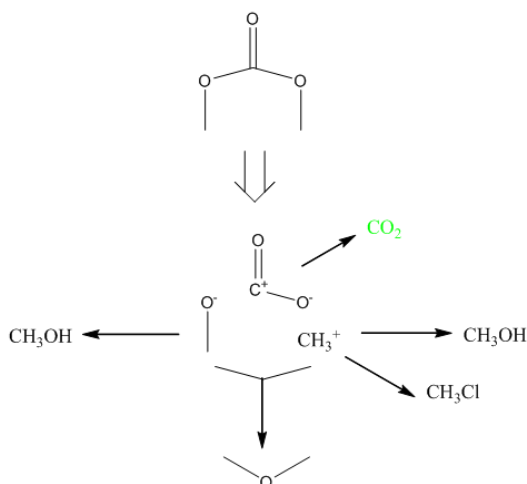
Figure 1.7 : Analyse rétrosynthétique du DMC

Deux réactions de synthèse de carbonates dont les réactifs sont activés de manière similaire à ce qui a été stipulé pour le DME ont été identifiées. La première est la synthèse de carbonate cyclique ou de polycarbonate à partir d'époxyde[55-57] et la seconde est l'hydratation du CO_2 en acide carbonique catalysé par l'enzyme *Carbonic Anhydrase* [58-61].

On retrouve d'abord à la **Figure 1.8** le mécanisme réactionnel de formation du carbonate de propylène à partir de l'oxyde de propylène et du CO_2 en présence d'un complexe de zinc.[62] Le fonctionnement de cette réaction débute par la coordination d'une molécule d'époxyde par le zinc, suivie d'une ouverture de l'époxyde via l'assistance de l'un des ligands qui agit comme nucléophile sur l'époxyde. Après incorporation d'une molécule d'époxyde dans un monomère de zinc, il s'en suit une dimérisation qui résulte en un complexe actif à partir duquel la formation catalytique de carbonate cyclique se produit. C'est donc dans ce dimère que le CO_2 s'insère via une attaque nucléophile par la fonction alkoxyde rattachée au zinc, résultant en un intermédiaire bicarbonate. Cet intermédiaire bicarbonate agit ensuite en tant que nucléophile pour l'ouverture d'une seconde molécule d'époxyde, qui se referme ensuite en formant une molécule de carbonate cyclique et régénérant le dimère de zinc. Ainsi, la nucléophicité des alkoxydes et bicarbonates de zinc sont mis en en évidence et à profit lors de cette réaction au cours de laquelle une molécule de CO_2 est transformée en carbonate.
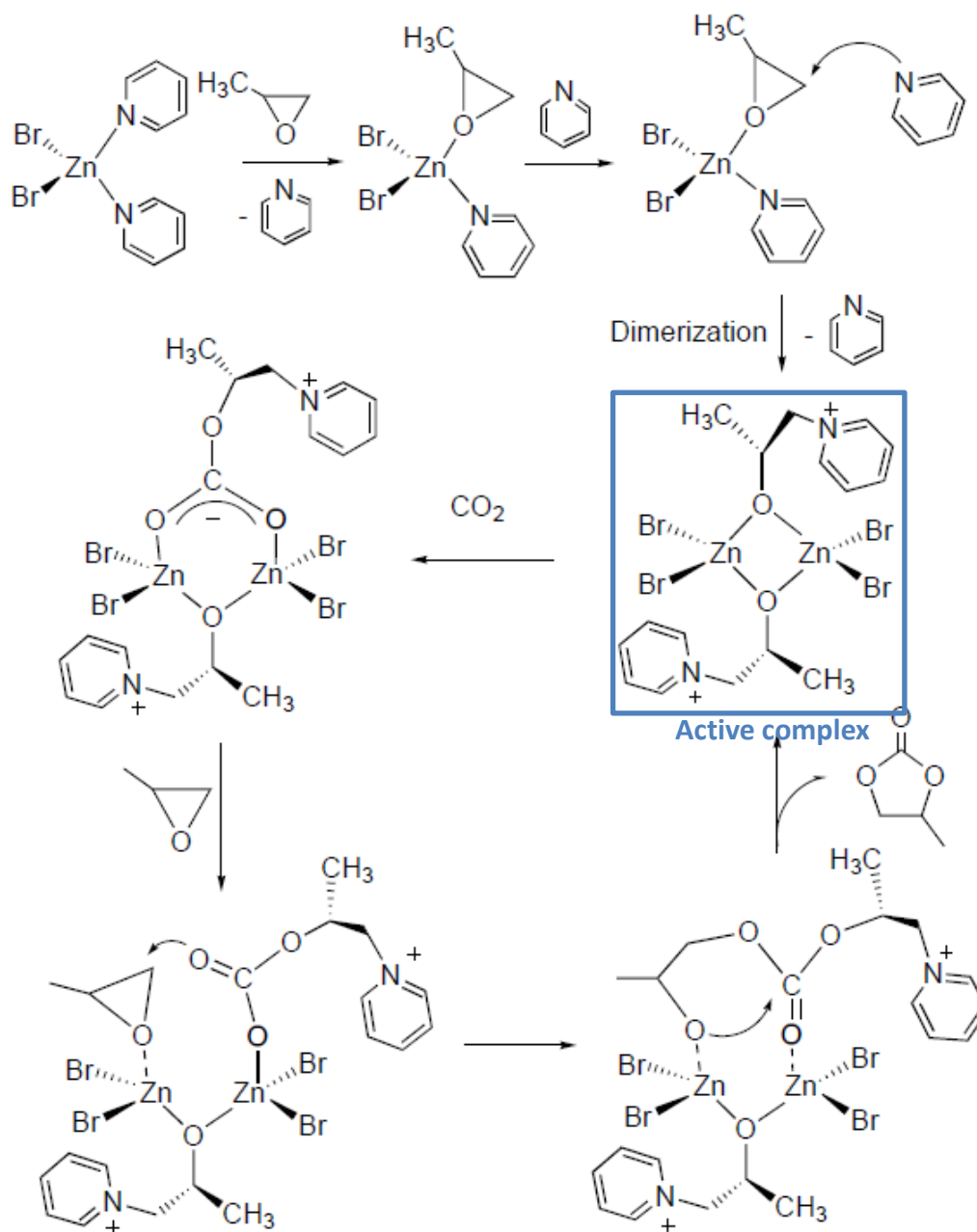
Figure 1.8 : Mécanisme de formation de carbonate cyclique par un complexe de zinc

Le fonctionnement de l'enzyme *Carbonique Anhydrase,* étroitement lié à tous les travaux visant à transformer le CO_2 en carbonates, est donné à la **Figure 1.9**. La *Carbonique Anhydrase* catalyse l'hydratation du CO_2 en acide carbonique à une vitesse 10^7 fois plus rapide que lorsque non catalysée. Le site actif de cette enzyme, ainsi que son mécanisme réactionnel (**Figure 1.9**), résument la réaction la plus rapide de transformation du CO_2 connue à ce jour.

La structure du site actif présenté a été extraite de la structure cristalline de l'enzyme en présence de ces substrats, accessible dans la banque de données de structure des protéines.[63]
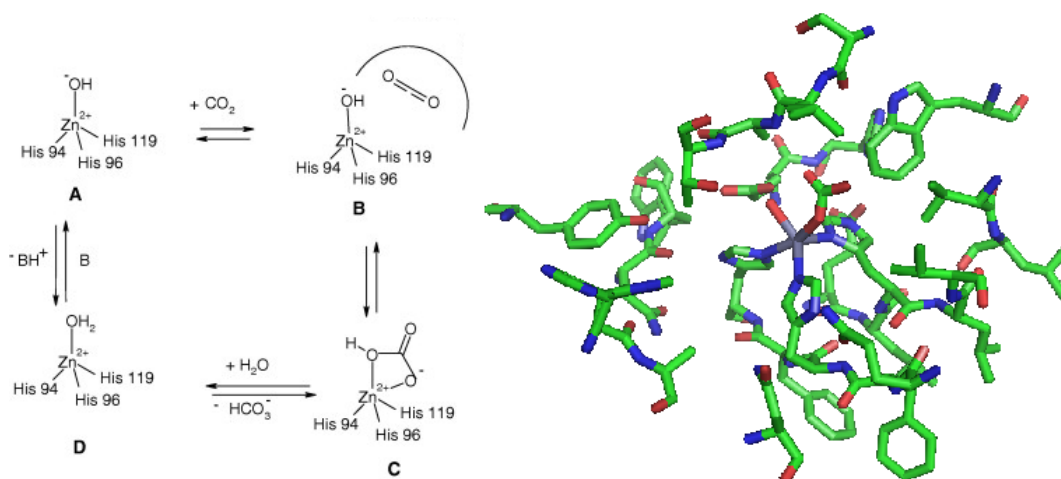
Figure 1.9 : Mécanisme réactionnel et structure du site actif de l'enzyme Carbonique Anhydrase

Ainsi, le site actif de la métallo-enzyme *Carbonique Anhydrase* est une porphyrine de zinc. Quatre résidus histidines se trouvent à proximité de l'atome de zinc, trois étant directement en coordination avec le métal, et le quatrième (His 64) agit de manière à évacuer des protons du site de réaction vers le liquide intracellulaire. Présumant que le cycle catalytique débute par la coordination d'une molécule d'eau par l'atome de zinc **D**, un proton est transféré à l'acide aminé His64 via un réseau de molécules d'eau, ce qui résulte en un intermédiaire hydroxyde de zinc et His64 protoné. Il s'en suit une rotation de His64 de manière à ce que le proton soit rejeté à l'extérieur du site réactionnel. En parallèle à ce mouvement de His64, la fonction hydroxyde de zinc effectue une attaque nucléophile sur une molécule de CO_2 produisant un intermédiaire bicarbonate de zinc. Le cycle catalytique est ensuite fermé via le déplacement de l'ion bicarbonate par une seconde molécule d'eau et régénère le site réactionnel initial.

La formation de tout intermédiaire lors de la réaction catalysée par l'enzyme *Carbonique Anhydrase* dépend d'un équilibre chimique (**Figure 1.10a**), dont l'activité préférentielle est hautement dépendante de la présence d'un milieu tampon, qui favorise la diffusion de protons (**Figure 1.10b**). En effet, il a été démontré qu'en absence de buffer, la constante de vitesse de la réaction de la métallo-enzyme est limitée à la vitesse de diffusion

des protons en solution soit $10^4 s^{-1}$, alors qu'elle peut atteindre jusqu'à $10^6 s^{-1}$ en présence d'un milieu tampon. Ainsi, l'étape limitante de la réaction d'hydratation du CO_2 dans le site actif de la *CA* est la formation de la fonction hydroxyde de zinc, via la déprotonation d'une molécule d'eau et la diffusion du proton à l'extérieur du site de réaction.

Il est intéressant de noter que l'ion bicarbonate, produit par la carbonique anhydrase, est une composante importante qui tamponne le liquide intracellulaire, et sa présence accélère la réaction d'hydratation du CO_2.
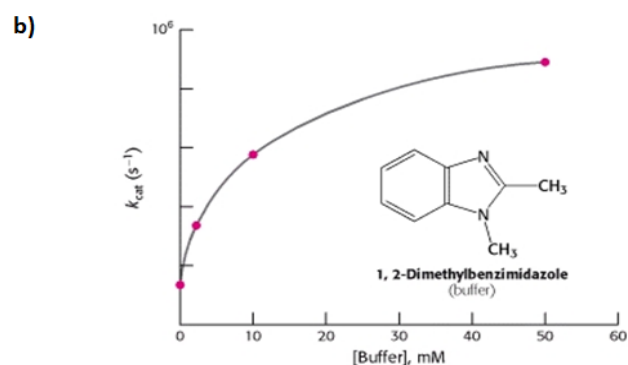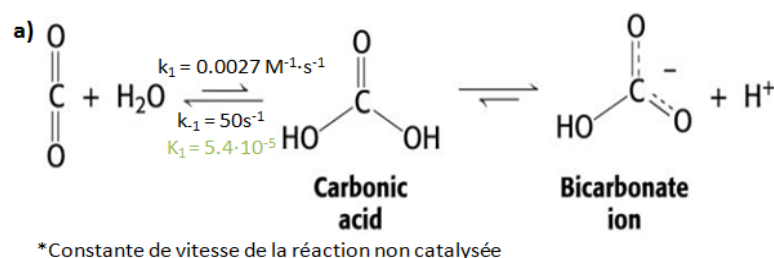
Figure 1.10 : a) Équilibre chimique de la réaction d'hydratation du CO_2 en absence de catalyse et à pH neutre b) Influence de la concentration de buffer sur la constante de vitesse de la réaction directe de l'enzyme carbonique anhydrase.

Ainsi, sachant que la réaction de formation de carbonate à partir d'époxyde est un processus réversible, tout comme l'hydratation du CO_2 par la *Carbonique Anhydrase*, la carboxylation du DME en DMC à été entrepris de manière à promouvoir un cycle catalytique similaire. Dans cette optique, la conception de catalyseurs hétérogènes a été effectuée dans le but d'activer le diméthyle éther de manière à promouvoir l'insertion du CO_2 tel que lors de la synthèse de carbonates à partir d'époxyde ou lors de l'hydratation du CO_2. Par étude de la réactivité du DME à la surface de divers catalyseurs, il à été identifié que les zéolites

protonées réagissent en phase gazeuse avec le diméthyle éther produisant du méthanol et générant une surface catalytique couverte de méthyllium (**Figure 1.11**). [64] Des études sur la formation de la forme méthoxonium des zéolites ont montré que lorsqu'exposés à un écoulement de MeOH ou DME, les protons zéolitiques sont échangés par des méthyllium à une température aussi basse que 120°C.[65-66]
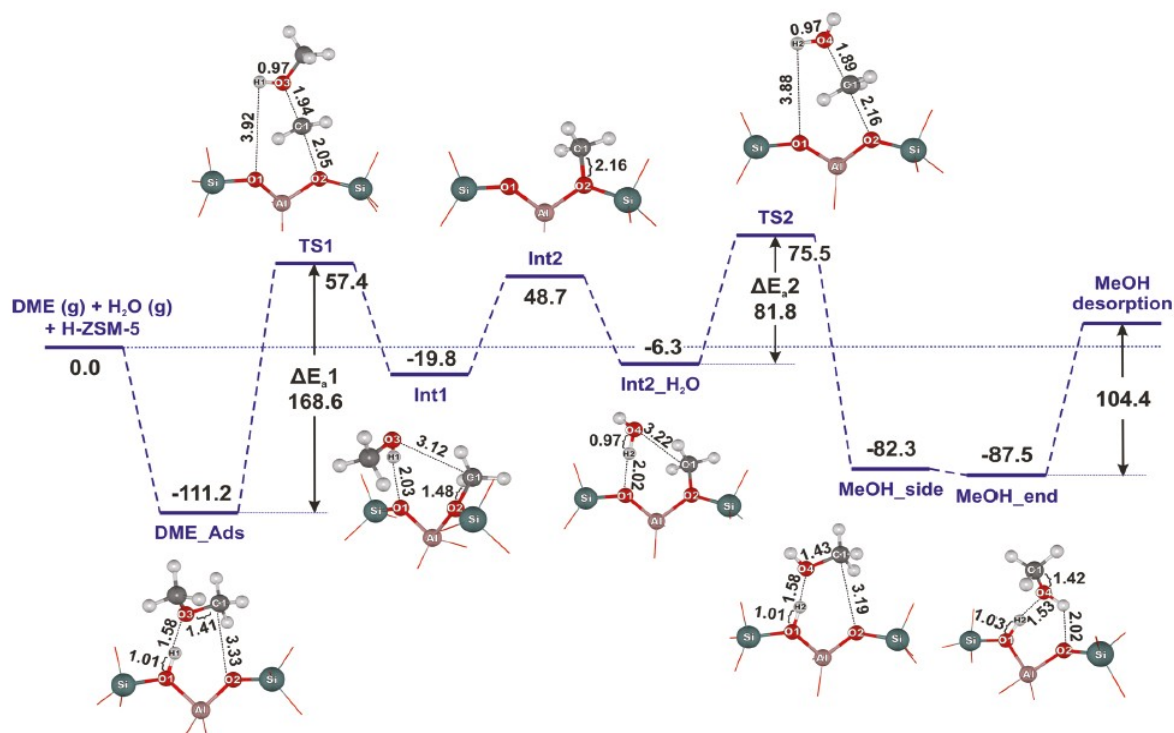
Figure 1.11 : Formation de méthyllium à la surface de zéolite et mécanisme d'hydrolyse du DME

Cependant, la partie méthoxy associée à la formation du cation méthyllium à partir du DME quitte le site actif sous forme de méthanol lorsque la réaction est effectuée sur une forme de zéolite protoné. Une attention a donc été portée à l'échange des protons zéolitiques par des métaux. Ainsi, les sites à l'intérieur des zéolites sur lesquels le DME est brisé en CH_3^+ et CH_3O^- ne produiraient plus de méthanol tel qu'avec la forme proton, mais plutôt des méthoxyde de métal. Le choix du métal à positionner dans la structure zéolitique devait donc être choisi judicieusement et dû à ses antécédents pour ce qui a trait à la synthèse de carbonates, le zinc a été le candidat en tête de liste.

Par la suite, la structure de la zéolite influence également grandement la réactivité du complexe catalytique. Après évaluation de la structure de plusieurs types de zéolite, c'est la *Faujasite* qui a été choisie, en raison de sa constitution présentant une abondance de sites constitués de 6 atomes tétragonaux (6T). Lorsqu'un métal est placé dans un site 6T, il est tricoordiné, tel que l'atome de zinc dans le site actif de l'enzyme carbonique anhydrase. L'évaluation théorique et expérimentale de l'activité de la faujasite échangée au zinc pour la carboxylation du diméthyle éther ainsi que la décarboxylation du diméthyle carbonate a ainsi été entreprise.

REFERENCES

1.   *Key world energy statistics*; International Energy Agency: 2011.

2.   Smol, J. P., Climate Change: A planet in flux. *Nature* **2012,** *483* (7387), S12-S15.

3.   Friedrich, T.; Timmermann, A.; Abe-Ouchi, A.; Bates, N. R.; Chikamoto, M. O.; Church, M. J.; Dore, J. E.; Gledhill, D. K.; Gonzalez-Davila, M.; Heinemann, M.; Ilyina, T.; Jungclaus, J. H.; McLeod, E.; Mouchet, A.; Santana-Casiano, J. M., Detecting regional anthropogenic trends in ocean acidification against natural variability. *Nature Clim. Change* **2012,** *2* (3), 167-171.

4.   Hungate, B. A.; Hampton, H. M., Ecosystem services: Valuing ecosystems for climate. *Nature Clim. Change* **2012,** *2* (3), 151-152.

5.   Shakun, J. D.; Clark, P. U.; He, F.; Marcott, S. A.; Mix, A. C.; Liu, Z.; Otto-Bliesner, B.; Schmittner, A.; Bard, E., Global warming preceded by increasing carbon dioxide concentrations during the last deglaciation. *Nature* **2012,** *484* (7392), 49-54.

6.   Cox, P. M.; Betts, R. A.; Jones, C. D.; Spall, S. A.; Totterdell, I. J., Acceleration of global warming due to carbon-cycle feedbacks in a coupled climate model. *Nature* **2000,** *408* (6809), 184-187.

7.   Singh, B. K.; Bardgett, R. D.; Smith, P.; Reay, D. S., Microorganisms and climate change: terrestrial feedbacks and mitigation options. *Nat Rev Micro* **2010,** *8* (11), 779-790.

8.   Sakakura, T.; Choi, J.-C.; Yasuda, H., Transformation of Carbon Dioxide. *Chemical Reviews* **2007,** *107* (6), 2365-2387.

9.   Pacheco, M. A.; Marshall, C. L., Review of Dimethyl Carbonate (DMC) Manufacture and Its Characteristics as a Fuel Additive. *Energy & Fuels* **1997,** *11* (1), 2-29.

10.   Tundo, P.; Selva, M., The Chemistry of Dimethyl Carbonate. *Accounts of Chemical Research* **2002,** *35* (9), 706-716.

11.   Santos, B. A. V.; Pereira, C. S. M.; Silva, V. M. T. M.; Loureiro, J. M.; Rodrigues, A. E., Kinetic study for the direct synthesis of dimethyl carbonate from methanol and CO2 over CeO2 at high pressure conditions. *Applied Catalysis A: General* **2013,** *455* (0), 219-226.

12.   Renaud, R.; Leitch, L. C., SYNTHESIS OF DEUTERATED DIMETHYL CARBONATE. *Canadian Journal of Chemistry* **1956,** *34* (2), 181-182.

13.   Cella, J. A.; Bacon, S. W., Preparation of dialkyl carbonates via the phase-transfer-catalyzed alkylation of alkali metal carbonate and bicarbonate salts. *Journal of Organic Chemistry* **1984,** *49* (6), 1122-1125.

14.   Fujinami, T.; Sato, S.; Sakai, S., A facile preperation of dialkyl carbonates from potassium carbonate and alkyl bromide by using organostannyl compounds as a catalyst. *Chemistry Letters* **1981,** *10* (6), 749.

15.   Kizlink, J., Synthesis of Dimethyl Carbonate from Carbon Dioxide and Methanol in the presence of Organotin compounds. *Collection of Czechoslovak Chemical Communications* **1993,** *58* (6), 1399-1402.

16.   Kizlink, J.; Pastucha, I., Preperation of Dimethyl Carbonate from Methanol and Carbon Dioxide in the presence of Sn(IV) and Ti(IV) Alkoxides and metal acetates. *Collection of Czechoslovak Chemical Communications* **1995,** *60* (4), 687-692.

17.   Kizlink, J.; Pastucha, I., Preperation of Dimethyl Carbonate from Methanol and Carbon Dioxide in the presence of organotin compounds. *Collection of Czechoslovak Chemical Communications* **1994,** *59* (9), 2116-2118.

18.   Wagner, A.; Loeffler, W.; Haas, B. Verfahren zur Herstellung von Dialkylcarbonat. 1994.

19.   Sakakura, T.; Saito, Y.; Okano, M.; Choi, J.-C.; Sako, T., Selective Conversion of Carbon Dioxide to Dimethyl Carbonate by Molecular Catalysis. *The Journal of Organic Chemistry* **1998,** *63* (20), 7095-7096.

20.   Sakakura, T.; Choi, J.-C.; Saito, Y.; Masuda, T.; Sako, T.; Oriyama, T., Metal-Catalyzed Dimethyl Carbonate Synthesis from Carbon Dioxide and Acetals. *The Journal of Organic Chemistry* **1999,** *64* (12), 4506-4508.

21.   Tsutomu, S.; Yotaro, O.; Inoue, N.; Masatsugu, M. Production of Dimethyl Carbonate. 1999.

22.   Yiling, T.; Ying, Q.; Li, C.; Jingang, F.; Li, W., Synthesis of dimethyl carbonate by supercritical CO2-feeding methanol and dimethyl ether. *Fuel Chemistry Division Preprints* **2002,** *47* (1), 267.

23.   Choi, J.-C.; Sakakura, T.; Sako, T., Reaction of Dialkyltin Methoxide with Carbon Dioxide Relevant to the Mechanism of Catalytic Carbonate Synthesis. *Journal of the American Chemical Society* **1999,** *121* (15), 3793-3794.

24.   Tomishige, K.; Sakaihori, T.; Ikeda, Y.; Fujimoto, K., A novel method of direct synthesis of dimethyl carbonate from methanol and carbon dioxide catalyzed by zirconia. *Catalysis Letters* **1999,** *58* (4), 225-229.

25.   Ikeda, Y.; Sakaihori, T.; Tomishige, K.; Fujimoto, K., Promoting effect of phosphoric acid on zirconia catalysts in selective synthesis of dimethyl carbonate from methanol and carbon dioxide. *Catalysis Letters* **2000,** *66* (1), 59-62.

26.   Tomishige, K.; Ikeda, Y.; Sakaihori, T.; Fujimoto, K., Catalytic properties and structure of zirconia catalysts for direct synthesis of dimethyl carbonate from methanol and carbon dioxide. *Journal of Catalysis* **2000,** *192* (2), 355-362.

27.   Yoshiki, I.; Mohammad, A.; Kaoru, F.; Tomishige, K., Structure of the active sites on H3PO4/ZrO2 catalyst for dimethyl carbonate synthesis from methanol and carbon dioxide. *Journal of Physical Chemistry B* **2001,** *105* (43), 10653-10658.

28.   Tomishige, K., Direct synthesis of dimethyl carbonate from methanol and carbon dioxide over solid oxide catalysts. *Current topics in catalysis* **2002,** *3*, 81-101.

29.   Tomishige, K.; Furusawa, Y.; Ikeda, Y.; Asadullah, M.; Fujimoto, K., CeO2−ZrO2 Solid Solution Catalyst for Selective Synthesis of Dimethyl Carbonate from Methanol and Carbon Dioxide. *Catalysis Letters* **2001,** *76* (1), 71-74.

30.   Tomishige, K.; Kunimori, K., Catalytic and direct synthesis of dimethyl carbonate starting from carbon dioxide using CeO2-ZrO2 solid solution heterogeneous catalyst: effect of H2O removal from the reaction system. *Applied Catalysis A: General* **2002,** *237* (1–2), 103-109.

31.   Jung, K. T.; Bell, A. T., An in Situ Infrared Study of Dimethyl Carbonate Synthesis from Carbon Dioxide and Methanol over Zirconia. *Journal of Catalysis* **2001,** *204* (2), 339-347.

32.   Xie, S.; Bell, A. T., An in situ Raman study of dimethyl carbonate synthesis from carbon dioxide and methanol over zirconia. *Catalysis Letters* **2000,** *70* (3), 137-143.

33.   Jiang, C.; Guo, Y.; Wang, C.; Hu, C.; Wu, Y.; Wang, E., Synthesis of dimethyl carbonate from methanol and carbon dioxide in the presence of polyoxometalates under mild conditions. *Applied Catalysis A: General* **2003,** *256* (1–2), 203-212.

34.   Lee, H.; Park, S.; Jung, J.; Song, I., Direct synthesis of dimethyl carbonate from methanol and carbon dioxide over H3PW12O40/CeXZr1−XO2 catalysts: Effect of acidity of the catalysts. *Korean Journal of Chemical Engineering* **2011,** *28* (7), 1518-1522.

35.   La, K. W.; Jung, J. C.; Kim, H.; Baeck, S.-H.; Song, I. K., Effect of acid–base properties of H3PW12O40/CexTi1−xO2 catalysts on the direct synthesis of dimethyl carbonate from methanol and carbon dioxide: A TPD study of H3PW12O40/CexTi1−xO2 catalysts. *Journal of Molecular Catalysis A: Chemical* **2007,** *269* (1–2), 41-45.

36.   Wu, X. L.; Xiao, M.; Meng, Y. Z.; Lu, Y. X., Direct synthesis of dimethyl carbonate on H3PO4 modified V2O5. *Journal of Molecular Catalysis A: Chemical* **2005,** *238* (1–2), 158-162.

37.   Aouissi, A.; Al-Othman, Z. A.; Al-Amro, A., Gas-Phase Synthesis of Dimethyl Carbonate from Methanol and Carbon Dioxide Over Co1.5PW12O40 Keggin-Type Heteropolyanion. *International Journal of Molecular Sciences* **2010,** *11* (4), 1343-1351.

38.   Almusaiteer, K., Synthesis of dimethyl carbonate (DMC) from methanol and CO2 over Rh-supported catalysts. *Catalysis Communications* **2009,** *10* (7), 1127-1131.

39.   Cai, Q.; Jin, C.; Lu, B.; Tangbo, H.; Shan, Y., Synthesis of Dimethyl Carbonate from Methanol and Carbon dioxide using Potassium Methoxide as Catalyst under Mild Conditions. *Catalysis Letters* **2005,** *103* (3), 225-228.

40.   Bian, J.; Xiao, M.; Wang, S. J.; Lu, Y. X.; Meng, Y. Z., Novel application of thermally expanded graphite as the support of catalysts for direct synthesis of DMC from CH3OH and CO2. *Journal of Colloid and Interface Science* **2009,** *334* (1), 50-57.

41.   Bian, J.; Xiao, M.; Wang, S.-J.; Lu, Y.-X.; Meng, Y.-Z., Carbon nanotubes supported Cu–Ni bimetallic catalysts and their properties for the direct synthesis of dimethyl carbonate from methanol and carbon dioxide. *Applied Surface Science* **2009,** *255* (16), 7188-7196.

42.   Bian, J.; Xiao, M.; Wang, S.; Wang, X.; Lu, Y.; Meng, Y., Highly effective synthesis of dimethyl carbonate from methanol and carbon dioxide using a novel copper–nickel/graphite bimetallic nanocomposite catalyst. *Chemical Engineering Journal* **2009,** *147* (2–3), 287-296.

43.   Bian, J.; Xiao, M.; Wang, S. J.; Lu, Y. X.; Meng, Y. Z., Highly effective direct synthesis of DMC from CH3OH and CO2 using novel Cu–Ni/C bimetallic composite catalysts. *Chinese Chemical Letters* **2009,** *20* (3), 352-355.

44.   Shen, Y.; Meng, Q.; Huang, S.; Wang, S.; Gong, J.; Ma, X., Reaction mechanism of dimethyl carbonate synthesis on Cu/[small beta] zeolites: DFT and AIM investigations. *RSC Advances* **2012,** *2* (18), 7109-7119.

45.   Zhang, R.; Song, L.; Wang, B.; Li, Z., A density functional theory investigation on the mechanism and kinetics of dimethyl carbonate formation on Cu2O catalyst. *Journal of Computational Chemistry* **2012,** *33* (11), 1101-1110.

46.   Zhou, Y.; Wang, S.; Xiao, M.; Han, D.; Lu, Y.; Meng, Y., Novel Cu-Fe bimetal catalyst for the formation of dimethyl carbonate from carbon dioxide and methanol. *RSC Advances* **2012,** *2* (17), 6831-6837.

47.   Chen, Y.; Xiao, M.; Wang, S.; Han, D.; Lu, Y.; Meng, Y., Porous Diatomite-Immobilized Cu–Ni Bimetallic Nanocatalysts for Direct Synthesis of Dimethyl Carbonate. *Journal of Nanomaterials* **2012,** *2012*.

48.   Bian, J.; Wei, X. W.; Wang, L.; Guan, Z. P., Graphene nanosheet as support of catalytically active metal particles in DMC synthesis. *Chinese Chemical Letters* **2011,** *22* (1), 57-60.

49.   Bian, J.; Wei, X. W.; Jin, Y. R.; Wang, L.; Luan, D. C.; Guan, Z. P., Direct synthesis of dimethyl carbonate over activated carbon supported Cu-based catalysts. *Chemical Engineering Journal* **2010,** *165* (2), 686-692.

50.   Mikkelsen, M.; Jorgensen, M.; Krebs, F. C., The teraton challenge. A review of fixation and transformation of carbon dioxide. *Energy & Environmental Science* **2010,** *3* (1), 43-81.

51.   North, M.; Pasquale, R.; Young, C., Synthesis of cyclic carbonates from epoxides and CO2. *Green Chemistry* **2010,** *12* (9), 1514-1539.

52.   Yu, Z.; Xu, L.; Wei, Y.; Wang, Y.; He, Y.; Xia, Q.; Zhang, X.; Liu, Z., A new route for the synthesis of propylene oxide from bio-glycerol derived propylene glycol. *Chemical Communications* **2009,** (26), 3934-3936.

53.   Fu, Y.; Zhu, H.; Shen, J., Thermal decomposition of dimethoxymethane and dimethyl carbonate catalyzed by solid acids and bases. *Thermochimica Acta* **2005,** *434* (1–2), 88-92.

54.   Selva, M.; Fabris, M.; Perosa, A., Decarboxylation of dialkyl carbonates to dialkyl ethers over alkali metal-exchanged faujasites. *Green Chemistry* **2011,** *13* (4), 863-872.

55.   Yang, Y.; Hayashi, Y.; Fujii, Y.; Nagano, T.; Kita, Y.; Ohshima, T.; Okuda, J.; Mashima, K., Efficient cyclic carbonate synthesis catalyzed by zinc cluster systems under mild conditions. *Catalysis Science & Technology* **2012,** *2* (3), 509-513.

56.   Omae, I., Recent developments in carbon dioxide utilization for the production of organic chemicals. *Coordination Chemistry Reviews* **2012,** *256* (13–14), 1384-1405.

57.   Razali, N. A. M.; Lee, K. T.; Bhatia, S.; Mohamed, A. R., Heterogeneous catalysts for production of chemicals using carbon dioxide as raw material: A review. *Renewable and Sustainable Energy Reviews* **2012,** *16* (7), 4951-4964.

58.   Sattler, W.; Parkin, G., Low temperature NMR spectroscopic investigation of a zinc bicarbonate compound: Thermodynamics of bicarbonate formation by insertion of CO2 into the zinc hydroxide bond of []ZnOH. *Polyhedron* **2012,** *32* (1), 41-48.

59.   Bottoni, A.; Lanza, C. Z.; Miscione, G. P.; Spinelli, D., New Model for a Theoretical Density Functional Theory Investigation of the Mechanism of the Carbonic Anhydrase: How Does the Internal Bicarbonate Rearrangement Occur? *Journal of the American Chemical Society* **2004,** *126* (5), 1542-1550.

60.   Lipton, A. S.; Heck, R. W.; Ellis, P. D., Zinc Solid-State NMR Spectroscopy of Human Carbonic Anhydrase: Implications for the Enzymatic Mechanism. *Journal of the American Chemical Society* **2004,** *126* (14), 4735-4739.

61.   Maupin, C. M.; McKenna, R.; Silverman, D. N.; Voth, G. A., Elucidation of the Proton Transport Mechanism in Human Carbonic Anhydrase II. *Journal of the American Chemical Society* **2009,** *131* (22), 7598-7608.

62.   Kim, H. S.; Kim, J. J.; Lee, S. D.; Lah, M. S.; Moon, D.; Jang, H. G., New Mechanistic Insight into the Coupling Reactions of CO2 and Epoxides in the Presence of Zinc Complexes. *Chemistry – A European Journal* **2003,** *9* (3), 678-686.

63.   Eriksson, A. E.; Jones, T. A.; Liljas, A., Refined structure of human carbonic anhydrase II at 2.0 Å resolution. *Proteins: Structure, Function, and Bioinformatics* **1988,** *4* (4), 274-282.

64.   Namuangruk, S.; Meeprasert, J.; Khemthong, P.; Faungnawakij, K., A Combined Experimental and Theoretical Study on the Hydrolysis of Dimethyl Ether over H-ZSM-5. *The Journal of Physical Chemistry C* **2011,** *115* (23), 11649-11656.

65.   Wang, W.; Seiler, M.; Hunger, M., Role of Surface Methoxy Species in the Conversion of Methanol to Dimethyl Ether on Acidic Zeolites Investigated by in Situ Stopped-Flow MAS NMR Spectroscopy. *The Journal of Physical Chemistry B* **2001,** *105* (50), 12553-12558.

66.   Wang, W.; Buchholz, A.; Seiler, M.; Hunger, M., Evidence for an Initiation of the Methanol-to-Olefin Process by Reactive Surface Methoxy Groups on Acidic Zeolite Catalysts. *Journal of the American Chemical Society* **2003,** *125* (49), 15260-15267.

2. A thermodynamic resolution of Dimethyl Carbonate decarboxylation and the first example of its reversibility: Dimethyl Ether carboxylation

Jean-Francois Lacroix [1], Armand Soldera [2] and Jean-Michel Lavoie [1*]*

[1] J.F. Lacroix, Prof. Dr. J.M. Lavoie

Chaire de recherche industrielle sur l'éthanol cellulosique

2   Prof. Dr. A. Soldera

Laboratoire de chimie physique moléculaire

RÉSUMÉ

Il a été montré que la décarboxylation du diméthyle carbonate (DMC) et la carboxylation du diméthyle ether (DME) sont deux réactions en éruilibre, équilibre chimique dans lequel le CO_2 est impliqué. La décarboxylation du DMC en DME et CO_2 a été cinétiquement et thermodynamiquement résolue, ce qui a permis d'obtenir les conditions opératoires avec lesquelles la carboxylation du DME est thermodynamiquement favorable. L'obtention de la carboxylation du DME qui en a découlée, représente le premier exemple d'insertion du CO_2 dans une fonction éther aliphatique. Cette étude a été effectuée en utilisant un réacteur à lit fixe contenant un catalyseur faujasite échangé avec du zinc. Ce catalyseur a été conçu dans le but de reproduire avec le DMC et le DME, l'équilibre chimique d'hydratation du CO_2 par l'enzyme carbonique anhydrase (*CA*).

ABSTRACT

Dimethyl carbonate (DMC) decarboxylation and Dimethyl Ether (DME) carboxylation were found to be a system under equilibrium in which CO_2 is the cornerstone. DMC decarboxylation to DME and CO_2 was thermodynamically and kinetically resolved, which allowed obtaining conditions in which DME carboxylation is thermodynamically favourable. Subsequent demonstration of DME carboxylation represents the first exemple of CO_2 insertion in an aliphatic ether function. This study was carried out using a continuous fixed bed reactor loaded with zinc-exchanged faujasite catalyst, designed to mimic the reaction mechanism of CO_2 hydration by the enzyme Carbonic Anhydrase.

2.1   Introduction

Using a continuous bench-scale reactor loaded with zinc exchanged faujasite (Zn-FAU), we have demonstrated that Dimethyl Carbonate (DMC) decomposition to Dimethyl Ether (DME) and CO_2 is a reversible process. During the past twenty years, development of an efficient catalyst for bulk production of dimethyl carbonate (DMC) from CO_2 and methanol has been pursued given its economical interest as oxygenated fuel additive as well as for its potential as a green methylating agent and solvent.[1-5] However, catalyst development for methanol carboxylation to DMC has shown to be hindered not only by CO_2 kinetics inertia, but also by an important reaction inhibition caused by water co-production.[6] Actually, the only industrially scalable method for producing DMC from methanol and CO_2 is the water-free reaction sequence involving epoxide carboxylation to cyclic carbonate followed by transesterification with methanol producing DMC and the 1,2-diol associated to the initial oxirane.[7-9] As this DMC synthesis process also involves converting an epoxide into a 1,2-diol, the economic viability of the process is highly dependent on downstream usage of the diol, either as an added-value co-product from the reaction or as a feed to regenerate epoxide.[10-11]

Herein, we present the thermodynamic resolution of DMC decarboxylation to DME and the first example of DME carboxylation to DMC [Eq. 2.1]. DME carboxylation is a novel water free and direct synthetic path to DMC from CO_2 with 100% atoms efficiency.

$$\diagdown_O\diagup\ +\ CO_2\ \underset{\longrightarrow}{\overset{cat,\ \Delta}{\longleftarrow}}\ \diagdown_O\overset{\displaystyle O}{\underset{O}{\|}}_{\diagup} \qquad\qquad (2.1)$$
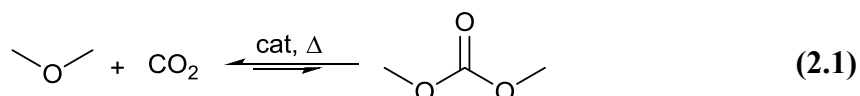
DMC decarboxylation to DME and CO_2 is a known process and its reversibility is found to be the results of a temperature dependant chemical equilibrium, as previously demonstrated in cyclic carbonates synthesis.[12-15] The catalyst used in this work is a zinc-loaded faujasite at its near full exchange capacity. It has been designed in order to mimic the zinc prosthetic group and reactivity of the active site of the enzyme *Carbonic Anhydrase* (*CA*). The metalloenzyme induces CO_2 hydration through equilibrium displacement promoted by a tri-coordinated Zn^{II} porphyrin, aided by a histidine residue that acts as proton shuttle between the reaction site and the bulk solution.[16] The faujasite framework consists of sodalite cages connected through hexagonal prisms, which result in a structure made of 4T and 6T rings (T

for tetrahedral atoms) with diffusion channels of 7.4Å aperture.[17-19] Previous work on single crystals XRD characterization of the zinc-exchanged faujasite has demonstrated that preferential location of metals is at a first instance in the sodalite cages, then at the surface of supercages 6T rings. Characterization of Zn-FAU synthesized through wet impregnation as in this work was also found to have abundance of zinc located 6T ring sites.[20] These zinc located 6T ring sites are accessible to substrates for reaction and as in the *CA* active site; the acidic zinc center is in a three coordination state.[20-21] The electron density and geometrical analyses of the *CA* active Zinc centre and substrate accessible zinc exchanged faujasite 6T rings site are given in **Figure 2.1** and **Table 2.1**. The analysis of the *CA* active site was carried out directly on the crystal structure of the enzyme while the zinc-loaded faujasite 6T ring site has been artificially reconstituted through DFT structure optimization at the ONIOM(M06/6-31g(d),SBKJC VDZ:PM6) theory level. Charges of both sites were then obtained by full DFT single point calculation. Larger cluster and description of the method used for obtaining these structures is provided in the supporting information.
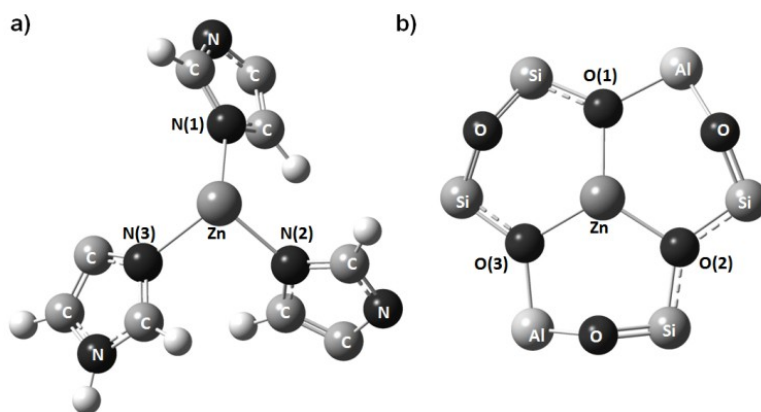
Figure 2.1 : Zinc environment in a) Carbonic Anhydrase metalloporphyrin b) Zinc exchanged faujasite 6T ring

Table 2.1. Bond length and charge density of a) Carbonic Anhydrase Zn porphyrin b) Zinc exchanged faujasite 6T ring

a)	Zn	N(1)	N(2)	N(3)
Charge[a]	0.577	-0.491	-0.481	-0.534
Zn[b]	2.06[c]	2.06	2.03	2.08
b)	Zn	O(1)	O(2)	O(3)
Charge[a]	0.950	-0.884	-0.901	-0.887
Zn[b]	1.92[c]	1.90	1.93	1.93

[a] Mulliken charges[b] Distance (Å) [c] Average distance (Å) to ligand

The acid strength of the faujasite material is known to activate DME in a similar fashion as H_2O activation by the metallo-enzyme. The induction of CO_2 hydration by the metalloenzyme is initiated by the activation of a water molecule to reversibly produce a zinc hydroxide center in which CO_2 insertion occurs, while a proton is taken away by a proximal basic function.[22-24] Comparatively, the first steps of numerous heterogeneous reactions such as hydrolysis, carbonylation, and DTO involving a gas flow of DME at the surface of zeolites, is the DME acid-promoted C-O bond cleavage resulting in the formation of a surface methoxonium and adsorbed methanol intermediate.[25-27] Consequently, promoting the same reaction pattern at the surface of zinc-exchanged faujasite potentially results in the reversible formation of adjacent zinc-methoxide and surface methoxonium active complex, analog to the *CA* key intermediates in which CO_2 insertion occur.

2.2 Experimental

2.2.1 Catalyst synthesis

The catalyst was prepared from zeolite Y CBV 600 (Faujasite) in his hydrogen cation nominal form with SiO_2/Al_2O_3 ratio of 5.2, purchased from Zeolyst International. Zinc(II) was loaded in CBV 600 using $Zn(NO_3)_2 \cdot 6H_2O$ salt with purity higher than 98%, purchased from Sigma Aldrich. Zn-FAU was prepared by Brønsted acid sites neutralisation using the incipient wetness method, a fully scalable synthesis procedure which does not require solvents other than water. Specifically, to a 1L round bottom flask containing 400mL of deionised water at

60°C, were gradually added CBV 600 (75g, 0.322 mol of Al, 1 equivalent) while stirring under air. The resulting solution were vigorously stirred at 60°C during 2h, then $Zn(NO_3)_2 \cdot 6H_2O$ (38.32g, 0.129 mol Zn, 0.45 equivalent) was added slowly. The resulting mixture was stirred overnight at 60°C under atmospheric conditions. Without any filtration, water was removed under vacuum (-32 PSIG) at 90°C, resulting in a white thick and solid crust. The solid has been kept in the 1L round bottom flask and place in an air stationary oven at 105°C for 24h. The solid has then been transfer in a 5 inches diameter quartz tube and place in a high temperature tube furnace and calcinated at 723K under a 1L·min⁻¹ air flow. The calcinations procedure which involves slow temperature increase ramp was completed with a final heating stage of 4h at 723K, which is slightly above the zinc oxide Hüttig temperature, temperature at which ZnO mobility is occurring on a catalytic surface.[28] The post calcinations material (Zn-FAU) was still a white thick and solid crust which was then crushed and sifts. The particles with size fractions ranging from 1.4 to 2.5 millimetres where collected (85.2g) and stored under dry atmosphere for characterization and catalyst activity measurement. The materials were characterized all along the synthesis procedure using XRD, XRF, SEM and SAXS analysis. The different characterization procedures are provided in supporting information.

2.2.2 Reactor

Catalyst testing was carried out using a bench-scale reactor. The setup consisted of a tubular fixed bed reactor with internal diameter of 19.05mm, where the catalyst was immobilized between two layers of inert material (Silicon Carbide). The catalyst bed temperature was controlled using a tube furnace with homogeneous temperature gradient, and internal temperatures were monitored by a thermocouple with the head carefully placed in the middle of the reactive zone. Temperature and pressure were graphically monitored at several points of the reactor, to guarantee that reagents were reaching the catalyst as gaseous species and that no pressures build up was occurring. The CO_2 flow was controlled using a high precision mass flow controller, while liquefied DME or DMC were pumped continuously and subsequently vaporized in the heated inlet stream. The reactor outlet composition was quantified using gas chromatography system, an AGILENT 7820A, equipped with a FID

detector and a DB624 column. The GCMS was an AGILENT 7890A equipped with VL MSD triple axis detector 5975C and DB624 column, was used for outlet stream composition analysis.

2.2.3 Catalyst activity measurements

Typical procedure for DMC decarboxylation experiments consisted to pre-heat the reactor inlet, outlet and catalyst containing area under a 1L•min^{-1} N$_2$ flow. The inlet and outlet stream were heated to 398 K and the catalyst internal temperature was set to a desired temperature. Once the reactor temperature, pressure and flow were stabilized at the desired reaction conditions, liquid DMC was added continuously in the inlet stream at a rate of 0.02mL (liq)·min^{-1} using a diaphragm pump.

Dimethyl Ether carboxylation experiments was carried out following a similar procedure as describe for DMC decarboxylation. 1.5L$_{(gas)}$ ·min^{-1} of CO$_2$ was used as vector gas during pre-reaction setup conditioning and liquefied DME was added using a high pressure syringe pump. Typically, the reactor inlet and outlet stream was heated to 398 K, the catalyst internal temperature at 313 K, while pressurizing the setup to 400 psig. Once the setup was stabilized at the predefined conditions and under a CO$_2$ flow, Dimethyl Ether (0.372 mL·min^{-1}) was added in the inlet stream in a ratio CO$_2$/DME of 10.

2.3 Results and discussion

2.3.1 Catalyst characterization

The catalyst were prepared with an intended zinc to alumina ratio of 0.45, in order to avoid formation of zinc bridged oxide sites, while maximizing zinc loading and hence the presence of substrates accessible internal surface sites.[29] Using XRD powder analysis, it was verified after each synthetic step that the faujasite structure remained unchanged. **Figure 2.2c** presents diffraction pattern superposition of the 5-35° characteristic regions of the synthesized material pre and post calcination, with the commercial faujasite. It confirmed that the faujasite framework remained identical all along the metal exchanged procedure, and that zinc atoms

are all extra framework located. In addition, the absence of ZnO signal in the XRD powder pattern supports that zinc atoms are well dispersed and linked to the activated oxygen of the framework. To verify that mesoporosity was unaffected by metal loading, surface analysis was carried out using a 20-150keV electron beam in Scanning electron microscopy (SEM). Picture of H-FAU **2.2a** and Zn-FAU **2.2b** show that the structure remained mesoporous and therefore that reactants meso-diffusion is physically unlimited.
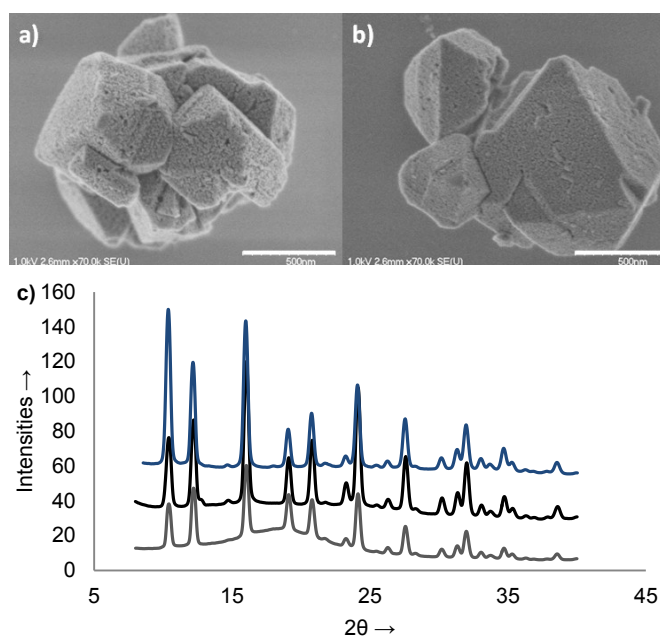
Figure 2.2 : SEM picture of a) H-FAU b) Zn-FAU c) XRD diffraction pattern superposition of the commercial Faujasite (grey), Zn-FAU pre-calcination (black) and Zn-FAU post-calcination (blue).

Table 2.2. Elemental composition of the materials along the synthesis procedure, determined by XRF analysis. [a]

	Commercial Faujasite	Zinc loaded Faujasite	Zn-FAU post-calcination
SiO2	70.88	45.01	62.38
Al2O3	21.89	14.17	19.33
ZnO	0	11.88	14.78
LOI (%)	7.25	29.08	3.53
Si/Al	2.74	2.59	2.74
Zn/Al	0.00	0.51	0.48

[a] Masse % of metal oxide composition of the catalyst

The zinc to alumina ratio was monitored along the metal exchange process using X-Ray Fluorescence (XRF) analysis (**Table 2.2**). A final Zn/Al ratio of 0.48 was obtained, compared to the planned value of 0.45. Mesostructural particle size also remained unaffected by the aqueous and thermal treatment of the material. The average meso-particle radius distribution of the commercial and zinc exchanged faujasite are 5.83 nm and 5.81 nm respectively, as demonstrated by small angle X-ray scattering (SAXS).

2.3.2 Catalyst activity

At each evaluated reaction conditions, the reaction was maintained at steady state for at least 2h, until three identical GC injections were obtained. In order to observe any catalyst deactivation, initial conditions were retrieved at the end of each 8-10h run. For experiments in which temperature was kept below 360K, initial activity was always retrieved, indicating that the catalyst did not deactivate. On the other hand, catalyst darkening associated to coke formation was observed after experiments in which temperature above 400K was studied. Our efforts being focused on the characterization of the equilibrium point between DMC and DME, DMC decarboxylation has only been studied with the purpose to collect thermodynamic and kinetic data.
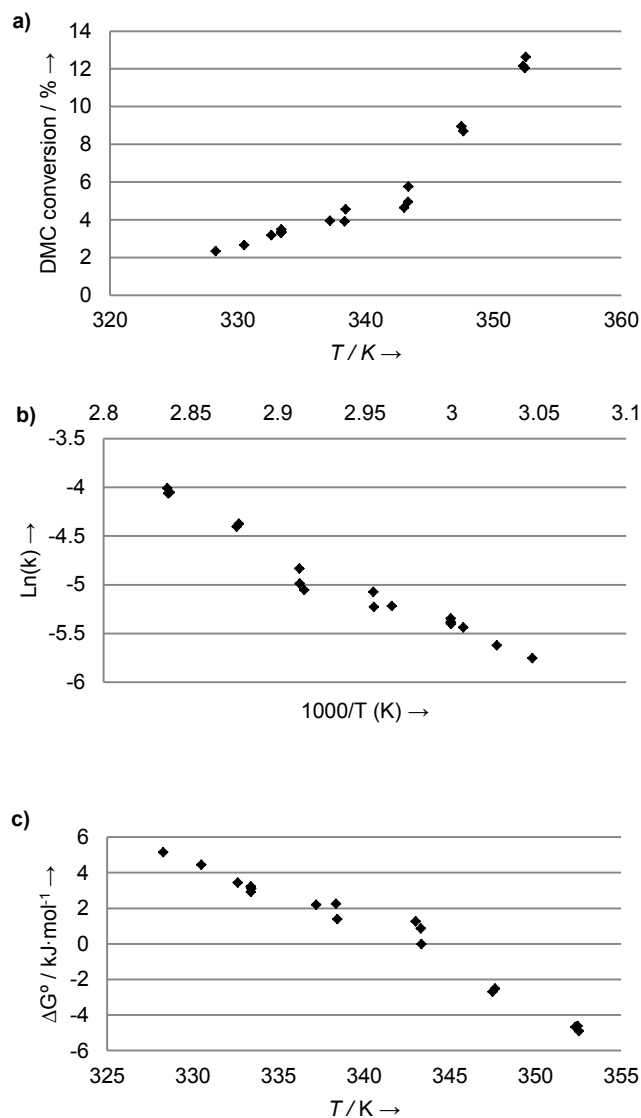
Figure 2.3 : a) Temperature effect on DMC decarboxylation to DME and CO_2 on Zn-FAU b) corresponding Arrhenius plot c) variation of equilibrium free energy in function of temperature. Reaction conditions: $65g_{cat}$(150 mL), $1L_{(gas)} \cdot min^{-1}$ N_2 (GHSV 400h^{-1}), $0.02mL_{(liq)} \cdot min^{-1}$ DMC (LHSV 0.008h^{-1}), 1 bar.

The activity of the synthesized zinc-exchanged faujasite material towards DMC decarboxylation as a function of temperature is given in **Figure 2.3a**. The reaction is found to begin at a temperature slightly below 325K and increase rapidly while maintaining a perfect selectivity for DME and CO_2. The conversion was maintained below 12% in order to remain in the kinetics linearity domain of the reaction, which allowed obtention of an accurate

kinetics resolution of the reaction (**Figure 2.3b**).[30] It permitted identifying that at the surface of Zn-FAU, DMC and DME are thermodynamically separated by apparent activation energy of 66.7kJ/mol, while the entropic pre-exponential terms is $1,21 \cdot 10^8 s^{-1}$. The Arrhenius plot also shows that the decarboxylation reaction proceeds with a rate of $3.2 \cdot 10^{-3}$ s^{-1} at 328K. This reaction is presenting an ideal kinetically limited profile: reactant and product diffusion is occurring at higher rate than the reaction. Further data analysis allowed defining reaction equilibrium free energy variation in function of the temperature (**Figure 2.3c**). It is found that at the surface of Zn-FAU, the decarboxylation reaction is thermodynamically favourable at temperature above 345K, and that CO_2 insertion in DME is accessible below this temperature.

Figure 2.4a shows the temperature effect on DME carboxylation at the surface of Zn-FAU. In correlation with the DMC decarboxylation thermodynamic results, DMC formation was observed at low temperature and showed a negative temperature effect. Exposing Zn-FAU to a continuous 10:1 CO_2:DME flow and catalyst contact time of 7.45s at 325K led to a maximal DME conversion of 0.4% without any trace of product other than DMC. The effect of pressure was evaluated between 7.8 and 28.2 bar, but conversion variation remained undetectable. On the other side, increasing gas velocity resulted in an increase of the catalyst activity. At 360K and under 28.2 bar, the conversion increased from 0.25% to 0.35% by varying the CO_2/DME ratio from 10 to 50. Identical results were obtained when diluting the reaction with N_2 at constant 10:1 CO_2/DME ratio. This suggests that flow velocity rather than reactants equivalent is at the origin of the activity variation, and therefore that reactants and products diffusion at the catalyst surface is a possible limitation.
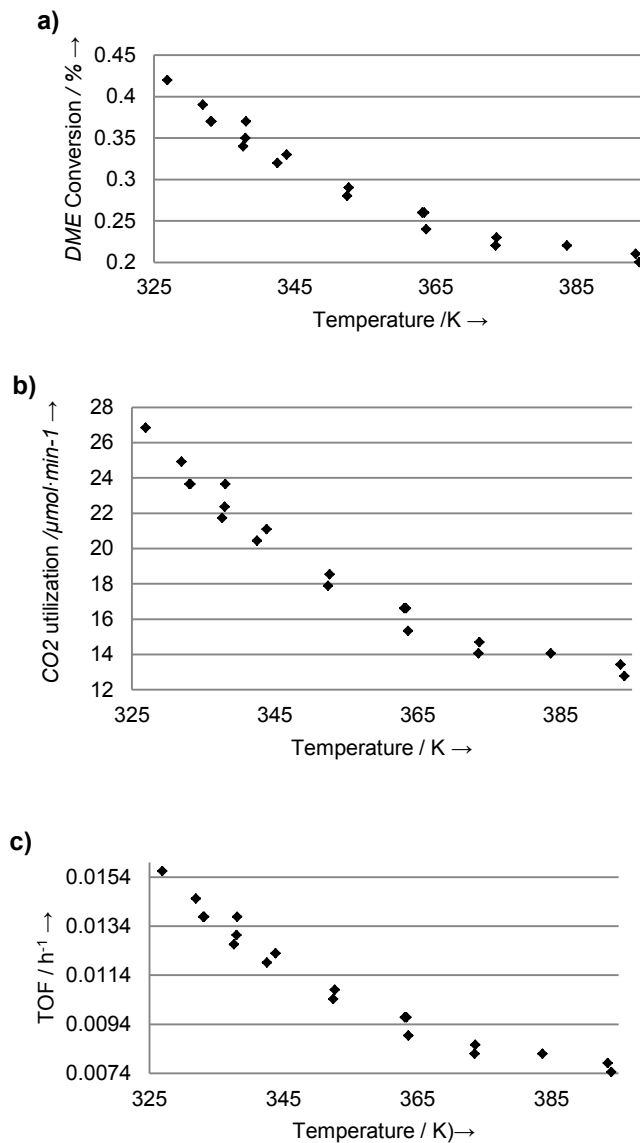
Figure 2.4 : a) Temperature effect on DME carboxylation on Zn-FAU b) Amount of CO$_2$ converted c) Turnover frequency for DME carboxylation. Reaction conditions: 57g$_{cat}$(125 mL), CO$_2$/DME mol ratio 10, 1.5L$_{(gas)}$·min^{-1} CO$_2$ (GHSV=720h^{-1}), 0.37mL$_{(liq)}$·min^{-1} DME (LHSV=0.18h^{-1}), 28.2 bar

Figure 2.4b show the amount of CO$_2$ valorised into DMC during DME carboxylation reaction at the surface of Zn-FAU, while **Figure 2.4c** present turnover frequency (TOF/h^{-1}) of the reaction, based on the total zinc content of the material. Such a system has the potential to become industrially relevant if conversion can be increase sufficiently to allow isolating DMC from the outlet stream, but would require an important DME and CO$_2$ recycling loop.

2.4 Conclusions

In summary, using heterogeneous Zinc exchanged faujasite catalyst, designed to reproduce with DME and DMC the *carbonic cnhydrase* equilibrium mechanism, it was demonstrated that dimethyl carbonate decarboxylation is reversible, resulting into the first example of CO_2 insertion into an aliphatic ether function. A typical temperature influence of carbonates formation/decomposition was observed, lower temperature being preferable to CO_2 insertion and higher temperature being favourable to CO_2 release. From kinetics measurement on the DMC decarboxylation reaction, we found that when proceeding under a kinetically controlled regime, the equilibrium is separated by apparent activation energy of $66.7 kJ \cdot mol^{-1}$. Such an energetic barrier amplitude is typical to methyllium transfer in zeolites,[25] suggesting that the equilibrium is driven by zinc methoxide/surface methoxonium formation. DME carboxylation being found to occur at low temperature, reactants and products surface state and diffusion are found to potentially be limiting. The reaction was attempted using packed bed reactor at gaseous state, but actual results orient future development towards utilization of trickle bed or slurry reactors, in which the heterogeneous reaction is carried out by interacting homogeneous solution of reactants and products with the solid catalyst. Further mechanistical analysis will be carried in order to orient design of second generation catalysts with improve performance for DME carboxylation.

Supporting information

Experimental details and supplementary data associated with this article can be found with the online version at:

Acknowledgements

REFERENCES

1.	Tundo, P.; Selva, M., The Chemistry of Dimethyl Carbonate. *Accounts of Chemical Research* 2002, *35* (9), 706-716.

2.	Wen, L.-b.; Xin, C.-Y.; Yang, S.-C., The effect of adding dimethyl carbonate (DMC) and ethanol to unleaded gasoline on exhaust emission. *Applied Energy* 2010, *87* (1), 115-121.

3.	Rounce, P.; Tsolakis, A.; Leung, P.; York, A. P. E., A Comparison of Diesel and Biodiesel Emissions Using Dimethyl Carbonate as an Oxygenated Additive. *Energy & Fuels* 2010, *24* (9), 4812-4819.

4.	Pacheco, M. A.; Marshall, C. L., Review of Dimethyl Carbonate (DMC) Manufacture and Its Characteristics as a Fuel Additive. *Energy & Fuels* 1997, *11* (1), 2-29.

5.	Schäffner, B.; Schäffner, F.; Verevkin, S. P.; Börner, A., Organic Carbonates as Solvents in Synthesis and Catalysis. *Chemical Reviews* 2010, *110* (8), 4554-4581.

6.	Sakakura, T.; Kohno, K., The synthesis of organic carbonates from carbon dioxide. *Chemical Communications* 2009, *0* (11), 1312-1330.

7.	Buysch, H.-J., Carbonic Esters. In *Ullmann's Encyclopedia of Industrial Chemistry*, Wiley-VCH Verlag GmbH & Co. KGaA: 2000.

8.	Cokoja, M.; Bruckmeier, C.; Rieger, B.; Herrmann, W. A.; Kühn, F. E., Transformation of Carbon Dioxide with Homogeneous Transition-Metal Catalysts: A Molecular Solution to a Global Challenge? *Angewandte Chemie International Edition* 2011, *50* (37), 8510-8537.

9.	Cokoja, M.; Bruckmeier, C.; Rieger, B.; Herrmann, W. A.; Kühn, F. E., Umwandlung von Kohlendioxid mit Übergangsmetall-Homogenkatalysatoren: eine molekulare Lösung für ein globales Problem? *Angewandte Chemie* 2011, *123* (37), 8662-8690.

10.	Rebsdat, S.; Mayer, D., Ethylene Glycol. In *Ullmann's Encyclopedia of Industrial Chemistry*, Wiley-VCH Verlag GmbH & Co. KGaA: 2000.

11.	Yu, Z.; Xu, L.; Wei, Y.; Wang, Y.; He, Y.; Xia, Q.; Zhang, X.; Liu, Z., A new route for the synthesis of propylene oxide from bio-glycerol derived propylene glycol. *Chemical Communications* 2009, (26), 3934-3936.

12.	Selva, M.; Fabris, M.; Perosa, A., Decarboxylation of dialkyl carbonates to dialkyl ethers over alkali metal-exchanged faujasites. *Green Chemistry* 2011, *13* (4), 863-872.

13.	Fu, Y.; Zhu, H.; Shen, J., Thermal decomposition of dimethoxymethane and dimethyl carbonate catalyzed by solid acids and bases. *Thermochimica Acta* 2005, *434* (1–2), 88-92.

14.   Bolívar-Diaz, C. L.; Calvino-Casilda, V.; Rubio-Marcos, F.; Fernández, J. F.; Bañares, M. A., New concepts for process intensification in the conversion of glycerol carbonate to glycidol. *Applied Catalysis B: Environmental* 2013, *129* (0), 575-579.

15.   Ema, T.; Miyazaki, Y.; Koyama, S.; Yano, Y.; Sakai, T., A bifunctional catalyst for carbon dioxide fixation: cooperative double activation of epoxides for the synthesis of cyclic carbonates. *Chemical Communications* 2012, *48* (37), 4489-4491.

16.   Domsic, J. F.; Williams, W.; Fisher, S. Z.; Tu, C.; Agbandje-McKenna, M.; Silverman, D. N.; McKenna, R., Structural and Kinetic Study of the Extended Active Site for Proton Transfer in Human Carbonic Anhydrase II. *Biochemistry* 2010, *49* (30), 6394-6399.

17.   Inayat, A.; Knoke, I.; Spiecker, E.; Schwieger, W., Assemblies of Mesoporous FAU-Type Zeolite Nanosheets. *Angewandte Chemie International Edition* 2012, *51* (8), 1962-1965.

18.   Inayat, A.; Knoke, I.; Spiecker, E.; Schwieger, W., Mesoporöse Nanoschichtaggregate vom Zeolithtyp FAU. *Angewandte Chemie* 2012, *124* (8), 1998-2002.

19.   Isambert, A.; Angot, E.; Hebert, P.; Haines, J.; Levelut, C.; Le Parc, R.; Ohishi, Y.; Kohara, S.; Keen, D. A., Amorphization of faujasite at high pressure: an X-ray diffraction and Raman spectroscopy study. *Journal of Materials Chemistry* 2008, *18* (47), 5746-5752.

20.   Seo, S.; Kim, H.; Park, M.; Lim, W., Synthesis and structural refinement of fully dehydrated fully Zn2+-exchanged zeolite Y (FAU), |Zn35.5|[Si121Al71O384]-FAU. *J Porous Mater* 2011, *18* (1), 47-56.

21.   Frising, T.; Leflaive, P., Extraframework cation distributions in X and Y faujasite zeolites: A review. *Microporous and Mesoporous Materials* 2008, *114* (1–3), 27-63.

22.   Bottoni, A.; Lanza, C. Z.; Miscione, G. P.; Spinelli, D., New Model for a Theoretical Density Functional Theory Investigation of the Mechanism of the Carbonic Anhydrase: How Does the Internal Bicarbonate Rearrangement Occur? *Journal of the American Chemical Society* 2004, *126* (5), 1542-1550.

23.   Lipton, A. S.; Heck, R. W.; Ellis, P. D., Zinc Solid-State NMR Spectroscopy of Human Carbonic Anhydrase: Implications for the Enzymatic Mechanism. *Journal of the American Chemical Society* 2004, *126* (14), 4735-4739.

24.   Maupin, C. M.; McKenna, R.; Silverman, D. N.; Voth, G. A., Elucidation of the Proton Transport Mechanism in Human Carbonic Anhydrase II. *Journal of the American Chemical Society* 2009, *131* (22), 7598-7608.

25.   Namuangruk, S.; Meeprasert, J.; Khemthong, P.; Faungnawakij, K., A Combined Experimental and Theoretical Study on the Hydrolysis of Dimethyl Ether over H-ZSM-5. *The Journal of Physical Chemistry C* 2011, *115* (23), 11649-11656.

26.   Boronat, M.; Martínez-Sánchez, C.; Law, D.; Corma, A., Enzyme-like Specificity in Zeolites: A Unique Site Position in Mordenite for Selective Carbonylation of Methanol and

Dimethyl Ether with CO. *Journal of the American Chemical Society* 2008, *130* (48), 16316-16323.

27.   Yamazaki, H.; Shima, H.; Imai, H.; Yokoi, T.; Tatsumi, T.; Kondo, J. N., Direct Production of Propene from Methoxy Species and Dimethyl Ether over H-ZSM-5. *The Journal of Physical Chemistry C* 2012, *116* (45), 24091-24097.

28.   Moulijn, J. A.; van Diepen, A. E.; Kapteijn, F., Catalyst deactivation: is it predictable?: What to do? *Applied Catalysis A: General* 2001, *212* (1–2), 3-16.

29.   Kazansky, V. B.; Serykh, A. I., Unusual localization of zinc cations in MFI zeolites modified by different ways of preparation. *Physical Chemistry Chemical Physics* 2004, *6* (13), 3760-3764.

30.   Hill, I. M.; Hashimi, S. A.; Bhan, A., Kinetics and mechanism of olefin methylation reactions on zeolites. *Journal of Catalysis* 2012, *285* (1), 115-123.

2.5 Supporting Information

A thermodynamic resolution of Dimethyl Carbonate decarboxylation and the first example of its reversibility: Dimethyl Ether carboxylation

Jean-François Lacroix, Armand Soldera* and Jean-Michel Lavoie*

2.5.1 Carbonic Anhydrase and Faujasite active site analysis

The active site analysis of the enzyme Carbonic Anhydrase has been made from the *human carbonic anhydrase II* crystal structure available in the *RCSB Proteine Data Bank*, PDB # 3U47. The active site analysis of the Zinc exchanged faujasite has been made based on the crystal structure of the faujasite material, available in the database of zeolite structure from the *Structure Comission* of the *International Zeolite Association* (IZA-SC), framework type FAU. In the case of *CA*, a water free 8Å residues cluster was extracted from the crystal structure of the protein using the program *PyMOL*, and the valence of the subsequent cluster was completed to neutral with hydrogen using the *Gauss View 5.0* program (**Figure 2.5a).** The Zn(II) faujasite 6T ring site was computationally reconstituted in a faujasite supercage cluster, extracted from the faujasite crystal structure. In the faujasite 6T ring site, two silicon atoms haves been replaced with two aluminium atoms, after which the valence of the site was completed to neutral by the addition of the Zn(II) atom. The valence of the outer layer atoms of the faujasite cluster was also completed to neutral using hydrogen atoms (**Figure 2.5b**).
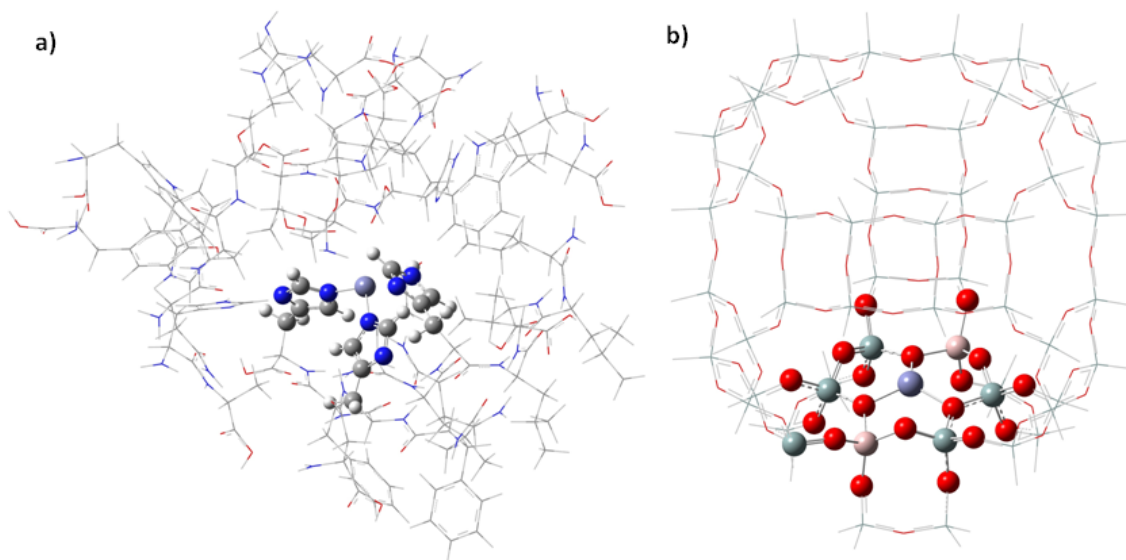
Figure 2.5 : a) Carbonic Anhydrase cluster b) faujasite cluster with Zn(II) 6T ring

The atomic distances were directly available from the crystal structure, atomic charge haves been obtained from Density Functional Theory (DFT) calculations. In both cases, for the *CA* cluster and faujasite cluster, the calculation method was the same. The functional which has been used is the *M06*. It was previously proved accurate for evaluating structures in which long range interactions are significant.[1] The *6-31g(d) basis set was* used for any atoms other than Zinc. The Zinc atoms haves been treated with the *SBKJC VDZ effective core potential*. Atomic charges of the *CA* active site have been obtained from a single point calculation, while the faujasite cluster was energetically optimized as it was not an original structure. This optimization has been carried out by dividing the structure in three layers. The non site participating atoms were treated with the semi empirical *PM6* method. The atoms other than Zn(II) in the active site were treated with the DFT *M06/6-31g(d)* method. Finally, the Zinc atom was treated using the *M06* functional and the *SBKJC VDZ* effective core potential. Final atomic charges of the faujasite optimized cluster have been refined to the same level of theory as for the *CA* cluster by single point calculation. The geometrical and charges comparison of both sites is given in **figure 2.1** of the present article. The calculations have been made using Gaussian 09 and the command lines to carry out calculations to get energetically optimized structures are as follow:

Optimization: *# opt oniom(m06/genecp:pm6) nosymm scf=qc geom=connectivity*

Single Point: *# m06/genecp nosymm scf=qc geom=connectivity*

Genecp referring to *6-31G(D)* and *SBKJC VDZ ECP*

2.5.2 Preparation of Zn-FAU

The catalyst was prepared from a CBV 600 zeolite Y (Faujasite) in his hydrogen cation nominal form and with a ratio SiO_2/Al_2O_3 of 5.2 as indicated by the supplier; Zeolyst International. Zinc(II) has been loaded in CBV 600 using $Zn(NO_3)_2 \cdot 6H_2O$ with purity higher than 98%, purchased from Sigma Aldrich. Zn-FAU was prepared by the following procedure. To a 1L round bottom flask containing 400mL of deionised water at 60°C, were gradually added CBV 600 (75g, 0.322 mol of Al, 1 equivalent) while stirring under air. The resulting solution were vigorously stirred at 60°C during 2h, then $Zn(NO_3)_2 \cdot 6H_2O$ (38.32g, 0.129 mol Zn, 0.45 equivalent) was added slowly. The resulting mixture was stirred overnight at 60°C under air. Without any filtration, water was removed under vacuum (-32 PSIG) at 90°C, resulting in a white thick and solid crust. The solid has been kept in the 1L round bottom flask and place in an air stationary oven at 105°C for 24h. The solid has then been transfer in a 5 inches diameter quartz tube and place in a high temperature tube furnace. While a continuous air flow of 1L·min⁻¹ was passed through the material in the quartz tube, the zinc loaded CBV 600 has been calcinated following the program describe in **Figure 2.6**. The pre-calcination material contained a significant amount of water and nitric acid and consequently, the calcinations were carried out through slow temperature increase ramp, in order to prevent the structure to collapse under an acidic thermal treatment.
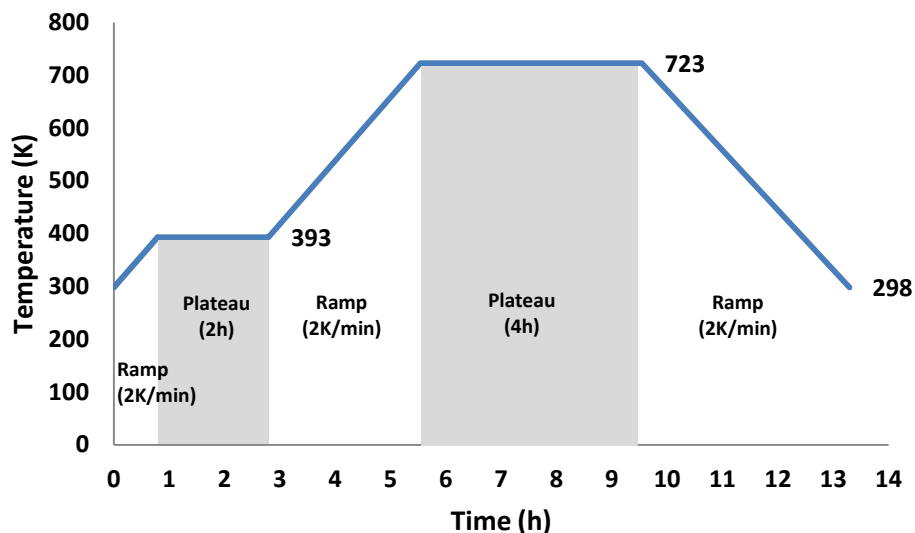
Figure 2.6 : Temperature programmed calcinations under an air flow of 1L·min⁻¹

The post calcinations material (Zn-FAU) was still a white thick and solid crust which was then crushed and sifts. The particles with size fractions ranging from 1.4 to 2.5 millimetres where then collected (85.2g) and stored under dry atmosphere for characterization and catalyst activity measurement.

2.6   Characterization

2.6.1 Powder XRD analysis

X-ray powder diffraction analysis has been made using a *Bruker APEX DUO X-Ray* diffractometer. The sample preparation and scans procedure were as follow. The powder was mixed with paratone oil to obtain a paste like sample. This sample was cut to approximately 0.3mm³ and place on a steel needle and mounted in the instrument. 6 correlated runs with Phi Scan of 360° and exposures time of 360 seconds were collected with the Cu micro-focus anode (1.54184Å) and the signal was detected with a *CCD APEX II* detector located at 150 mm from the sample. These runs, from -12 to -72 2θ and 6 to 36ω, where then treated and integrated with the *XRW² Eval Bruker* software to produce the X-Ray powder pattern from

approximately 7⁰ to 80⁰ 2θ range. The pattern was treated with *Diffrac.Eva* version 2.0 from Bruker and the matching was done with the International Center for Diffraction Data (ICDD[®]) PDF-2 (2011) release.

2.6.2 Powder XRD analysis of CBV 600

The obtained XRD powder pattern of the commercial faujasite CBV 600 is presented in **figure 2.7**. The typical 5-35 2θ characteristics region of the faujasite is well defined and it is found that the material have a crystallinity degree of 66.2%, with 33.8% of amorphous phase. The low crystallinity degree of the material is highlighted by the presence of the broad peak between 13 and 22 2θ, but the matching with the reference powder pattern of the faujasite zeolite is perfect.
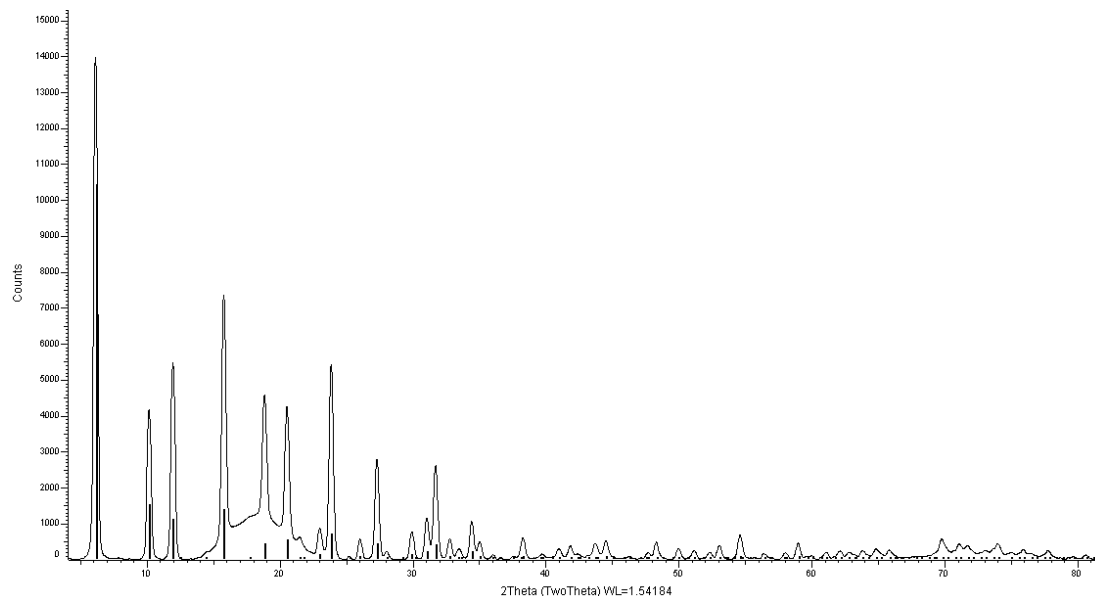
Figure 2.7: XRD powder pattern of CBV 600 (black) and reference pattern peak (lines)

2.6.3 XRD Powder pattern of zinc loaded CBV 600

The XRD powder pattern of the pre-calcination zinc loaded material is given in **figure 2.8**. It is confirmed that the aqueous treatment, water evaporation and the 105°C drying step did not affect the faujasite structure. An increase of the crystallinity degree of the material is remarkable, with 78.5% of crystalline phase and 21.5% of amorphous phase compare to 66.2% and 33.8% respectively for the commercial CBV 600. Such an increase in crystallinity after aqueous treatment of the CBV 600 material has been previously observed and is attributed to a flushed away of remaining impurities from the commercial synthesis of CBV 600.[2]
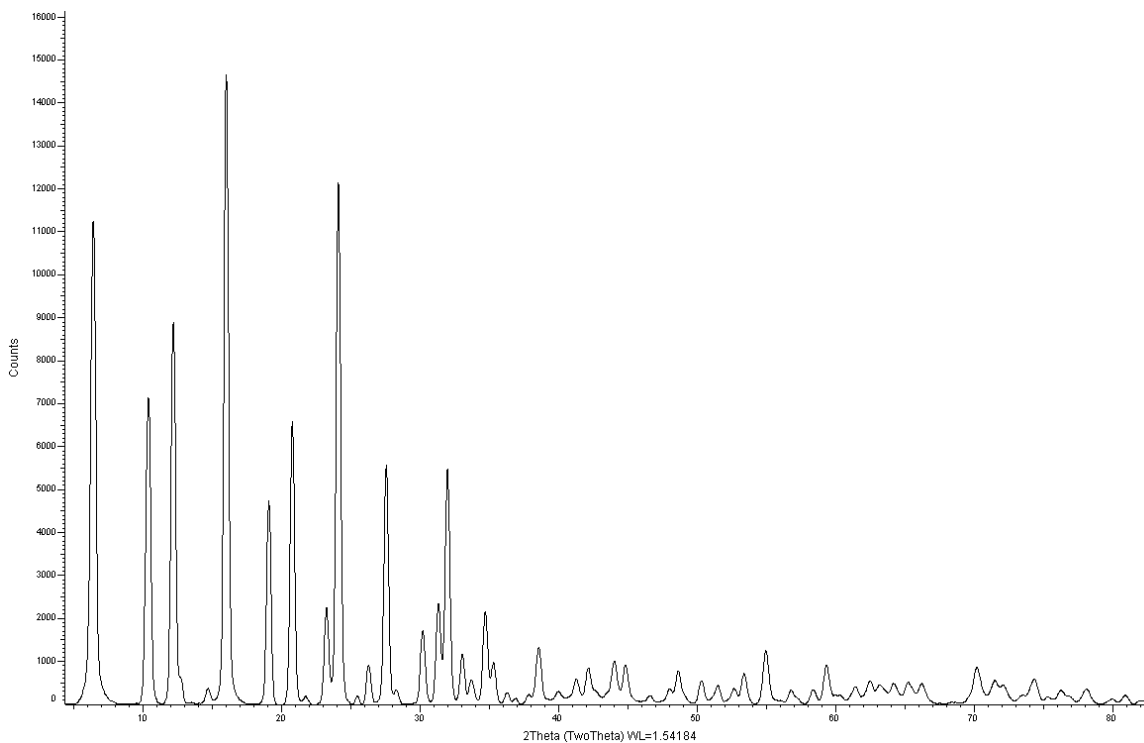
Figure 2.8 : XRD powder pattern of the pre-calcination Zinc loaded CBV 600

2.6.4 XRD powder pattern of Zn-FAU

The XRD powder pattern of the post calcinations zinc loaded CBV 600 (Zn-FAU) is given in **figure 2.9**. The faujasite structure remained intact after the thermal treatment, and the crystallinity degree of the material remained essentially the same as obtained for the pre-calcination material with 80% of crystalline phase and 20% of amorphous phase. The absence of the characteristic signal of ZnO (2θ of 32, 37 and 43) in the powder pattern of Zn-FAU support that zinc sintering did not happen during calcinations and that they are well disperse and in coordination with the activated oxygen of the faujasite structure.
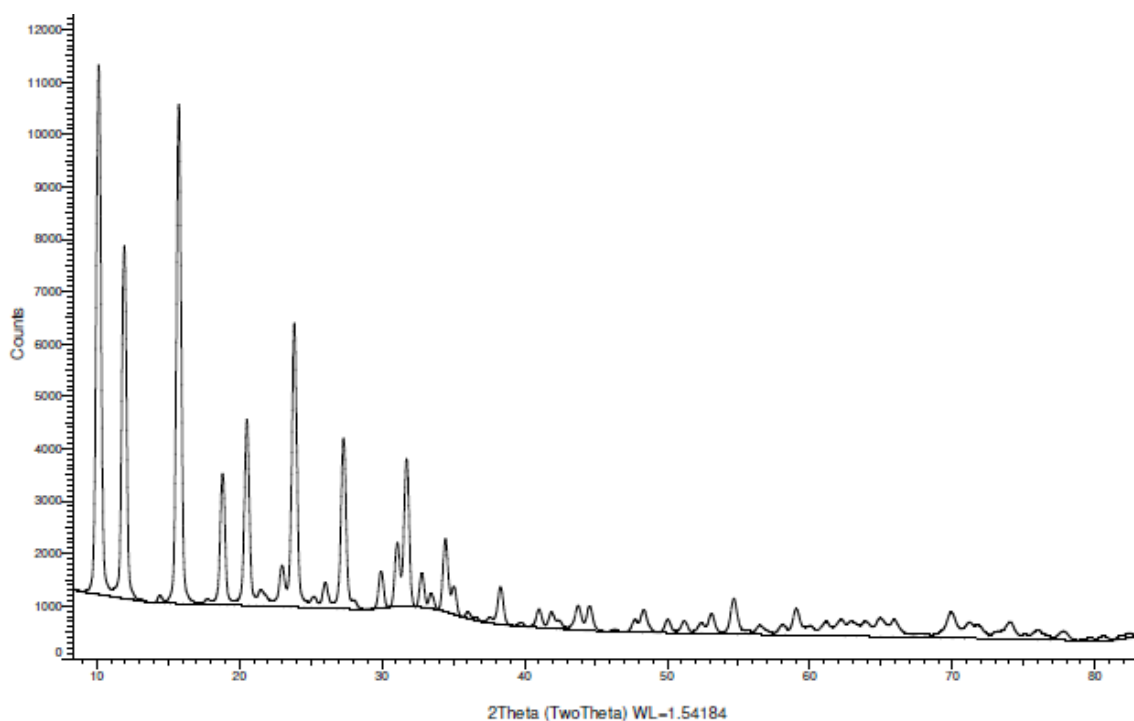
Figure 2.9: XRD powder pattern of Zn-FAU

The superposition of the diffraction pattern showed in **figure 2.7 – 2.9** is given in **figure 2.2** of the present article.

2.7 X-Ray fluorescence analysis

The general procedure for determining the elemental composition of the material using XRF analysis is as follow. The sample was prepared using the fused bead method. 0.7 g of sample was mixed with 7g of melting agents; 4.67g of $Li_2B_4O_7$, 2.30 g of $LiBO_2$ and 0.035g of LiBr. The solid solution has been melted at 1473 K with heating steps plateau of 2.5 min at 873K, 0.5 min at 1173 K, 1.0 min at 1323 K, 1.5 min at 1423 K and 10.5 min at 1473 K. The resulting melted solution has been allowed to cool to room temperature resulting in a glass pellets which was analysed with $K\alpha$ ray using an AXIOS PANanalytical instrument. The elemental composition of the material along the synthesis procedure is given in **table 2.3**. The mass loss resulting from the glass pellets procedure is associated to water in the case of CBV 600 and Zn-FAU, nitric acid add to water in the case of Zn(II) + CBV 600.

Table 2.3: Elemental composition (mass %) of the materials along the catalyst synthesis

Oxydes	CBV 600	Zn(II) + CBV	Zn-FAU
SiO_2	70.878	45.07	62.382
Al_2O_3	21.889	14.169	19.325
ZnO	0.000	11.881	14.775
CuO	0,026	0.021	0.022
Fe_2O_3	0,011	0,007	0,012
SO_3	0,014	0,011	0,019
Mass loss on	7,245	29,081	3,529
Si/Al	2.74	2.59	2.74
Zn/Al	0.00	0.51	0.48

*Mass loss related to material melting and glass pellets making procedure

2.8 Scanning electron microscopy

The scanning electron microscopy analysis has been carried out using a *FEG-SEM S-4700* instrument from *HITACHI*. The imaging measurement has been made in secondary electron mode with a work distance of 2.6 mm and maximal objective focus. Pictures at 300, 500 and 1000 nm scale of CBV 600 and Zn-FAU are given in **Figure 2.10**.
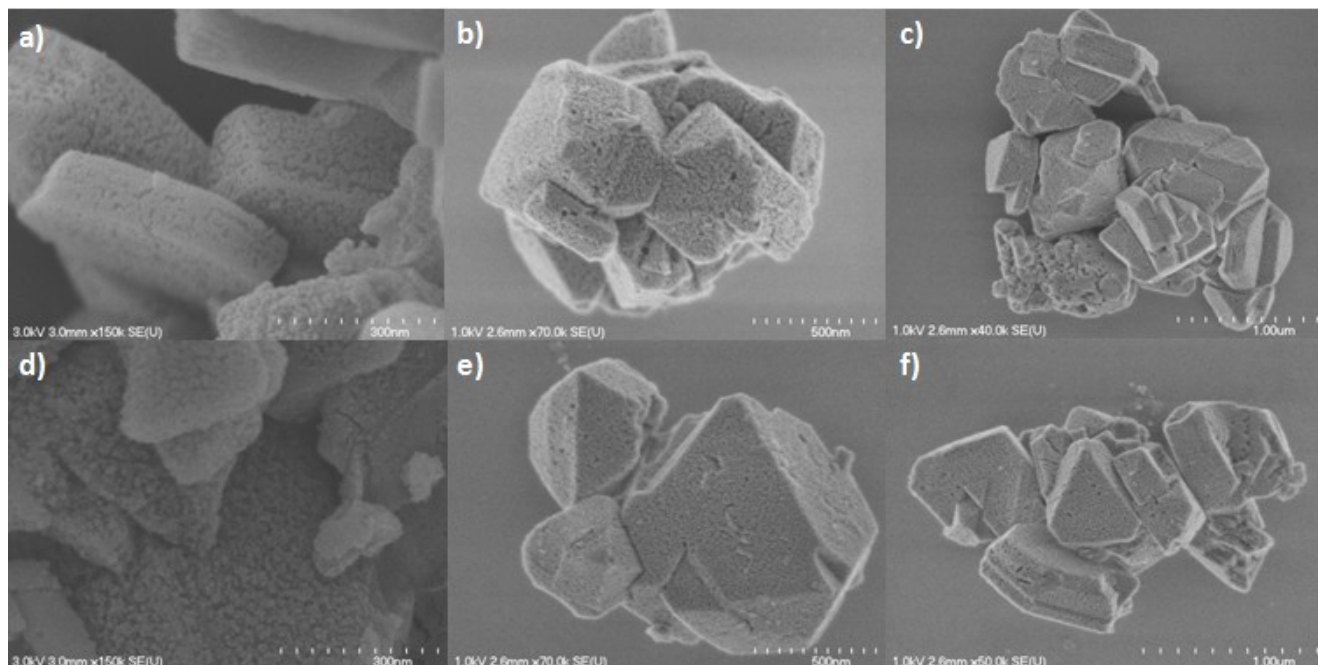
Figure 2.10: SEM picture of CBV 600 a), b) and c) and Zn-FAU d), e) and f)

2.9   Small Angle X-Ray Scattering (SAXS) analysis

SAXS analysis of CBV 600 and Zn-FAU has been carried out using a *Bruker AXS Nanostar* system equipped with a microfocus copper anode at 45 kV / 0.65 mA, *MONTAL OPTICS* and a *VANTEC 2000 2D* detector placed at 68.35 mm from the samples. The instrument has been pre-calibrated with a Silver Behenate standard. The samples were measured on an adhesive blanks tape. The blanks were measured first and subtracted to the sample measurement data. The diffracted intensities were then integrated from 0.2 to 6.3 2θ and treated with *Primus GNOM 3.0* programs from ATSAS 2.3 softwares to determine the particle sizes by pair distance distribution. Samples exposure times during data collection were 500 seconds/sample.

Figure S6 show that CBV 600 and Zn-FAU are constituted of mesoparticles with relatively homogeneous size distribution. The SAXS pattern of CBV 600 and Zn-FAU has been processed to obtain the pair distance distribution function (**Figure 2.11 and 2.12**), from which the averages mesoparticles radius of the material was obtained.
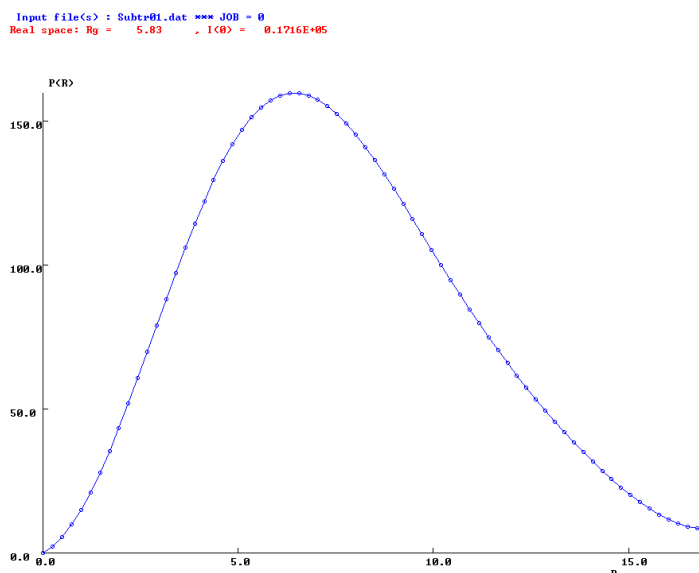
Figure 2.11: Pair distances distribution function of CBV 600
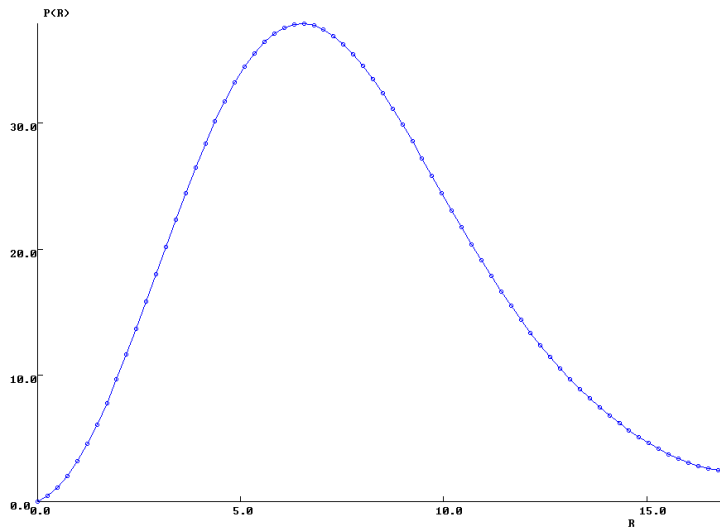
Figure 2.12: Pair distances distribution function of Zn-FAU

The average mesoparticle radius for CBV 600 and Zn-FAU are 5.83 nm and 5.81 nm respectively.

2.10 Reactor

The setup used for catalytic experiment is homemade and build on ¼ SS 316 tubing and Swagelok fitting, conceived to be operable at pressure varying from atmospheric to 2000 PSIG. The reactor oven allowed varying reaction temperature from room temperature to 1373 K. The reactor pressure limitation during DME carboxylation experiments was the pressure of the CO_2 cylinder. The pressure of the CO_2 cylinder was 600 PSIG and its associated mass flow controller required a minimal ΔP of 100 PSIG from the inlet to the outlet to remain in the specification domain for high accuracy. Consequently, the maximal reachable pressure during DME carboxylation was 500 PSIG. The setup pressure was manually controlled using a back pressure valve. The stream ID of the reactor is given in **figure 2.13**, with a physical picture in **figure 2.14**.
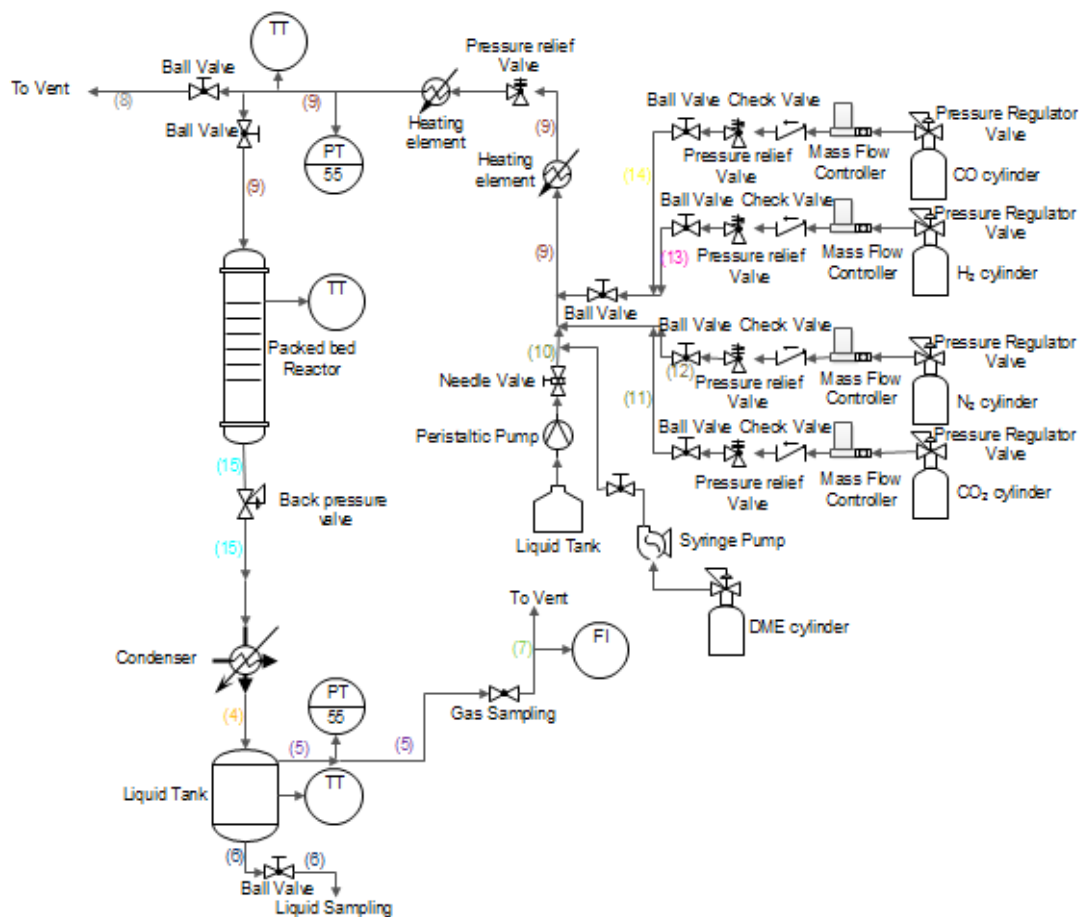
Figure 2.13: Stream ID of the flow reactor used for catalyst activity experiments

Figure 2.14: Gas flow reactor used for DME carboxylation and DMC decarboxylation

2.11 Decarboxylation and Carboxylation Reaction

The typical procedure for DMC decarboxylation experiments consisted to pre-heat the reactor inlet, outlet and catalyst containing area under a 1L•min^{-1} N2 flow. The inlet and outlet stream were heated to 398 K and the catalyst internal temperature was set to a desired temperature. Once the reactor temperature, pressure and flow were stabilized at the desired conditions, liquid DMC was added continuously at a rate of 0.02mL (liq)·min^{-1} using a diaphragm pump.

Dimethyl Ether carboxylation experiments has been carried out following a similar procedure as describe for DMC decarboxylation. 1.5L (gas) ·min^{-1} of CO_2 was used as vector gas during pre-reaction setup conditioning and liquid DME was added continuously from a high pressure tank using a high pressure syringe pump. The setup pressure was kept above the DME vapour pressure in the pump during each experiment for retaining DME properly in the pump piston chamber. Typically, the reactor inlet and outlet stream was heated to 398 K, the catalyst internal temperature at 313 K, while pressurizing the setup to 400 PSIG. Once   the setup was stabilized at the predefined conditions and under a CO_2 flow of 1.5L (gas) ·min^{-1}, Dimethyl Ether (0.372 mL·min^{-1}) was introduced in a ratio CO_2/DME of 10.

Catalyst temperature variations during experiments have been made by 5K increments. After condition modification, the reaction generally take 90 min to stabilise in the case of DMC decarboxylation and 180min in the case of DME carboxylation. The reactor outlet composition was quantified using gas chromatography system, the *AGILENT 7820A*, equipped with a FID detector and a *DB624* column. GCMS, *AGILENT 7890A* equipped with *VL MSD triple axis* detector *5975C* and *DB624* column, was used for outlet stream composition analysis. GC-MS (ESI) DME fragments m/z obtained: 30, 31, 32, 42, 43, 44, 45, 46, 47, 48; reference: 30, 31, 32, 33, 42, 43, 44, 45, 46, 47, 48. DMC fragments m/z obtained: 31, 32, 33, 42, 43, 44, 45, 46, 59, 60, 61, 90; reference: 31, 32, 33, 42, 43, 44, 45, 46, 59, 60, 61, 62, 90.

REFERENCES

1.   Zhao, Y.; Truhlar, D., The M06 suite of density functionals for main group thermochemistry, thermochemical kinetics, noncovalent interactions, excited states, and transition elements: two new functionals and systematic testing of four M06-class functionals and 12 other functionals. *Theoretical Chemistry Accounts: Theory, Computation, and Modeling (Theoretica Chimica Acta)* **2008,** *120* (1), 215-241.

2.   Felice, V.; Tavares, A. C., Faujasite zeolites as solid electrolyte for low temperature fuel cells. *Solid State Ionics* **2011,** *194* (1), 53-61.

3. Dimethyl Carbonate decarboxylation: Structural resolution of the rate-determining step

Jean-Francois Lacroix [1], Armand Soldera [2] and Jean-Michel Lavoie [1*]*

[1]   J.F. Lacroix and Prof. Dr. J.M. Lavoie

Industrial Research Chair on Cellulosic Ethanol

[2]   Prof. Dr. A. Soldera

Molecular physical-chemistry laboratory

RÉSUMÉ

Notre groupe a récemment démontré que la décarboxylation du diméthyle carbonate (DMC) en diméthyle ether (DME) et CO_2 est un processus réversible. Cet équilibre chimique a été défini suivant l'hypothèse qu'il se produit de manière similaire à l'hydratation du CO_2 par l'enzyme anhydrase carbonique (*CA*). Cette hypothèse a été vérifiée en corrélant des calculs théoriques aux mesures expérimentales de décarboxylation du DMC à la surface du catalyseur faujasite échangé au zinc, ce qui a permis de résoudre la structure de l'état de transition entre le DMC et le DME. La structure chimique représentant notre modèle théorique utilisé pour les calculs est constituée d'une section de la structure DRX de la faujasite, composé de 54 atomes tétrahedral (54T), section qui sert de support à un site réactionnel composé de 6 atomes tétrahedral (6T). Ce modèle a été séparé en deux couches calculatoires; le site de réaction 6T traité en DFT et le reste du modèle traité de façon semi-empirique. Le modèle a été résolu au niveau théorique M06/6-31++g(d)/SBKJC_VDZ_ECP:PM6 en utilisant la méthode ONIOM. La réaction a été évaluée en fonction de mécanismes réactionnels comportant de une à trois structures de transition, de manière parallèle aux intermédiaires connus pour l'enzyme *CA*. Les mécanismes en une et deux étapes ont été corrélé aux mesures expérimentales et n'ont pas différé selon le mode de calcul 6-31g(d) et 6-31g(d,p). C'est en ajoutant de la diffusivité sur les orbitales *s* et *p*, avec les modèles de base 6-31++g(d) et 6-31+g(d,p) que les mécanismes en une et deux étapes ont été différentiés. Il en découle que la décarboxylation du DMC se produit en une seule étape, via la migration intramoléculaire d'un ion méthyllium. L'énergie d'activation expérimentale de la réaction est de $66.7 kJ \cdot mol^{-1}$, alors que l'énergie d'activation théorique du chemin réactionnel en une seule étape est de $68.7 kJ \cdot mol^{-1}$ tel qu'obtenue avec le set de base 6-31++g(d).

ABSTRACT

Our group has recently demonstrated that dimethyl carbonate (DMC) decarboxylation to dimethyl ether (DME) and carbon dioxide is a reversible process. This chemical equilibrium was defined following the hypothesis that the reactions are occurring via a reaction mechanism similar to the equilibrium found in the enzyme *Carbonic Anhydrase* (*CA*) which catalyzes CO_2 hydration. By correlating theoretical calculations to experimental measurements at the surface of a zinc exchanged faujasite catalyst, the reaction mechanism and rate limiting transition structure for DMC decarboxylation was elucidated. A computational model consisting of a faujasite 54T supercage cluster, was used as framework for the actual zinc-located 6T ring reaction site. The calculation cluster was separated in two layers, the reaction site which was treated in density functional theory (DFT) and the faujasite supercage backbone treated in molecular dynamics. The structures were resolved up to the M06/6-31++g(d)/SBKJC_VDZ_ECP:PM6 level of theory using the n-layered integrated molecular orbital and molecular mechanics (ONIOM) method. The reaction was evaluated to proceed from a 1 to 3 steps reaction coordinate scheme according to the known intermediates of the Carbonic Anhydrase reaction mechanism. The 2-step and concerted mechanism was found to correlate with the experimental measurement and appeared to be indistinguishable using the 6-31g(d) and 6-31g(d,p) basis set. It was by adding s and p diffusivity in the model, with the 6-31++g(d) and 6-31+g(d,p) basis that those two reaction schemes were differentiated, further allowing to state that DMC decarboxylation to DME and CO_2 is occurring via a surface-promoted intra molecular methyl transfer following a fully concerted mechanism. The experimental activation energy was found to be $66.7 kJ \cdot mol^{-1}$ and the computationally resolved rate limiting structure of the fully concerted reaction mechanism presented activation energy of $68.7 kJ \cdot mol^{-1}$ at the 6-31++g(d) theory level.

Keywords: Dimethyl Carbonate • Decarboxylation • Mechanism • Carbon Dioxide • DFT

3.1 Introduction

The current energetic consumption profile and land-use of our society generate an annual amount of CO_2 estimated to $3.5 \cdot 10^{11}$ tons, with approximately half of this emitted CO_2 taken up by combined land and ocean carbon reservoirs, consequently accumulating an important fraction in the atmosphere.[1-2] Even if the influence of this environmental disequilibrium by society is still under debate,[3] a general agreement on the necessity of reducing the green-house gas emissions was accepted and common efforts undertaken.[4] The utilization of CO_2 for the production of valuable chemicals via catalytic conversion is one of the most economically relevant ways to mitigate industrial release of this the green house gases.[5] Carbon dioxide catalytic conversion into value added products is globally pursued following three main reaction scheme: hydrogenation to formic acid or methanol, high temperature reforming with short alkanes and carbonates synthesis.[5-10] Carbon dioxide being the carbon form with the highest oxidation degree, its catalytic conversion requires a co-reactant with a low oxidation degree and therefore a high energy content.[11] Recently, we have demonstrated the existence of a chemical equilibrium where CO_2 is the cornerstone linking dimethyl carbonate and dimethyl ether (**Equation 3.1**), the later been industrially accessible from MeOH dehydration or directly from syngas using a modified version of the MeOH catalyst.[12-17] Depending on the origin of the feedstock used to produce MeOH and DME, a completely sustainable DMC production process can be developed in addition to CO_2 valorization.

(3.1)
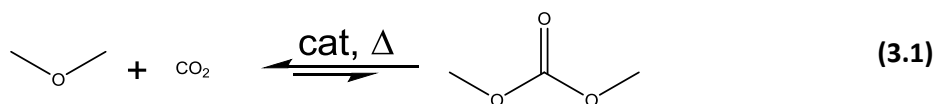
During the past twenty years, development of an efficient catalyst for DMC bulk production starting with methanol and CO_2 has been pursued given its economical interest as oxygenated fuel additive as well as for its potential as a green methylating agent.[18-20] However, catalyst development for MeOH carboxylation was found to be hindered not only by CO_2 kinetic inertia but also by water coproduction that showed to highly inhibit the reaction via equilibrium displacement towards reactants.[21-22] As a consequence, catalysts presented

short lifetime and low conversion.[23-25] It was found that *in-situ* removal of water using acetals and ortho esters significantly enhance reaction conversion, but this approach was not found to be economically viable. Dimethyl ether carboxylation and dimethyl carbonate decarboxylation was also recently found to be under equilibrium, as novel water free and CO_2 based synthetic route to dimethyl carbonate.

To further understand the equilibrium prevailing between DMC and DME, we carried out the computational resolution of dimethyl carbonate decarboxylation, with full correlation to experimental measurements. Using a continuous fixed bed reactor, dimethyl carbonate decarboxylation to DME and CO_2 was previously reported quantitatively at the surface of metal-exhanged zeolite.[26-27] Here we present our computational resolution of the reaction at the surface of the zinc-exchanged faujasite catalyst (Zn-FAU), which has been used to demonstrate the existence of the equilibrium between DMC and DME. Dimethyl carbonate decarboxylation was resolved according to the CO_2 hydration reaction mechanism that occurs in the active site of the enzyme *Carbonic Anhydrase* (**Figure 3.1a**). [28-30]
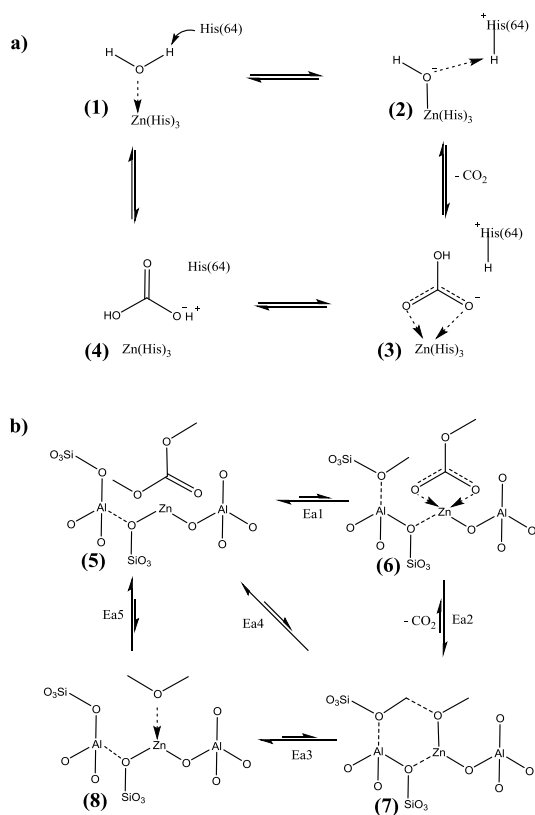
Figure 3.1 : a) CO$_2$ hydration mechanism in Carbonic Anhydrase active site b) evaluated reaction path for DMC decarboxylation in Zn-FAU

The first step of carbon dioxide hydration by the metallo-enzyme is the adsorption of a water molecule at the surface of the zinc center **(1)**, follow by proton transfer via a water molecules network to the proximal His64 buffer residue, resulting in a zinc hydroxide and protonated His64 intermediate **(2)**. This proton transfer step is believed to be the rate limiting step of CO_2 hydration by the enzyme and was the object of numerous studies on the *CA* active site reactivity.[30-35] The subsequent step is carbon dioxide insertion in the Zn-OH function, while His64 transfers the proton to the bulk solution. The resulting bicarbonate **(3)** is then displaced from the reaction site **(4)** by another water molecule, which re-initiates the catalytic cycle. Bicarbonate production from Carbonic Anhydrase is the fastest known reaction in which carbon dioxide is involved, the most active form of the metallo-protein having a turnover rate of $\sim 10^6 \cdot s^{-1}$.[36-37]

Surface methylation of H-zeolite under a DME gaseous flow, producing an intermediate such as **(7)** (**Figure 3.1b**), occur similarly to how water is activated by the metallo-enzyme. The methylated form of zeolite was previously characterized experimentally and its mechanism of formation resolved computationally.[38-40] This intermediate is a key in several zeolite promoted DME reactions such as DTO and carbonylation.[41-42] Dimethyl carbonate being recognized to be a better methylating agent than DME, formation of reaction intermediate **(6)** was anticipated to be found within the DMC decarboxylation mechanism.[43]

Dimethyl carbonate decarboxylation was consequently evaluated to occur either through a 1,2 or 3 step reaction coordinate scheme, involving similar reaction intermediates as known for the *Carbonic Anhydrase* mechanism. Initially, the thermodynamic study was carried out using a cost effective calculation method, which was further refined to gain accuracy between the theoretical model and the experimental measurements. At the light of this work, we obtain that with an optimized model, it is possible to estimate computationally and with good accuracy the amplitude of rate limiting barrier of reactions at the surface of metal exchanged zeolite catalysts.

3.2 Results and Discussion

3.2.1 Experimental results

The measured Dimethyl Carbonate conversion to Dimethyl Ether and CO_2 at the surface of Zn-FAU as function of temperature is given in **Figure 3.2a**, and the associated Arrhenius plot in **Figure 3.2b**. It is found that at the surface of zinc exchanged faujasite, DMC decarboxylation conversion increase from 2% at 328K to 12.5% at 355K. A reaction selectivity of 100% to DME and CO_2 remained constant in the screened temperature range, no side products were detected during the experiments. From the linear fit of the Arrhenius plot in the form of **Equation 3.2** (experimental section), we proved that DMC decarboxylation is a monomolecular first order reaction with apparent activation energy of 66.7kJ·mol^{-1}.
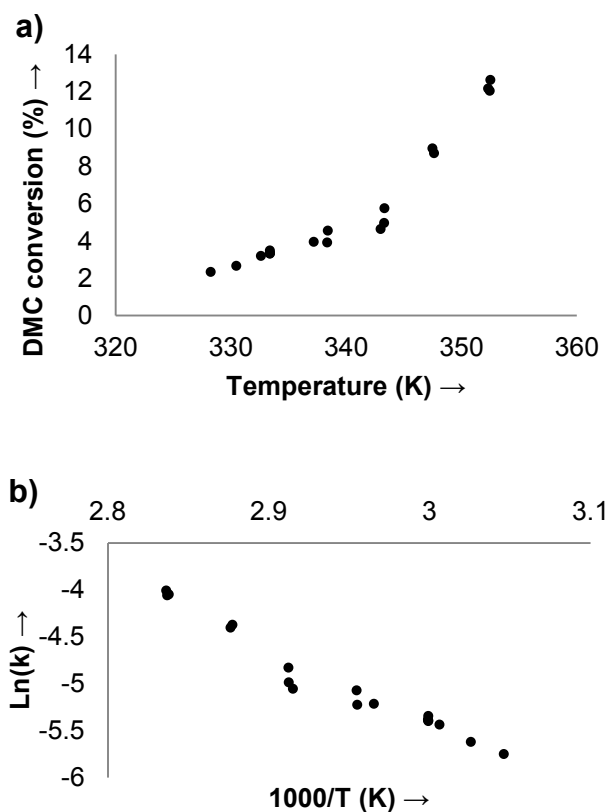
Figure 3.2 : a) Temperature effect on DMC decarboxylation to DME and CO_2 on Zn-FAU b) corresponding Arrhenius plot. Reaction conditions: 65g$_{cat}$(150 mL), 1L$_{(gas)}$·min^{-1} N$_2$ (GHSV=400h^{-1}), 0.02mL$_{(liq)}$·min^{-1} DMC (LHSV=0.008h^{-1}), 1 bar

The quasi-perfect linear fit of the reaction into an Arrhenius plot also shows that the reaction was under a kinetically controlled regime. Apparent activation energy in the magnitude order of 66.7kJ·mol^{-1} was previously reported for numerous zeolite-promoted reactions involving methylium transfer transition states, the typical energetic barrier for surface methylation/demethylation of zeolites at their proton nominal form being ~57.4kJ·mol^{-1}. The difference in apparent activation energy between DMC decarboxylation at the surface of Zn-FAU and surface methylation of protonated zeolites highlight the acid strength decrease between the Brønsted and Lewis acid form of the material.[44-48]

3.2.2 Computational reaction mechanism analysis

The elucidation of dimethyl carbonate decarboxylation rate limiting step at the surface of Zn-FAU was researched amongst the intermediates formation in accordance to the *Carbonic Anhydrase* reaction mechanism. The reaction was theoretically evaluated to proceed from a stepwise mechanism that involves three different transition structures, to a fully concerted mechanism where the transformation is occurring through a single transition structure. The reaction path which involves concerted reaction steps were obtained by the combination of single step of the stepwise mechanism. For clarity, **Figure 3.3-3.5** show transition states and intermediates structures only at the surface of the 6T ring site without the faujasite backbone. All structures were obtained and cut from the 54T calculations cluster given in **Figure 3.7** (computational details).

3.2.3 The stepwise mechanism

The stepwise mechanism **(Figure 3.3)**, which involves three transition structures and three intermediates, is the exact replicate of the *Carbonic Anhydrase* reaction mechanism. All three reaction paths evaluated through this work begin by the adsorption of a single Dimethyl Carbonate molecule **(5)** at the surface of the zinc located 6T ring reaction site.

Figure 3.3: Stepwise thermodynamic reaction scheme of dimethyl carbonate decarboxylation. Resolve computationally at the M06/6-31g(d), SBKJC VDZ theory level

Dimethyl Carbonate adsorption **(5)** energy is found to be -162.7kJ·mol^{-1}, after which follows a DMC demethylation/surface methylation step **(Ea1)**, affording a zinc bicarbonate/surface methyllium intermediate **(6.1)**. This intermediate energy is measured to be -81.4kJ·mol^{-1}, for a ΔE of 81.3kJ·mol^{-1} from the initial DMC adsorbate **(5)**. The intrinsic thermodynamic barrier associated to **Ea1** is 195.0kJ·mol^{-1}, with apparent activation energy of 32.3kJ·mol^{-1}. This low energetic barrier reflects the well known application of DMC as an environmentally friendly methylating agent: catalytic methylation reactions using DMC is known to be efficiently catalyzed at the surface of the sodium nominal form of the Faujasite material.[49-52] Intermediate **(6.1)** is highly similar to the *CA* Lindskog intermediate which results from CO$_2$ insertion in the zinc hydroxide group.[28] The following step is therefore a rearrangement of the Zinc bicarbonate group as known for the Lindskog intermediate, affording a more reactive species **(6.2)**. Several studies on the *Carbonic Anhydrase* active site mechanism have demonstrated that this rearrangement results from an equilibrium between two bicarbonate rotamers.[53] In the metalloenzyme pocket, the outward bicarbonate was

described to be 13.4-17.2kJ·mol^{-1} more stable than the inward bicarbonate.[54-55] The same trend is observed in the present case with a ΔE of 10.7kJ·mol^{-1} in favor of the outward bicarbonate. The bicarbonate rearrangement is followed by CO_2 release from the zinc bicarbonate function **(Ea2)** generating the zinc methoxide/surface methylated intermediate **(7)**. The intrinsic barrier for this step is found to be 78.6kJ·mol^{-1}, for apparent activation energy of 7.9kJ·mol^{-1}. The zinc bicarbonate intermediate **(6.2)** is 73.8kJ·mol^{-1} more stable than the zinc methoxide intermediate **(7)**, the later being thermodynamically unfavorable with energy of 3.1kJ·mol^{-1}. The low activation energy for CO_2 release/insertion and higher stability of the bicarbonate function versus the methoxide function is in agreement with the well known aptitude of zinc metal for carboxylation reaction, which involve CO_2 insertion in Zn-OR function.[56-59] The final step of the stepwise dimethyl carbonate decarboxylation mechanism is the zinc methoxide methylation by the adjacent zeolitic surface methyllium **(Ea3)**. This step is found to have an intrinsic energetic barrier of 124.8kJ·mol^{-1} and shows to be highly restricted by apparent activation energy of 127.9kJ·mol^{-1}. Comparatively, at the surface of the zeolite ZSM-5 at its proton nominal form, the apparent activation energy of a similar step was experimentally measured to be 76.5kJ·mol^{-1}. The thermodynamic difference between H-ZSM-5 and Zn-FAU for a reaction step which involves a surface methyllium transfer from an activated oxygen toward a methoxide function is attributed to the surface mobility difference between a Zn(II) and an H$^+$ species. The resulting adsorbed DME and CO_2 complex **(8.1)** is the most stable structure of the entire reaction scheme, with adsorption energy of -170.9kJ·mol^{-1}.

The overall thermodynamic rate-determining step of dimethyl carbonate decarboxylation through a fully stepwise mechanism is the methyllium transfer **(Ea3)** between the zeolite surface and the zinc methoxide group. With apparent activation energy of 127.9kJ·mol^{-1} for the Zn-OMe methylation step, it shows that dimethyl carbonate decarboxylation is very unlikely to proceed through a fully stepwise reaction path. Even if DMC demethylation and CO_2 release steps were found to occur with lower energetic barrier than the experimental apparent activation energy of 66.7kJ·mol^{-1}, formation of a zinc-methoxide/surface methylated intermediate is unrealistic.

3.2.4 The half concerted mechanism

The half concerted dimethyl carbonate decarboxylation mechanism **(Figure 3.4)**, was obtained by combining the carbon dioxide released step **(Ea2)** and the zinc methoxide methylation **(Ea3)** step previously described in the fully stepwise reaction scheme.
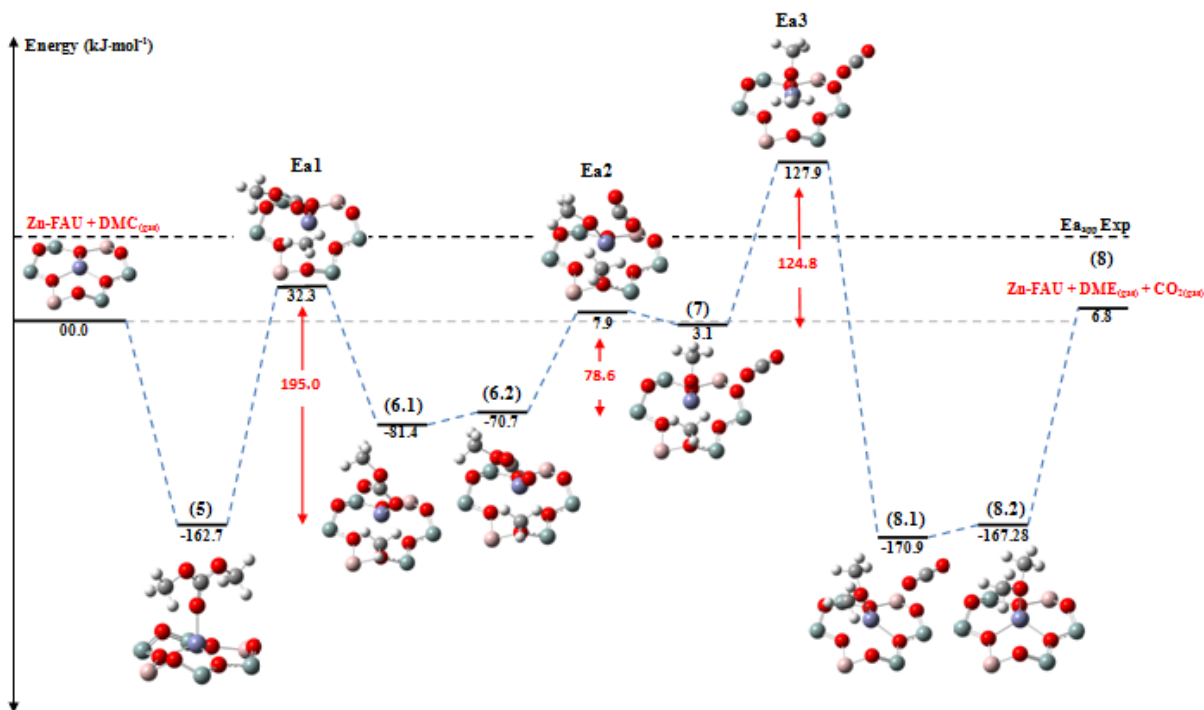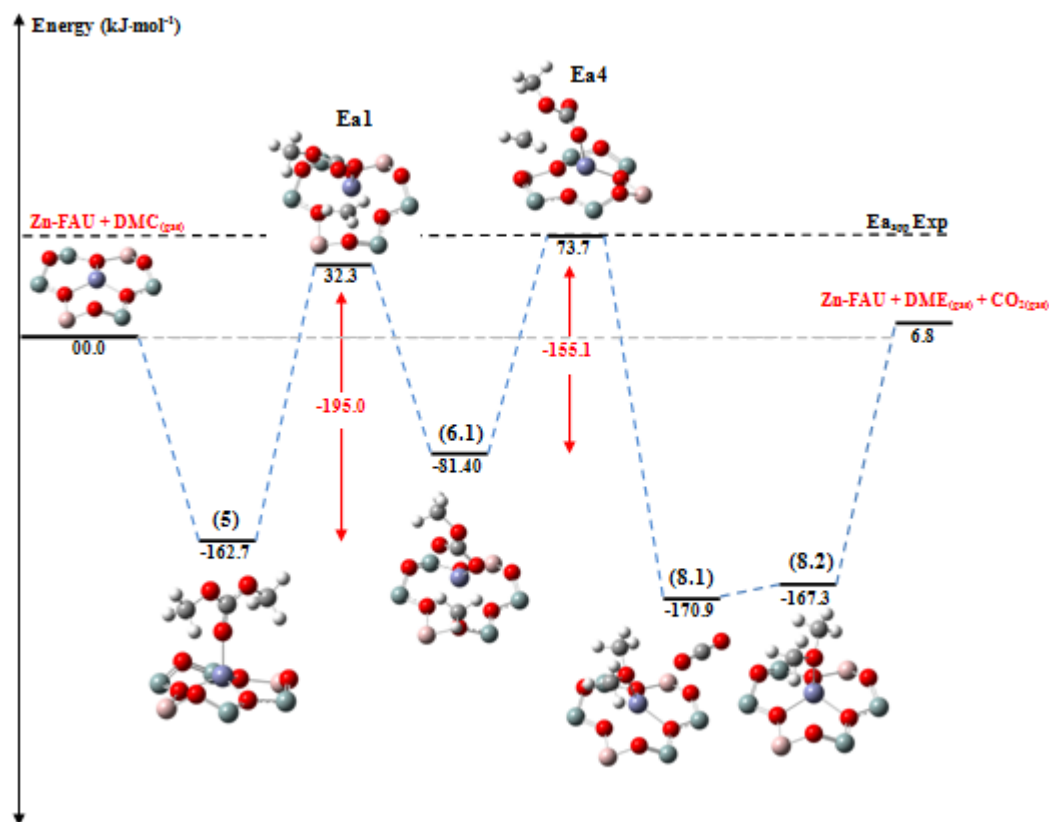

Figure 3.4: Half concerted thermodynamic reaction scheme of dimethyl carbonate decarboxylation. Resolve computationally at the M06/6-31g(d),SBKJC VDZ theory level.

Starting from adsorbed DMC **(5)**, follows the DMC demethylation/zeolite methylation step **(Ea1)** to afford the zinc bicarbonate/methylated faujasite intermediate **(6.1)** with apparent activation energy of 32.3kJ·mol^{-1}, a non-limiting step that would be undetectable experimentally through a kinetic and thermodynamic analysis. The subsequent step is the bicarbonate methylation step **(Ea4)**, in a similar fashion to the reverse of **(Ea1)**, the difference

being that the methylium transfer occurs between activated oxygen at the surface and the bicarbonate methoxide oxygen, rather than the initial carboxylate oxygen. This step results into the concerted CO_2 release and DME formation starting from the zinc bicarbonate and methylated faujasite intermediate. Following this reaction path, an important energetic barrier decrease is obtained for the methyllium transfer step **(Ea4)** that lead to DME and CO_2, compared to **(Ea3)** of the stepwise mechanism. The intrinsic transition barrier of **(Ea4)** is 155.1kJ·mol^{-1}, with apparent activation energy of 73.7kJ·mol^{-1}. The energetic difference between methoxide and bicarbonate methylation is attributed to the higher stability of the bicarbonate intermediate **(6.1)** compared to the methoxide intermediate **(7)**, as well as to a higher movement freedom degree of the bicarbonate function, which allowed accommodating a methyllium transfer structure in a more favorable geometrical arrangement. The limiting energetic barrier of the half-concerted reaction mechanism therefore is the bicarbonate methylation step **(Ea4)** with apparent activation energy of 73.7kJ·mol^{-1}. This transition structure is thus found to relate with the experimentally measured activation energy of 66.7kJ·mol^{-1} and will consequently be further considered as the potential reaction rate-determining transition structure for DMC decarboxylation.

3.2.5 The concerted mechanism

The dimethyl carbonate decarboxylation concerted mechanism which contains a single transition structure **(Ea5)** results from the combination the DMC demethylation/zeolite surface methylation **(Ea1)** with the zinc methoxide methylation steps **(Ea3) (Figure 3.5)**.
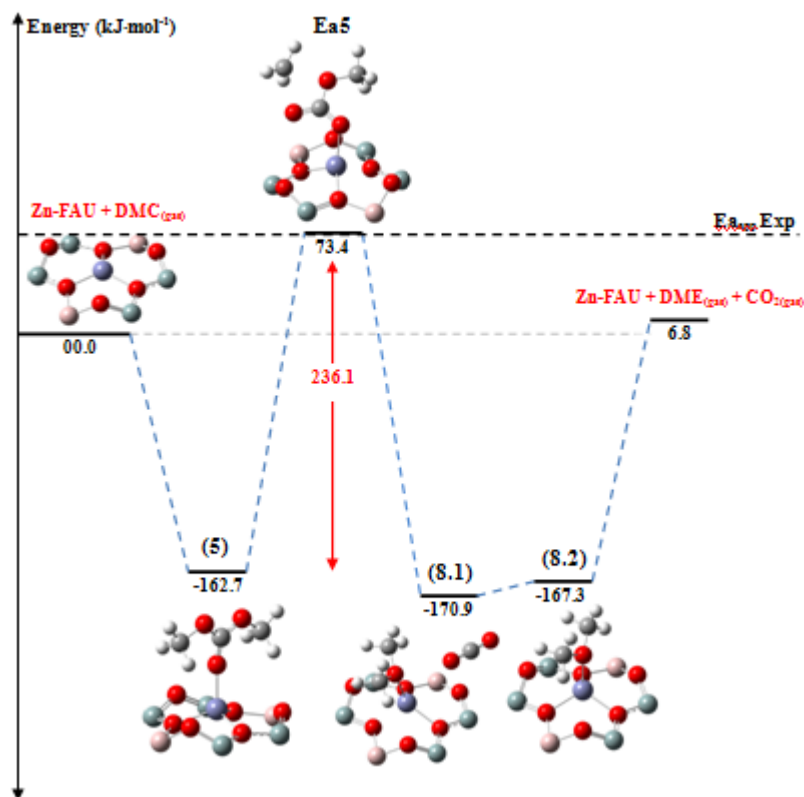
Figure 3.5: Concerted thermodynamic reaction scheme of dimethyl carbonate decarboxylation. Resolve computationally at the M06/6-31g(d),SBKJC VDZ theory level

Starting from adsorbed DMC **(5)**, the transition structure is initiated by the interaction of a DMC methyl group with activated oxygen at the catalytic surface, in the same manner as for the DMC demethylation step **(Ea1)**. In the case of the stepwise and half concerted mechanism, this initial interaction resulted in a transiting methyllium species between a carboxylate oxygen and activated oxygen of the support. In the actual mechanism, the adjacent DMC methoxide function is brought in closer proximity to this transiting methylium species, causing a deflection of the vibration mode towards the adjacent methoxide rather than towards activated oxygen of the faujasite support. The resulting concerted transition structure **(Ea5)** therefore involves a migrating methyllium species that is stabilized by a carboxylate, methoxide and activated oxygen, with a transition motion between the carboxylate and methoxide oxygen. This transition structure allows direct DMC decarboxylation to DME and CO_2 in a single step without formation of intermediates involving the faujasite framework.

The intrinsic energetic barrier associated with this transition structure is 236.1kJ·mol^{-1}, with apparent activation energy of 73.4kJ·mol^{-1}. The theoretical energetic barrier of the concerted DMC decarboxylation mechanism is thus also found to also correlate with the experimental activation energy of 66.7kJ·mol^{-1}, consequently making the concerted DMC decarboxylation reaction path to be another potential structure of the reaction rate-determining step.

3.2.6 Basis set effect on model accuracy

In order to differentiate both potential rate-limiting transition structure obtained from fast structure screening using the 6-31g(d) basis set, **(Ea4)** and **(Ea5)** was reevaluated using basis set with higher polarization and diffusion in the ONIOM high layer. The effect of basis set diffusivity and polarization on the energetic barrier associated to **(Ea4)** and **(Ea5)** is summarized in **Table 3.1**.

Table 3.1: Non-metal ONIOM high layer basis set influence on model accuracy		
Basis set	Ea4 (kJ·mol^{-1})	Ea5 (kJ·mol^{-1})
6-31g(d)	73.7	73.4
6-31g(d,p)	71,0	70,9
6-31+g(d,p)	77,6	71,1
6-31++g(d)	79,2	68,7
Experimental	66,7	

It is found that the half-concerted and concerted mechanism which was thermodynamically quasi-identical with the 6-31g(d) basis set are clearly differentiated by adding diffusivity on the s and p function. The two mechanism were readily separated from each other by the 6-31+g(d,p) basis set which add s and p diffusivity on the atoms other than hydrogen's in the high layer. Expansion of the diffusivity to the hydrogen atoms with the 6-31++g(d) basis set afforded the most accurate model with theoretical apparent activation energy of 68.7kJ·mol^{-1} for the concerted mechanism and 79.2kJ·mol^{-1} for the half concerted mechanism. On the other hand, the addition of polarization in the system was found to have

negligible influence on model accuracy and did not allow differentiating the theoretical reaction scheme in which **(Ea4)** and **(Ea5)** are the rate limiting structures. Even if the 6-31g(d,p) basis set allowed obtaining data with slightly increase correlation with the experimental measurements, it did not showed to be better suited than 6-31g(d) for the differentiation of highly similar reaction path at the surface of metal exchanged zeolite system. Quasi identical energetic barrier of 71.0kJ·mol^{-1} and 70.9kJ·mol^{-1} was obtained with the 6-31g(d,p) basis set for the half-concerted and concerted mechanism respectively. The 6-31g(d) basis set was therefore used efficiently for cost effective analysis of the rate-determining step of DMC decarboxylation, but further refinement of the model with heavier basis set was required to resolve the reaction with high theoretical accuracy. By adding polarization and diffusion function to the high layer basis set, wider van der waals interactions were considered on the reactive species, interactions to which theoretical accuracy is found to be directly related.

3.2.7 Reaction rate limiting step analysis

The basis set refined model allowed distinguishing two quasi-identical thermodynamic reaction paths previously obtained with the 6-31g(d) basis set, affording the structure of the DMC decarboxylation rate limiting step (**Figure 3.6**). The transition state consists of a migrating methyllium species stabilized by a methoxy and carboxylate oxygen located at 2.2Å and 2.3Å respectively, as well as by Si-O framework oxygens situated at 3.3Å from the transiting group. The vibration frequency at 393.4cm^{-1} associated to the reaction progression clearly shows the CO_2 and DME formation. In parallel to the methyllium transfer from the carboxylate towards the methoxy oxygen, the bicarbonate C-O bond breaking and methoxy-methyllium bond forming related to dimethyl ether formation is evidenced. The vibration motions also involve CO_2 release, marked by the carbonyl unfolding motion.
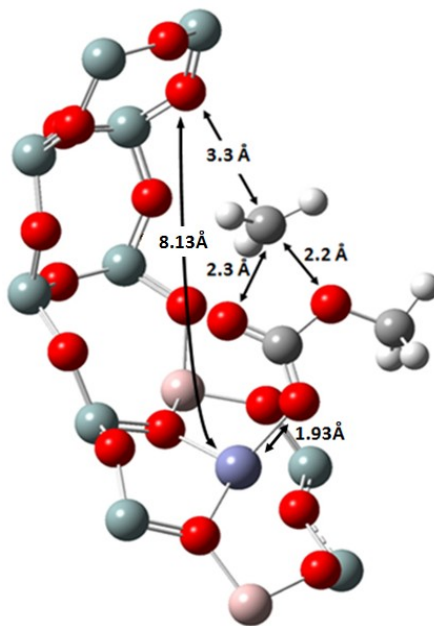
Figure 3.6: Reaction limiting transition structure of Dimethyl Carbonate decarboxylation at the surface of Zn-FAU

From the transition state structure, we can observe that the reaction is initiated from the DMC cis-trans conformer. Consequently, the DMC trans-trans conformer adsorbate has to rearrange into its cis-trans conformer via rotation of a methoxy group in order to reach its reactive conformation.[60] The interactions of DMC carboxylate oxygen with the acidic zinc center and trans methyl σ* with framework oxygen results in an important polarization and weakening of the trans methoxy C-O bond. The transition state is found to occur within a volume radius in the magnitude order of 4Å without any observable significance of the surface location of the metal. The framework oxygen which is found to interact closely in the transition state interestingly belongs to the silica backbone rather than being aluminum activated oxygen. The reaction site oxygen which bear the highest electron densities are the ones in coordination with the aluminum atoms, but these are not found to play any role in the reaction other than allowing electron delocalization and stabilizing the zinc metal. Catalytic site geometry is therefore found to be as important as its electronic strength.

3.3   Conclusions

In summary, the structure of dimethyl carbonate decarboxylation rate limiting step was fully resolved through correlation of experimental measurements and theoretical calculations. The reaction was evaluated according to the water hydration *Carbonic Anhydrase* reaction mechanism, from a stepwise to a fully concerted mechanism. DMC decarboxylation rate-determining step was effectively resolved amongst formation of intermediates and transition structures similar to the one describe in the CO_2 hydration mechanism by the metalloenzyme. From a fast structure screening using the 6-31g(d) basis set, we obtained two highly similar reaction schemes which correlated to experimental measurements: the half concerted mechanism involving the formation of a methylated faujasite intermediate and the concerted mechanism which lead directly to DME and CO_2 in a single step. Both of these reaction schemes showed a theoretical thermodynamic limiting barrier in the magnitude order of $73 kJ \cdot mol^{-1}$ using the 6-31g(d) basis set, while the stepwise mechanism was found to uncorrelated to experimental measurements with a theoretical apparent activation energy of $128.0 kJ \cdot mol^{-1}$. It is found that at the surface of Zn-FAU, transition structure and intermediates concerning DME only are unfavorable compare to the structures in which CO_2 is involve.

It was by increasing diffusivity of the non metal ONIOM high layer basis set that the concerted and half concerted mechanisms were differentiated. On another hand, polarization increase in the basis set was found to be a negligible calculation factor compared to diffusion when resolving theoretically reactions at the surface metal exchanged zeolite. Amongst the basis set which has been used, it is the 6-31++g(d) which allowed obtaining the best theoretical accuracy and efficiently allowed differentiating the concerted and half concerted reaction mechanism, with activation energy of $68.7 kJ \cdot mol^{-1}$ and $79.2 kJ \cdot mol^{-1}$ respectively. The refined calculation model with increased basis set diffusivity and van der waals interactions dispersion is therefore found to be highly effective at resolving theoretically the rate-determining structure of catalytic reactions in zeolites. In addition, the lighter 6-31g(d) basis set was proved to be efficient at identifying rapidly relevant structures, with acceptable accuracy.

From the structure of the rate limiting step of DMC decarboxylation, we showed that reaction site geometry is as important as its electronic strength. DMC decarboxylation initiation is found to require both an acid and base component, placed in an appropriate geometry within a reaction site radius of 4Å. The surface coordinating sphere of the metal which possess the highest electronic density is found to be uninvolved in the reaction. As the reaction is found to proceed without formation of intermediates in which the metal and faujasite framework are involves, further study on the influence of metal nature on this system will provide highly valuable information on the DME/DMC equilibrium.

3.4 Experimental Section

3.4.1 Catalyst synthesis and experimental measurements

Zn-FAU was synthesized from CBV 600 (H-FAU) with Si/Al of 2.74 available from *Zeolyst international* and $Zn(NO_3)_2 \cdot 6H_2O$, purchased from *Sigma Aldrich*. Zinc loading in Faujasite has been carried out using the incipient wetness method, followed by a drying step at 105**°**C and calcinations at 450**°**C under a 1L·min^{-1} air flow.[61] H-FAU was exchanged with Zn(II) at its near full capacity, with a final Zn/Al ratio of 0.48. Thermodynamic and kinetic analyses of DMC decarboxylation were carried out using a homemade gas flow reactor loaded with 65g of catalyst. The average particle size of the material was between 1.4 and 2.5 mm, avoiding preferential gas flow paths in the catalytic bed. The reaction was diluted with nitrogen and the conversion was maintained below 12% in order to remain in the kinetic linearity domain of the reaction.[47] The reactor outlet composition was quantified using the gas chromatography system AGILENT *7820A* equipped with a FID detector and a *DB624* column. An *AGILENT 7890A* GCMS equipped with the *VL MSD triple axis* detector *5975C* and *DB624* column was used for outlet stream characterization. A detailed description of catalyst synthesis, characterization and reaction setup was reported in our previous report.

The experimental kinetic resolution of DMC decarboxylation was carried out by varying temperature at constant flow and reactants catalyst contact time. The reaction rate constant was calculated following the Arrhenius first order **Equation (3.2)** for gas flow packed bed

reactor, where *[DMC]in* and *[DMC]out* are DMC concentration in the reactor inlet and outlet stream and *t* is the gas flow catalyst contact time.

$$ln\left(\frac{[DMC]_{in}}{[DMC]_{out}}\right) = kt \qquad\qquad (3.2)$$

Reaction activation energy was consequently defined from the slope of the resulting Arrhenius function.

3.4.2 Computational method

The 54T faujasite supercage cluster used for theoretical calculations is given in **Figure 3.7**. The cluster structure was cut from the faujasite crystal structure at its nominal proton form and the outer silicon boundary atoms valence was completed to neutral by the addition of hydrogen, oriented in the Si-O crystal structure directions and with bond length of 1.47Å. The 6T ring reaction site was artificially reconstituted by substitution of two opposite silicon atoms from the crystal structure by aluminum atoms, the resulting site valence was neutralized by the addition of a Zn(II) atom.

The cluster was separated in two layers using the ONIOM scheme as depicted in **Figure 3.7**. The reaction site consisting of 5 Si and 2 Al atoms represented as ball and stick was treated in DFT using the M06 functional and was fully allowed to relax during optimization. The basis set SBKJC VDZ ECD was specifically assigned to the zinc atom, while 6-31g(d) type basis set was used for the Al, Si, O, C and H atoms completing the DFT layer. The second layer, presented as wireframe, was frozen and treated with the semi-empirical PM6 method.

The M06 DFT basis set was built by Zhao & Truhlar with the purpose of estimating accurately long range dispersion interactions in large clusters.[62] The combination of semi-empirical and M06 DFT calculation methods using the ONIOM scheme was previously reported to be highly accurate compared to experimental results for situations involving catalytic reactions at the surface of zeolite materials.[40, 63-64] The addition of transition metals in the model however significantly increases computational cost and complexity in the mathematical model, as the overall model involve a calculation method that allows two DFT

basis sets to superpose within the same layer, in addition to the information transfer between the QM/MM boundary layer. The 6-31g(d) type and SBKJC VDZ ECP basis set superposition in the m06 functional and its hybridization with the semi empirical PM6 method was found to proceed very smoothly, allowing direct and clean convergence of micro-iteration optimization.[65]
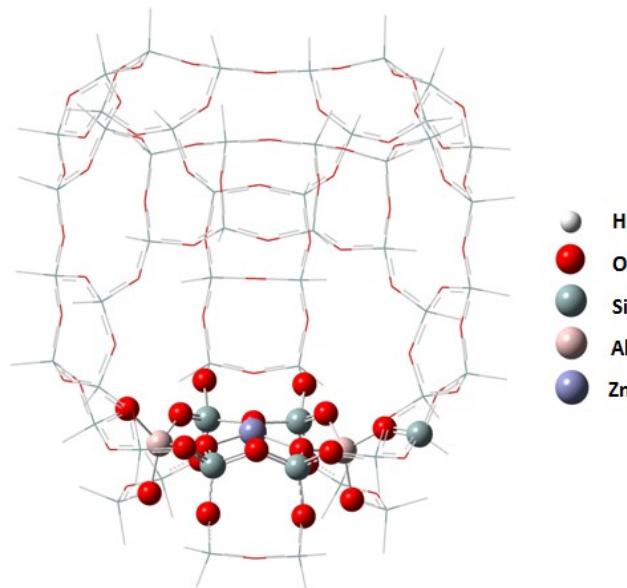
Figure 3.7: Faujasite 54T supercage cluster

Structure optimization and identification of the reaction rate limiting step were carried out using the ONIOM(M06/6-31g(d), SBKJC VDZ ECP:PM6) calculation method in the *Gaussian 09* package. Geometries optimization convergence criteria were set at a quadratic mean deviation of 0,026kJ·mol^{-1} with maximal optimization step size of 10 radians. Orbital symmetry of the final wave function was held from one iteration to the next and kept unconstrained. The validity of each structure was confirmed from a vibrational analysis, all reaction intermediates describe in this work have no negative imaginary frequencies and transition states have only one negative imaginary frequency in accordance to the reaction under evaluation. Vibrational analysis was carried out from frequency calculations using the same calculation method as for geometry optimization. Final structure energies were refined by full DFT single point of the ONIOM optimized structure using M06/6-31g(d), SBKJC VDZ ECP command line. Following the resolution of the rate-limiting barrier, the model accuracy was improved by using basis set with increase polarization and diffusion for the Al, Si, C, O and H atoms of the DFT layer.

REFERENCES

1. Ballantyne, A. P.; Alden, C. B.; Miller, J. B.; Tans, P. P.; White, J. W. C., Increase in observed net carbon dioxide uptake by land and oceans during the past 50 years. *Nature* **2012,** *488* (7409), 70-72.

2. Schimel, D. S.; House, J. I.; Hibbard, K. A.; Bousquet, P.; Ciais, P.; Peylin, P.; Braswell, B. H.; Apps, M. J.; Baker, D.; Bondeau, A.; Canadell, J.; Churkina, G.; Cramer, W.; Denning, A. S.; Field, C. B.; Friedlingstein, P.; Goodale, C.; Heimann, M.; Houghton, R. A.; Melillo, J. M.; Moore, B.; Murdiyarso, D.; Noble, I.; Pacala, S. W.; Prentice, I. C.; Raupach, M. R.; Rayner, P. J.; Scholes, R. J.; Steffen, W. L.; Wirth, C., Recent patterns and mechanisms of carbon exchange by terrestrial ecosystems. *Nature* **2001,** *414* (6860), 169-172.

3. Sheffield, J.; Wood, E. F.; Roderick, M. L., Little change in global drought over the past 60 years. *Nature* **2012,** *491* (7424), 435-438.

4. UNFCC, Communication Received from Parties in Relation to the Listing in the Chapeau of the Copenhagen Accord. 2010 ed.; UNFCC: http://unfccc.int/meetings/cop_15/copenhagen_accord/items/5276.php.

5. Mikkelsen, M.; Jorgensen, M.; Krebs, F. C., The teraton challenge. A review of fixation and transformation of carbon dioxide. *Energy & Environmental Science* **2010,** *3* (1), 43-81.

6. Li, L.; Zhao, N.; Wei, W.; Sun, Y., A review of research progress on CO_2 capture, storage, and utilization in Chinese Academy of Sciences. *Fuel* **2013,** *108* (0), 112-130.

7. Quadrelli, E. A.; Centi, G.; Duplan, J.-L.; Perathoner, S., Carbon Dioxide Recycling: Emerging Large-Scale Technologies with Industrial Potential. *ChemSusChem* **2011,** *4* (9), 1194-1215.

8. Amouroux, J.; Siffert, P., Carbon dioxide: a raw material and a future chemical fuel for a sustainable energy industry. *IOP Conference Series: Materials Science and Engineering* **2011,** *19* (1), 012001.

9.	Budzianowski, W. M., Negative carbon intensity of renewable energy technologies involving biomass or carbon dioxide as inputs. *Renewable and Sustainable Energy Reviews* **2012,** *16* (9), 6507-6521.

10.	Razali, N. A. M.; Lee, K. T.; Bhatia, S.; Mohamed, A. R., Heterogeneous catalysts for production of chemicals using carbon dioxide as raw material: A review. *Renewable and Sustainable Energy Reviews* **2012,** *16* (7), 4951-4964.

11.	Sakakura, T.; Choi, J.-C.; Yasuda, H., Transformation of Carbon Dioxide. *Chemical Reviews* **2007,** *107* (6), 2365-2387.

12.	Moradi, G. R.; Nazari, M.; Yaripour, F., Statistical analysis of the performance of a bi-functional catalyst under operating conditions of LPDME process. *Chemical Engineering Journal* **2008,** *140* (1–3), 255-263.

13.	Hassanpour, S.; Taghizadeh, M.; Yaripour, F., Preparation, Characterization, and Activity Evaluation of H-ZSM-5 Catalysts in Vapor-Phase Methanol Dehydration to Dimethyl Ether. *Industrial & Engineering Chemistry Research* **2010,** *49* (9), 4063-4069.

14.	Liu, D.; Yao, C.; Zhang, J.; Fang, D.; Chen, D., Catalytic dehydration of methanol to dimethyl ether over modified γ-Al2O3 catalyst. *Fuel* **2011,** *90* (5), 1738-1742.

15.	Hosseininejad, S.; Afacan, A.; Hayes, R. E., Catalytic and kinetic study of methanol dehydration to dimethyl ether. *Chemical Engineering Research and Design* **2012,** *90* (6), 825-833.

16.	Mao, D.; Xia, J.; Zhang, B.; Lu, G., Highly efficient synthesis of dimethyl ether from syngas over the admixed catalyst of CuO–ZnO–Al2O3 and antimony oxide modified HZSM-5 zeolite. *Energy Conversion and Management* **2010,** *51* (6), 1134-1139.

17.	Kang, S.-H.; Bae, J. W.; Kim, H.-S.; Dhar, G. M.; Jun, K.-W., Enhanced Catalytic Performance for Dimethyl Ether Synthesis from Syngas with the Addition of Zr or Ga on a Cu−ZnO−Al2O3/γ-Al2O3 Bifunctional Catalyst. *Energy & Fuels* **2010,** *24* (2), 804-810.

18.	Wen, L.-b.; Xin, C.-Y.; Yang, S.-C., The effect of adding dimethyl carbonate (DMC) and ethanol to unleaded gasoline on exhaust emission. *Applied Energy* **2010,** *87* (1), 115-121.

19.	Rounce, P.; Tsolakis, A.; Leung, P.; York, A. P. E., A Comparison of Diesel and Biodiesel Emissions Using Dimethyl Carbonate as an Oxygenated Additive. *Energy & Fuels* **2010,** *24* (9), 4812-4819.

20.	Pacheco, M. A.; Marshall, C. L., Review of Dimethyl Carbonate (DMC) Manufacture and Its Characteristics as a Fuel Additive. *Energy & Fuels* **1997,** *11* (1), 2-29.

21.	Eta, V.; Ma□ki-Arvela, P. i.; Leino, A.-R.; Kordás, K. n.; Salmi, T.; Murzin, D. Y.; Mikkola, J.-P., Synthesis of Dimethyl Carbonate from Methanol and Carbon Dioxide: Circumventing Thermodynamic Limitations. *Industrial & Engineering Chemistry Research* **2010,** *49* (20), 9609-9617.

22.   Bustamante, F.; Orrego, A. F.; Villegas, S.; Villa, A. L., Modeling of Chemical Equilibrium and Gas Phase Behavior for the Direct Synthesis of Dimethyl Carbonate from CO_2 and Methanol. *Industrial & Engineering Chemistry Research* **2012,** *51* (26), 8945-8956.

23.   Sakakura, T.; Kohno, K., The synthesis of organic carbonates from carbon dioxide. *Chemical Communications* **2009,** *0* (11), 1312-1330.

24.   Keller, N.; Rebmann, G.; Keller, V., Catalysts, mechanisms and industrial processes for the dimethylcarbonate synthesis. *Journal of Molecular Catalysis A: Chemical* **2010,** *317* (1–2), 1-18.

25.   Dai, W.-L.; Luo, S.-L.; Yin, S.-F.; Au, C.-T., The direct transformation of carbon dioxide to organic carbonates over heterogeneous catalysts. *Applied Catalysis A: General* **2009,** *366* (1), 2-12.

26.   Fu, Y.; Zhu, H.; Shen, J., Thermal decomposition of dimethoxymethane and dimethyl carbonate catalyzed by solid acids and bases. *Thermochimica Acta* **2005,** *434* (1–2), 88-92.

27.   Selva, M.; Fabris, M.; Perosa, A., Decarboxylation of dialkyl carbonates to dialkyl ethers over alkali metal-exchanged faujasites. *Green Chemistry* **2011,** *13* (4), 863-872.

28.   Bottoni, A.; Lanza, C. Z.; Miscione, G. P.; Spinelli, D., New Model for a Theoretical Density Functional Theory Investigation of the Mechanism of the Carbonic Anhydrase: How Does the Internal Bicarbonate Rearrangement Occur? *Journal of the American Chemical Society* **2004,** *126* (5), 1542-1550.

29.   Lipton, A. S.; Heck, R. W.; Ellis, P. D., Zinc Solid-State NMR Spectroscopy of Human Carbonic Anhydrase: Implications for the Enzymatic Mechanism. *Journal of the American Chemical Society* **2004,** *126* (14), 4735-4739.

30.   Maupin, C. M.; McKenna, R.; Silverman, D. N.; Voth, G. A., Elucidation of the Proton Transport Mechanism in Human Carbonic Anhydrase II. *Journal of the American Chemical Society* **2009,** *131* (22), 7598-7608.

31.   Domsic, J. F.; Williams, W.; Fisher, S. Z.; Tu, C.; Agbandje-McKenna, M.; Silverman, D. N.; McKenna, R., Structural and Kinetic Study of the Extended Active Site for Proton Transfer in Human Carbonic Anhydrase II. *Biochemistry* **2010,** *49* (30), 6394-6399.

32.   Lesnichin, S. B.; Shenderovich, I. G.; Muljati, T.; Silverman, D.; Limbach, H.-H., Intrinsic Proton-Donating Power of Zinc-Bound Water in a Carbonic Anhydrase Active Site Model Estimated by NMR. *Journal of the American Chemical Society* **2011,** *133* (29), 11331-11338.

33.   Mikulski, R.; West, D.; Sippel, K. H.; Avvaru, B. S.; Aggarwal, M.; Tu, C.; McKenna, R.; Silverman, D. N., Water Networks in Fast Proton Transfer during Catalysis by Human Carbonic Anhydrase II. *Biochemistry* **2012,** *52* (1), 125-131.

34.   Riccardi, D.; Konig, P.; Guo, H.; Cui, Q., Proton Transfer in Carbonic Anhydrase Is Controlled by Electrostatics Rather than the Orientation of the Acceptor†. *Biochemistry* **2008,** *47* (8), 2369-2378.

35.   Silverman, D. N.; McKenna, R., Solvent-Mediated Proton Transfer in Catalysis by Carbonic Anhydrase. *Accounts of Chemical Research* **2007,** *40* (8), 669-675.

36.   Pocker, Y.; Janjic, N., Molecularity of water in enzymic catalysis. Application to carbonic anhydrase II. *Journal of the American Chemical Society* **1989,** *111* (2), 731-733.

37.   Toba, S.; Colombo, G.; Merz, K. M., Solvent Dynamics and Mechanism of Proton Transfer in Human Carbonic Anhydrase II. *Journal of the American Chemical Society* **1999,** *121* (10), 2290-2302.

38.   Wang, W.; Seiler, M.; Hunger, M., Role of Surface Methoxy Species in the Conversion of Methanol to Dimethyl Ether on Acidic Zeolites Investigated by in Situ Stopped-Flow MAS NMR Spectroscopy. *The Journal of Physical Chemistry B* **2001,** *105* (50), 12553-12558.

39.   Wang, W.; Buchholz, A.; Seiler, M.; Hunger, M., Evidence for an Initiation of the Methanol-to-Olefin Process by Reactive Surface Methoxy Groups on Acidic Zeolite Catalysts. *Journal of the American Chemical Society* **2003,** *125* (49), 15260-15267.

40.   Namuangruk, S.; Meeprasert, J.; Khemthong, P.; Faungnawakij, K., A Combined Experimental and Theoretical Study on the Hydrolysis of Dimethyl Ether over H-ZSM-5. *The Journal of Physical Chemistry C* **2011,** *115* (23), 11649-11656.

41.   Boronat, M.; Martínez-Sánchez, C.; Law, D.; Corma, A., Enzyme-like Specificity in Zeolites: A Unique Site Position in Mordenite for Selective Carbonylation of Methanol and Dimethyl Ether with CO. *Journal of the American Chemical Society* **2008,** *130* (48), 16316-16323.

42.   Yamazaki, H.; Shima, H.; Imai, H.; Yokoi, T.; Tatsumi, T.; Kondo, J. N., Direct Production of Propene from Methoxy Species and Dimethyl Ether over H-ZSM-5. *The Journal of Physical Chemistry C* **2012,** *116* (45), 24091-24097.

43.   Gooden, P. N.; Bourne, R. A.; Parrott, A. J.; Bevinakatti, H. S.; Irvine, D. J.; Poliakoff, M., Continuous Acid-Catalyzed Methylations in Supercritical Carbon Dioxide: Comparison of Methanol, Dimethyl Ether and Dimethyl Carbonate as Methylating Agents. *Organic Process Research & Development* **2010,** *14* (2), 411-416.

44.   Van der Mynsbrugge, J.; Visur, M.; Olsbye, U.; Beato, P.; Bjørgen, M.; Van Speybroeck, V.; Svelle, S., Methylation of benzene by methanol: Single-site kinetics over H-ZSM-5 and H-beta zeolite catalysts. *Journal of Catalysis* **2012,** *292* (0), 201-212.

45.   Van Speybroeck, V.; Van der Mynsbrugge, J.; Vandichel, M.; Hemelsoet, K.; Lesthaeghe, D.; Ghysels, A.; Marin, G. B.; Waroquier, M., First Principle Kinetic Studies of Zeolite-Catalyzed Methylation Reactions. *Journal of the American Chemical Society* **2010,** *133* (4), 888-899.

46.   Kumar, P.; Thybaut, J. W.; Svelle, S.; Olsbye, U.; Marin, G. B., Single-Event Microkinetics for Methanol to Olefins on H-ZSM-5. *Industrial & Engineering Chemistry Research* **2012,** *52* (4), 1491-1507.

47.   Hill, I. M.; Hashimi, S. A.; Bhan, A., Kinetics and mechanism of olefin methylation reactions on zeolites. *Journal of Catalysis* **2012,** *285* (1), 115-123.

48.   Lesthaeghe, D.; Horré, A.; Waroquier, M.; Marin, G. B.; Van Speybroeck, V., Theoretical Insights on Methylbenzene Side-Chain Growth in ZSM-5 Zeolites for Methanol-to-Olefin Conversion. *Chemistry – A European Journal* **2009,** *15* (41), 10803-10808.

49.   Tundo, P.; Selva, M., The Chemistry of Dimethyl Carbonate. *Accounts of Chemical Research* **2002,** *35* (9), 706-716.

50.   Bonino, F.; Damin, A.; Bordiga, S.; Selva, M.; Tundo, P.; Zecchina, A., Dimethyl Carbonate in the Supercages of NaY Zeolite: The Role of Local Fields in Promoting Methylation and Carboxymethylation Activity. *Angewandte Chemie* **2005,** *117* (30), 4852-4855.

51.   Selva, M.; Tundo, P.; Perosa, A., Reaction of Functionalized Anilines with Dimethyl Carbonate over NaY Faujasite. 3. Chemoselectivity toward Mono-N-methylation. *The Journal of Organic Chemistry* **2003,** *68* (19), 7374-7378.

52.   Bonino, F.; Damin, A.; Bordiga, S.; Selva, M.; Tundo, P.; Zecchina, A., Dimethyl Carbonate in the Supercages of NaY Zeolite: The Role of Local Fields in Promoting Methylation and Carboxymethylation Activity. *Angewandte Chemie International Edition* **2005,** *44* (30), 4774-4777.

53.   Sattler, W.; Parkin, G., Structural characterization of zinc bicarbonate compounds relevant to the mechanism of action of carbonic anhydrase. *Chemical Science* **2012,** *3* (6), 2015-2019.

54.   Mikulski, R. L.; Silverman, D. N., Proton transfer in catalysis and the role of proton shuttles in carbonic anhydrase. *Biochimica et Biophysica Acta (BBA) - Proteins and Proteomics* **2010,** *1804* (2), 422-426.

55.   Zheng, Y. J.; Merz, K. M., Mechanism of the human carbonic anhydrase II-catalyzed hydration of carbon dioxide. *Journal of the American Chemical Society* **1992,** *114* (26), 10498-10507.

56.   Cokoja, M.; Bruckmeier, C.; Rieger, B.; Herrmann, W. A.; Kühn, F. E., Transformation of Carbon Dioxide with Homogeneous Transition-Metal Catalysts: A Molecular Solution to a Global Challenge? *Angewandte Chemie International Edition* **2011,** *50* (37), 8510-8537.

57.   Correa, A.; Martín, R. n., Palladium-Catalyzed Direct Carboxylation of Aryl Bromides with Carbon Dioxide. *Journal of the American Chemical Society* **2009,** *131* (44), 15974-15975.

58.   Kobayashi, K.; Kondo, Y., Transition-Metal-Free Carboxylation of Organozinc Reagents Using CO2 in DMF Solvent. *Organic Letters* **2009,** *11* (9), 2035-2037.

59.   Cokoja, M.; Bruckmeier, C.; Rieger, B.; Herrmann, W. A.; Kühn, F. E., Umwandlung von Kohlendioxid mit Übergangsmetall-Homogenkatalysatoren: eine molekulare Lösung für ein globales Problem? *Angewandte Chemie* **2011,** *123* (37), 8662-8690.

60.   Reddy, S. K.; Balasubramanian, S., Liquid Dimethyl Carbonate: A Quantum Chemical and Molecular Dynamics Study. *The Journal of Physical Chemistry B* **2012,** *116* (51), 14892-14902.

61.   Kazansky, V. B.; Serykh, A. I., Unusual localization of zinc cations in MFI zeolites modified by different ways of preparation. *Physical Chemistry Chemical Physics* **2004,** *6* (13), 3760-3764.

62.   Zhao, Y.; Truhlar, D., The M06 suite of density functionals for main group thermochemistry, thermochemical kinetics, noncovalent interactions, excited states, and transition elements: two new functionals and systematic testing of four M06-class functionals and 12 other functionals. *Theoretical Chemistry Accounts: Theory, Computation, and Modeling (Theoretica Chimica Acta)* **2008,** *120* (1), 215-241.

63.   Boekfa, B.; Choomwattana, S.; Khongpracha, P.; Limtrakul, J., Effects of the Zeolite Framework on the Adsorptions and Hydrogen-Exchange Reactions of Unsaturated Aliphatic, Aromatic, and Heterocyclic Compounds in ZSM-5 Zeolite: A Combination of Perturbation Theory (MP2) and a Newly Developed Density Functional Theory (M06-2X) in ONIOM Scheme. *Langmuir* **2009,** *25* (22), 12990-12999.

64.   Maihom, T.; Pantu, P.; Tachakritikul, C.; Probst, M.; Limtrakul, J., Effect of the Zeolite Nanocavity on the Reaction Mechanism of n-Hexane Cracking: A Density Functional Theory Study. *The Journal of Physical Chemistry C* **2010,** *114* (17), 7850-7856.

65.   Vreven, T.; Morokuma, K.; Farkas, Ö.; Schlegel, H. B.; Frisch, M. J., Geometry optimization with QM/MM, ONIOM, and other combined methods. I. Microiterations and constraints. *Journal of Computational Chemistry* **2003,** *24* (6), 760-76

# 4.	Insight into metal exchanged faujasite catalytic site properties that favor DME carboxylation over DMC decarboxylation

Jean-Francois Lacroix[1], Armand Soldera[2] and Jean-Michel Lavoie[1]*

[1] J.F. Lacroix, Prof. Dr. J.M. Lavoie

Chaire de recherche industrielle sur l'éthanol cellulosique

[2] Prof. Dr. A. Soldera

Laboratoire de chimie physique moléculaire

RÉSUMÉ

L'activité relative de la faujasite échangée avec Zn(II), Cd(II), Hg(II), Sn(II) et Na$^+$ pour la décarboxylation du DMC et la carboxylation du DME a été évaluée en utilisant des calculs théoriques DFT. La structure chimique correspondant au modèle de calcul théorique utilisé est constituée d'une section de la structure DRX de la faujasite, composé de 54 atomes tétraédrique (54T) utilisés comme plateforme pour le site réactionnel qui contient 6 atomes tétraédrique (6T). Le modèle de calcul a été séparé en deux couches, le site de réaction 6T traité en DFT et le reste du modèle traité avec une méthode semi-empirique. Les structures ont été résolues jusqu'au niveau théorique M06/6-31g(d)/SBKJC_VDZ_ECP:PM6 en utilisant la méthode de calcul ONIOM. L'activité relative de la faujasite contenant les différents métaux pour la décarboxylation du DMC et la carboxylation du DME a été obtenue en estimant la constante d'équilibre, considérant les deux réactions comme ayant la même étape limitante. Il a été montré lors de cette étude qu'au sein de la série de catalyseur évaluée, seule Na-FAU a le potentiel de favoriser la carboxylation du DME par rapport à la décarboxylation du DMC. Les constantes de vitesse théoriques de Na-FAU sont cependant très faibles. Cd-FAU à présenté les constantes de vitesse les plus élevées tant pour l'insertion que pour le rejet du CO_2, alors que Sn et Hg-FAU ont présenté un potentiel réactionnel inférieur à Zn-FAU, structures antérieurement comparées aux mesures expérimental. L'analyse de la géométrie, des charges et des orbitales des réactions à la surface des différents sites ont permis d'observer des tendances et d'établir les paramètres clés des sites réactionnels qui permettent de favoriser la carboxylation du DME par rapport à la décarboxylation du DMC.

ABSTRACT

The relative activity of Zn(II), Cd(II), Hg(II), Sn(II) and Na$^+$ exchanged faujasite towards DMC decarboxylation and DME carboxylation was evaluated using Density Functional Theory (DFT). The theoretical model consists of a faujasite 54T supercage cluster, used as framework for the actual metal located 6T ring reaction site. The calculation cluster was separated in two layers, the reaction site which was treated in DFT and the faujasite supercage backbone treated in molecular dynamics. Structures were resolved at the M06/6-31g(d)/SBKJC_VDZ_ECP:PM6 level of theory using the n-layered integrated molecular orbital and molecular mechanics (ONIOM) method. The relative activity of the metal exchanged faujasite catalyst towards DMC decarboxylation and DME carboxylation was obtained from calculation of the equilibrium constant, considering both reactions to be rate limited by the same transition structure. It is found through this study that only Na-FAU shows the potential to favor DME carboxylation over DMC decarboxylation. Cd-FAU presented the highest reaction rate constant for both CO_2 insertion and release while Sn and Hg-FAU presented lower activity than the zinc exchanged faujasite structure; model previously correlated with experimental measurements. The reactivity difference between the different reaction sites was rationalized through geometrical, electron density and orbital's analysis, affording the key active site and reactants complexes properties that favor DME carboxylation over DMC decarboxylation.

KEY WORDS: Dimethyl carbonate · Dimethyl ether · CO_2 · zeolite · Catalysis · DFT

4.1 INTRODUCTION

Dimethyl carbonate (DMC) has received important consideration due to its potential utilization as oxygenated fuel additive, as well as a green methylating agent in replacement to phosgene which is still industrially massively utilized.[2-4] Efforts toward direct DMC synthesis from methanol and CO_2 have been pursued, having water as sole co-products.[1, 5-7] However, development of Methanol carboxylation was found to be under equilibrium control with reaction conversion being highly restricted by the co-produce water.[8-10] To overcome this issue, in-situ water removal using dehydrating agent such as acetals, orthoester and organocyanide was studied and found to successfully increase reaction conversion.[11-15] However, even if reaction conversion was improved by the addition of dehydrating agent, catalysts reaction rate remained very low and yet, no dehydrating agents have found industrial application. In our previous work which consisted to thermodynamically and kinetically resolved DMC decarboxylation to dimethyl ether (DME) and CO_2 at the surface of a zinc-exchanged faujasite catalyst, we found that this reaction is reversible (**Equation 4.1**). As for methanol carboxylation, dimethyl ether carboxylation appeared to be under equilibrium with low DME conversion to DMC. Further interest were then given to this chemical equilibrium, DFT calculation coupled with experimental measurements were applied for resolving the reaction mechanism of DMC decarboxylation.

$$ \text{(4.1)} $$
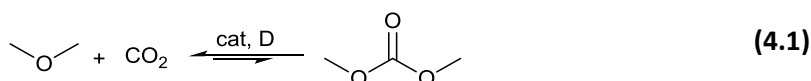
Here we present results relative to the application of the calculation method developed previously during the mechanistical analysis to computational catalyst screening. The aim of this work is to highlights catalytic sites properties which favors DME carboxylation over DMC decarboxylation. In a first instance, the thermodynamic and kinetic profile of the reactions at the surface of Zn(II), Cd(II), Hg(II), Sn(II) and Na$^+$ exchanged faujasite 6T ring site were investigated. Na$^+$, Zn(II), Cd(II) and Hg(II) interacts with reactants via an empty *3s*, *4s*,*5s* and *6s* empty orbital respectively, while Sn(II) adsorbs reactants in an empty *5p* orbital. Subsequent geometrical, electron density and orbitals analysis of the reaction sites, intermediates and transition structure allow defining the nature of the interactions between reactants and catalytic surface that favors equilibrium displacement toward DMC.

Specifically, the influence of metals size and charge density, while maintaining the orbital structure, was evaluated by comparing Na^+, Zn(II), Cd(II) and Hg(II), which all coordinate reactants in an empty *s* orbital. Further analysis of Sn(II) exchanged faujasite allows comparing reaction profile when carried out at the surface of a *s* or *p* empty orbital. The reaction coordinate and active site analysis were carried out comparatively with the zinc-exchanged faujasite model, which was previously correlated with experimental measurements.

4.2 Computational method

4.2.1 Calculation cluster, functional and basis set

The 54T faujasite supercage cluster used for calculations is given in **Figure 4.1**. The cluster structure was cut from the faujasite crystal structure at its nominal proton form and the outer silicon boundary atoms valence was completed to neutral by the addition of hydrogen oriented in the Si-O crystal structure directions, with bond length of 1.47Å. The 6T ring reaction site was artificially reconstituted by substitution of two opposite silicon atoms from the crystal lattice by aluminum atoms and the resulting site valence was completed to neutral by the addition of a divalent metal atom. In the case of Na-FAU, only one silicon atom of the 6T ring site was replaced by an aluminum atom.
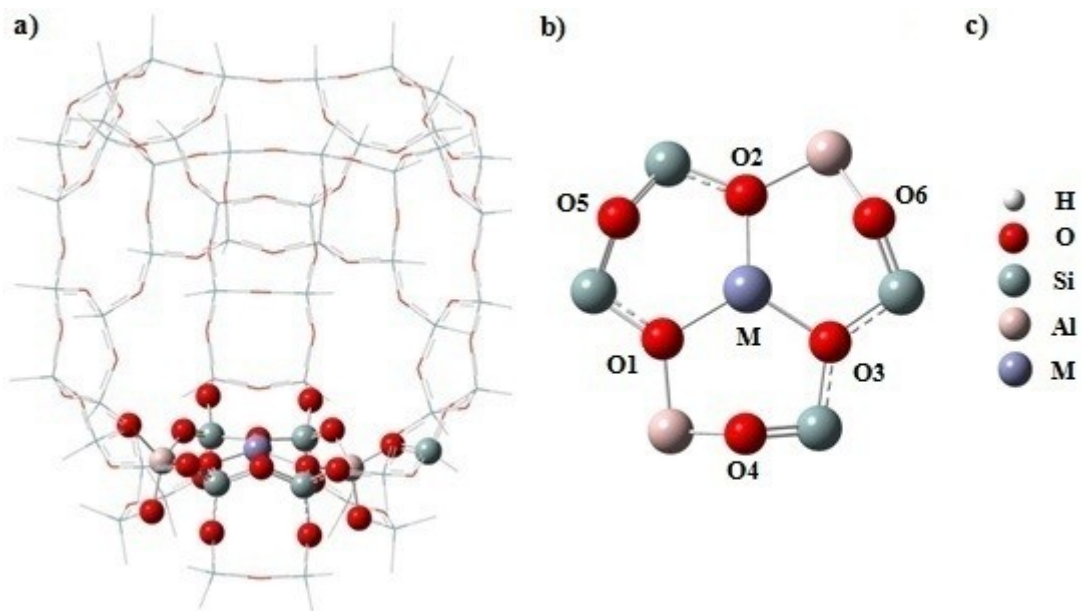
Figure 4.1: a) Metal exchanged faujasite supercage calculation cluster b) 6T ring site cut from calculation cluster c) atom color code

The cluster was separated in two layers using the ONIOM scheme as depicted in **Figure 4.1a**. The reaction site consisting of 5 Si and 2 Al atoms represented as ball and stick was treated in DFT using the M06 functional and was fully allowed to relax during optimization. The basis set SBKJC VDZ ECD was specifically assigned to the metal atoms, while 6-31g(d) basis set was applied to the Al, Si, O, C and H atoms, completing the DFT layer. The second layer, presented as wireframe, was frozen and treated with the semi-empirical PM6 method.

The M06 DFT functional was built by Zhao & Truhlar with the purpose of estimating accurately long range dispersion interactions in large clusters.[16] The combination of semi-empirical and M06 DFT calculation methods using the ONIOM scheme was previously reported to be highly accurate compared to experimental results for situations involving catalytic reactions at the surface of zeolite materials.[17-21] The addition of transition metals in the model however significantly increases computational cost and complexity in the mathematical model, as the overall cluster require a calculation method that allows two DFT basis sets to superpose within the high layer, in addition to the information transfer between the QM/MM boundary layer. The 6-31g(d) and SBKJC VDZ ECP basis set superposition in the M06 functional and its hybridization with the semi empirical PM6 method was found to proceed very smoothly, allowing direct and clean convergence of micro-iteration optimization.

4.2.2 Structure optimization

Structure optimization were carried out using the ONIOM(M06/6-31g(d), SBKJC VDZ ECP:PM6) calculation method in the *Gaussian 09* package. Geometries optimization convergence criteria were set at a quadratic mean deviation of 0.026kJ·mol^{-1} with maximal optimization step size of 10 radians. Orbital symmetry of the final wave function was held from one iteration to the next and kept unconstrained. The validity of each structure was confirmed from a vibrational analysis, all reaction intermediates described in this work have no negative imaginary frequencies and transition states have only one negative imaginary frequency, in accordance to the reaction under evaluation. Vibrational analysis was carried out from frequency calculations using the same calculation method as for geometry optimization. Final structure energies were refined by full DFT single point of the ONIOM optimized structure using M06/6-31g(d), SBKJC VDZ ECP command line.

4.2.3 Kinetic analysis

The kinetic analysis was carried out using the *Transition State Theory* (TST). (**Equation 4.2**) The reactions rate constants pre-exponential factor was estimated from the quotient of the partition function of the transition state and reactants, while the apparent activation energy was defined from the reaction coordinates.[22-24]

$$k = \frac{k_b T Q_{TS}}{h Q_{Re}} \cdot e^{\left(\frac{-Ea_{app}}{RT}\right)} \qquad (4.2)$$

In Equation 2, k_b, h and R are the *Boltzmann*, *Planck* and universal gas constant respectively. The first vibrational level was used as the zero point energy for calculating the partition function (Q) and the apparent activation energy is the zero point vibrational energy (ZPVE) energy difference between the highest energetic point of the reaction coordinates and the summation of reactants and catalytic surface at gas phase. The relative activity of the five metal exchanged faujasite structures toward DMC decarboxylation and DME carboxylation was then obtained through the expression of their equilibrium constant at 50°C and under 1 atm.

4.3 Results and discussion

4.3.1 Thermodynamic and kinetic analysis

Previous experimental-computational work which consisted to resolve DMC decarboxylation reaction mechanism at the surface of the zinc exchanged faujasite 6T ring site showed that the reaction proceed through a fully concerted reaction path. The conversion of DMC into DME and CO_2 was found to results from two main interactions. First, the polarization and weakening of DMC C-O σ bond induce by metal coordination and second, the interaction of the DMC trans methyl inflated LUMO with the HOMO of β,γ oxygens from an aluminum atom. The rate limiting structure which results from this mode of activation is a methyl transfer that occurs between carboxylate and methoxy oxygen of DMC, producing DME and CO_2 in a single step. The acidic metal center being at the origin of the primary interactions that promote the reaction, the influence of metal nature on the reaction thermodynamic and kinetic profile is here described.

The reaction coordinates of DMC decarboxylation/DME carboxylation at the surface of Na^+, Zn(II), Cd(II), Hg(II) and Sn(II) exchanged faujasite are shown in **Figure 4.2**. The energetic barrier amplitude of the reactions remained highly similar at the surface of the *IIB* metal exchanged faujasite (Zn-FAU, Cd-FAU and Hg-FAU). The computerized apparent activation energy is 73.4kJ·mol^{-1} at the surface of Zn-FAU, 66.9kJ·mol^{-1} at the surface of Hg-FAU and 64.0kJ·mol^{-1} at the surface of Cd-FAU. Those activation energies were calculated using the energies summation of M-FAU and DMC at gaseous state as the zero point of energy. The corresponding intrinsic reactions energetic barrier from DMC to DME and CO_2 is 236.2kJ·mol^{-1}, 212.1kJ·mol^{-1} and 201.0kJ·mol^{-1} at the surface of Zn, Cd and Hg exchanged faujasite respectively, while still in the same order, the intrinsic barrier for DME carboxylation is 244.3kJ·mol^{-1}, 250.1kJ·mol^{-1} and 236.9kJ·mol^{-1}. It is Cd-FAU that presents the lowest apparent activation energy, Hg-FAU which shows the lowest intrinsinc energetic barrier and Zn-FAU which have the most similar barrier amplitude for the forward and reverse reaction. It is Zn-FAU that presents the best affinity for DMC and Cd-FAU for DME and CO_2, with respective adsorption energy of -162.7kJ·mol^{-1} and -186.1kJ·mol^{-1}. Among the *IIB* series, Hg-FAU is the structure which has the lowest affinity with reactants on both side of the

equilibrium. It is due to this lower affinity toward reactants that Hg-FAU presents the tightest energetic profile.

Sn-FAU which interacts with reactants via an empty *5p* orbital and Na-FAU which coordinate via the *3s* orbital showed a reaction profile with important differences compare the *IIB* series. First, the apparent activation energy is 186.8kJ·mol^{-1} and 293.9kJ·mol^{-1} at the surface of Sn-FAU and Na-FAU respectively. DMC decarboxylation/DME carboxylation is thus significantly less thermodynamically favorable at the surface of Na^{+} and Sn(II) than at the surface of Zn(II), Cd(II) and Hg(II) exchanged faujasite. In addition, the affinity between reactants and Na and Sn-FAU is less favorable compare to the *IIB* series, as depicted in **Figure 4.2**. The energetic scheme also is significantly widen in the case of Na-FAU, with an energetic span of 412.0kJ·mol^{-1}. At the surface of Sn-FAU, the energetic barrier amplitude of 267.4kJ·mol^{-1} is in the same magnitude order than obtained with the *IIB* series, but with a less spontaneous profile as the entire reaction scheme is shift upward in the energy diagram. From the evaluated metal exchanged faujasite series, it is Sn-FAU which is found to adsorb reactants the most weakly with adsorption energy of -76.5kJ·mol^{-1} for DMC and -80.5kJ·mol^{-1} for DME and CO_2. DME and CO_2 consistently showed a higher adsorption exotherm than DMC at the surface of all five sites, indicating that at equal's desorption rate, catalyst surface will be DME and CO_2 rich.
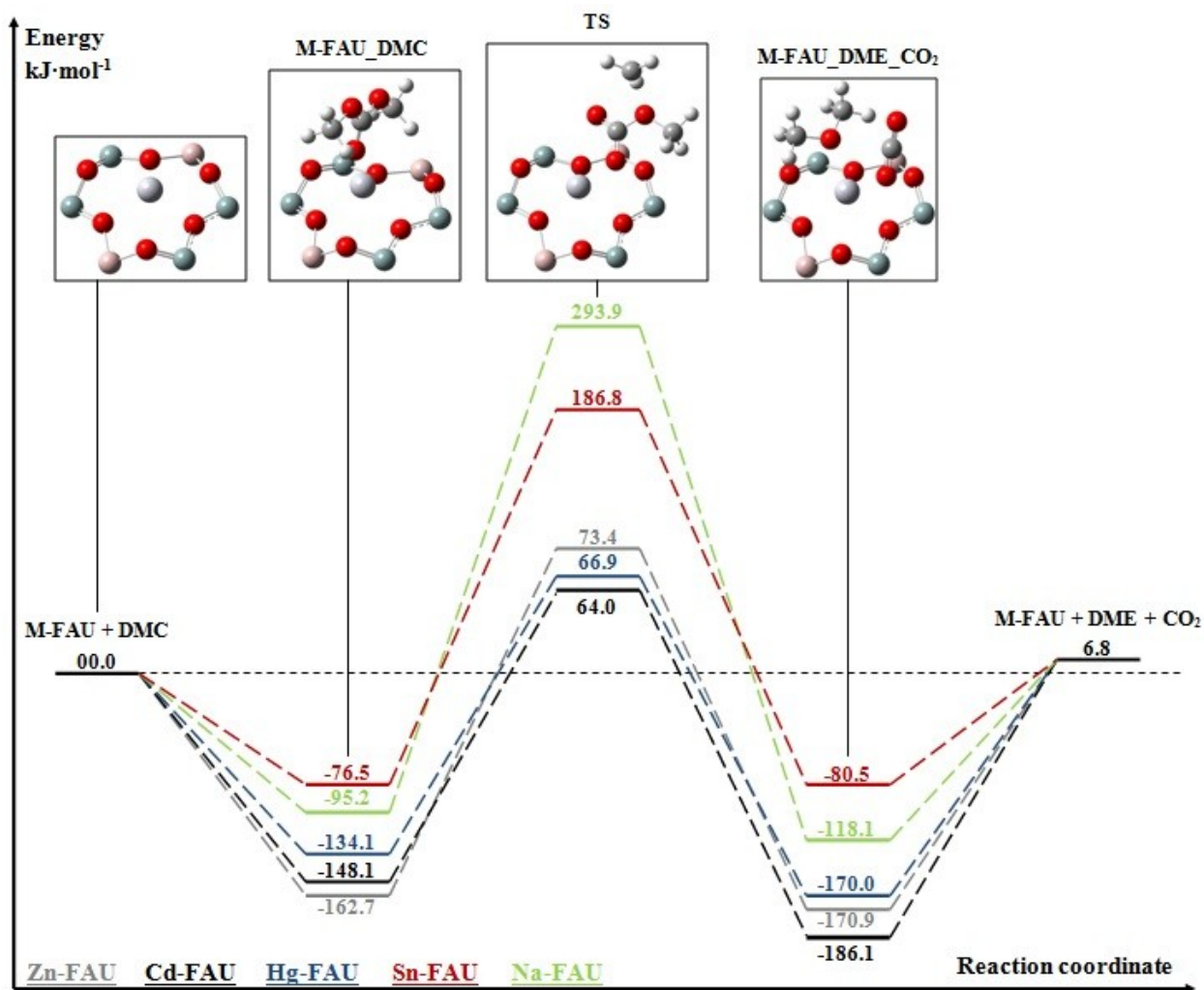
Figure 4.2: Thermodynamic profile of the DMC/DME equilibrium at the surface of the metal exchanged faujasite catalyst. Calculated using the M06(6-31g(d):SBKJC VDZ/PM6) method.

The computational kinetic analysis of DMC decarboxylation/DME carboxylation is summarized in **Table 4.1**, according to the transition state theory (**Equation 4.2**). The temperature at which DMC decarboxylation was experimentally observed to become favorable over DME carboxylation being in the magnitude order of 50°C at the surface of Zn-FAU, the kinetic analysis was carried out at this temperature.

Table 4.1: Computed rate constant, pre-exponential factor, activation energy and equilibrium constant for DMC decarboxylation and DME carboxylation[1]

Catalyst	DMC decarboxylation			DME Carboxylation			k_{DMC}/k_{DME}
	A (s^{-1})	Ea (kJ·mol^{-1})	k_{DMC} (s^{-1})	A (s^{-1})	Ea (kJ·mol^{-1})	k_{DME} (s^{-1})	
Na-FAU	$1.74 \cdot 10^{12}$	293.9	$5.17 \cdot 10^{-36}$	$3.31 \cdot 10^{12}$	293.9	$9.86 \cdot 10^{-36}$	0.5
Zn-FAU	$2.17 \cdot 10^{12}$	73.4	2.89	$1.27 \cdot 10^{12}$	73.4	2.33	1.2
Cd-FAU	$2.35 \cdot 10^{12}$	64.0	104	$1.54 \cdot 10^{12}$	64.0	68.4	1.5
Hg-FAU	$2.73 \cdot 10^{11}$	66.9	4.19	$3.01 \cdot 10^{12}$	66.9	1.76	2.4
Sn-FAU	$3.62 \cdot 10^{12}$	186.4	$2.20 \cdot 10^{-18}$	$1.99 \cdot 10^{11}$	186.4	$1.21 \cdot 10^{-19}$	18.2

[1] Kinetics parameters were computed for reaction conditions of 50°C and 1atm

The kinetic analysis show that among the five metal exchanged faujasite structures, only Na-FAU can promote favorably DME carboxylation over DMC decarboxylation with theoretical equilibrium constant ratio of 0.5. From the *IIB* series, DME carboxylation appeared to be more favorable at the surface of Zn-FAU, followed by Cd-FAU and Hg-FAU which show the higher equilibrium constant of the series with 2.4. From the metals that adsorb reactants in an empty *s* orbital, it is observed that decreasing metal size is favorable to DME carboxylation. On the other hand, Sn-FAU which interacts with reactants via an empty *5p* orbital present very low reaction rate constant and potential to promote DME carboxylation with equilibrium constant of 18.2. The *5p^0* coordination sphere of Sn-FAU is thus found to be less favorable to catalyze DMC decarboxylation/DME carboxylation compare to the other structures. It is interesting that when comparing catalytic site with similar orbital structure, high activation energy between DMC and DME tend to be favorable to DMC formation. Such result indicates that DME carboxylation is more likely to be under kinetic than thermodynamic control and consequently, reactants mode of adsorption and subsequent activation is a more determining factor than the energetic barrier to which the reaction is opposed.

4.3.2 Electronic, geometrical and orbital's analysis of the M-FAU 6T ring site

The mulliken population and metal coordinating bond length of Na^+, Zn(II), Cd(II), Hg(II) and Sn(II) exchanged faujasite 6T ring is summarized in **Table 4.2**.

Table 4.2: Charge and distances[1] involves in metal exchanged faujasite 6T ring site, computed at the M06(6-31g(d):SBKJC VDZ/PM6) theory level

Catalytic site	Metal charge[2]	O1 charge[2]	O2 charge[2]	O3 charge[2]	Distance[3] M-O1	Distance[3] M-O2	Distance[3] M-O3
Na-FAU	0.46	-0.72	-0.67	-0.68	2.28	2.39	2.31
Zn-FAU	0.95	-0.89	-0.88	-0.90	1.93	1.90	1.93
Cd-FAU	1.05	-0.77	-0.77	-0.75	2.20	2.16	2.18
Hg-FAU	0.86	-0.74	-0.74	-0.73	2.25	2.22	2.23
Sn-FAU	1.10	-0.80	-0.83	-0.79	2.43	2.19	2.31

[1]See Figure 1 for elements numbering [2]Mulliken charge population [3]Distance in angstrom (Å)

Properties analysis of metal exchanged faujasite 6T ring site presented in table 1 show the typical electronegativity increase along a period, with Zn, Cd and Hg exchanged structures. The metal electronegativity being related to the mulliken charge populations of its coordinating sphere, withdrawing the electron density of the faujasite support in its vicinity. Amongst the *IIB* metals series (Zn(II), Cd(II) and Hg(II)), it is zinc metal that has the highest electronegativity with an average mulliken population of -0.89 on its coordinating oxygen sphere, followed by Cd with -0.76 then Hg with -0.74. The distance between the coordinating oxygens and metals is also directly related to electronegativity within the *IIB* series: as high is the electronegativity, as tight is the complex.

However, due to an important difference of the orbitals nature of Sn(II) and oxidation degree of Na^+, site geometries and mulliken charge dispersion of those structures cannot be included in the *IIB* series trends. Nevertheless, Sn-FAU which has a p^0 coordination sphere, presents charges and geometrical profile highly similar to Cd-FAU, with a slight increase in complex bond length, metal charge density and electronegativity. For its part, Na-FAU shows

the lowest metal charge density, electronegativity and is the loosest complex. Those characteristics of Na-FAU reflect the well known application of this material for reactions that are catalyzed under basic conditions. The addition of Na^+ in a zeolite material results into an electron rich metal support with basic properties.[25-27]

A front view of the metal exchanged 6T ring HOMO-LUMO orbitals and associated energies which are involved in reactants coordination and transition state stabilization are shown in **Figure 4.3**. The nature difference between the $3s^0$, $4s^0$, $5s^0$, $6s^0$ and $5p^0$ coordination orbitals is illustrated by the LUMO orbitals of the complexes (**Figure 4.3a**). The $5p$ LUMO character of Sn is well distinguished from the s^0 series. While the s^0 series adsorb reactants in the same orbital prior to reactions, Sn-FAU interact with reactants via two distinct empty orbitals separated by a node. Even if it is Sn(II) which was found to have the highest charge density on the metal, it is this site which interacts the most weakly with reactants. Such a site orbital structure is thus found to be highly unfavorable to carboxylation and decarboxylation reaction compare to the other sites which have a coordination sphere which consist of an empty s orbital.

The LUMO structure of the *IIB* series remained similar very consistently (**Figure 4.3a**). One of the main distinction within this series results from metal size variation. Increasing metal size is accompanied by an amplification of the interactions with the 6T ring second row oxygen's; O4, O5 and O6 as labeled in **Figure 4.1**. The interactions increase with the second row oxygen's correlate with a charge density decrease on O1, O2 and O3. Metals charge dispersion within the 6T ring therefore become more important with larger metals, resulting in a complex in which charges are less concentrated and which is consequently more polarizable. From the s^0 metals series, only Na-FAU presents a significant deviation of the LUMO structure. While Zn(II), Cd(II) and Hg(II) LUMO remained highly similar, Na-FAU possess a more diffuse LUMO which results in a less important polarization effect on the faujasite backbone. Comparing the s^0 series allows observing that the LUMO energies correlate with DMC decarboxylation/DME carboxylation equilibrium constant. The LUMO energies of the metal exchanged faujasite decrease in the order Na^+, Zn(II), Cd(II) and Hg(II), which is the order in which DMC decarboxylation become more favorable over DME carboxylation. This indicate that metal exchanged faujasite site with high energy LUMO is favorable to DME carboxylation while DMC decarboxylation is favor by sites with low energy LUMO.
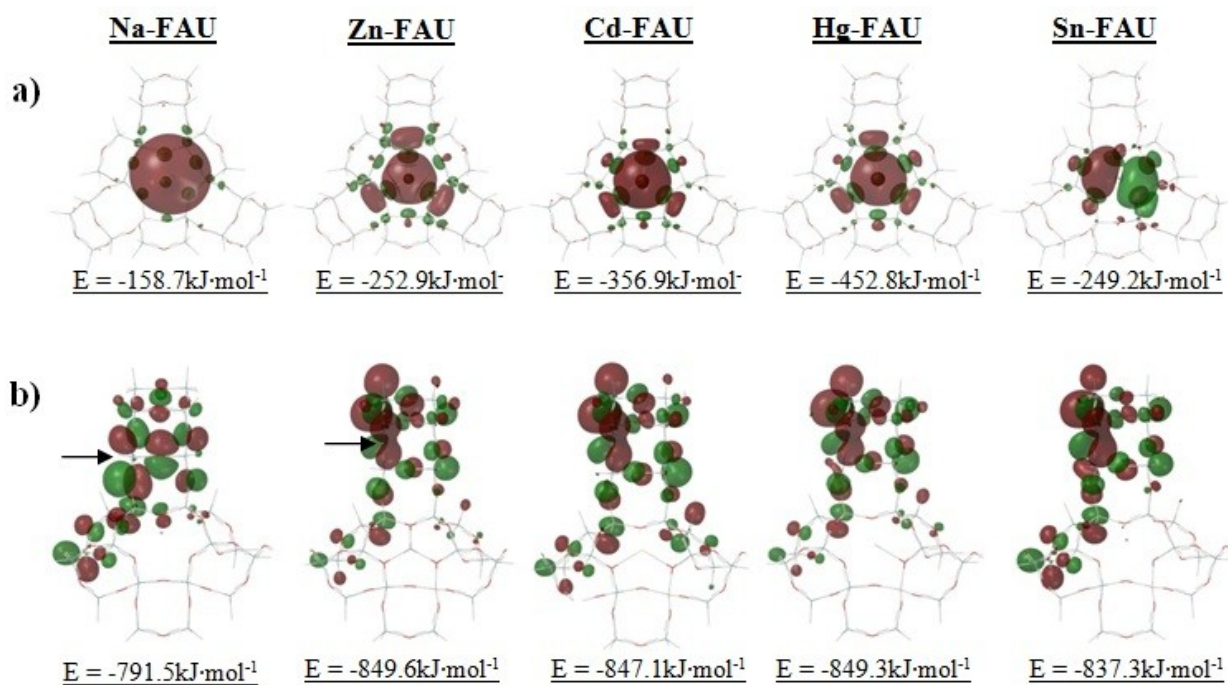
Figure 4.3: Metal exchanged faujasite 6T ring orbitals a) LUMO and b) HOMO. The arrows show the faujasite interacting HOMO during DMC decarboxylation transition structure.

The influence of metal loading on faujasite reaction interacting HOMO is shown in **Figure 4.3b**. Among the series, only Na-FAU present a distinct HOMO configuration, the HOMO of Sn, Zn, Cd and Hg faujasite being essentially structurally and energetically identical. From the mechanistical resolution of DMC decarboxylation, it was found that the transition structure was stabilized by the HOMO of β and γ oxygen's from aluminum of the faujasite support (**Figure 4.3b**). The loading of Zn, Cd, Hg and Sn in the faujasite results in the promotion of constructive interactions specifically between the β and γ oxygen's HOMO. This constructive interaction is not observed with Na-FAU, affording a site with an HOMO slightly higher in energy compare to the others structures. In the case of Na-FAU, the natural *p* character of the oxygen's HOMO remained intact. DMC decarboxylation at the surface of Na-FAU and Zn-FAU was reported to begin at 180°C and 50°C respectively, suggesting that such a constructive interaction between the β and γ oxygen's is beneficial to DMC decarboxylation.[28-29]

4.3.3 Geometrical and charge population analysis of adsorb reactants

The distances between the metals and substrates oxygen in coordination, between substrate methyl and the closest faujasite oxygen as well as between DME oxygen and CO_2 Carbon are summarized in **Table 4.3**. Mulliken charges of the metals, reactants oxygen in coordination, reactants methyl that interact with the support and CO_2 carbon are further given in **Table 4.4**. At the surface of all five sites, energetic minima of adsorb reactants were found to be identical, as shown in **Figure 4.2**.

Table 4.3: Geometrical parameters of adsorb reactants complexes[1]

Catalyst	M-O_{DMC}	CH_{3DMC}-O_{FAU}	M-O_{DME}	CH_{3DME}-O_{FAU}	M-O_{CO2}	O_{DME}-C_{CO2}
Zn-FAU	1.94	3.11	2.00	3.60	3.41	2.86
Cd-FAU	2.17	2.95	2.28	3.26	2.51	2.96
Hg-FAU	2.22	2.96	2.31	3.37	2.63	2.98
Sn-FAU	2.43	3.77	2.55	3.14	3.10	2.74
Na-FAU	2.18	3.14	2.35	3.26	2.41	2.77

[1] Distance in Angstrom (Å)

Table 4.4: Charge density dispersion of adsorb DMC, DME and CO_2 complexes[1]

Catalyst	$M_{(DMC)}$	$O_{(DMC)}$	$CH_{3(DMC)}$	$M_{(DME)}$	$O_{(DME)}$	$CH_{3(DME)}$	O_{CO2}	C_{CO2}
Zn-FAU	0.67	-0.50	-0.27	0.76	-0.53	-0.29	-0.36	0.76
Cd-FAU	0.88	-0.54	-0.28	0.90	-0.54	-0.29	-0.38	0.79
Hg-FAU	0.73	-0.52	-0.29	0.66	-0.52	-0.30	-0.36	0.78
Sn-FAU	1.07	-0.57	-0.29	1.03	-0.54	-0.25	-0.37	0.77
Na-FAU	0.30	-0.54	-0.28	0.23	-0.50	-0.30	-0.41	0.87

[1] Mulliken charge population

In the case of DMC complexes, the coordination bond length between the reactant and the metal is directly related to the adsorption energy (**Table 4.3**). Zn-FAU, which has the highest affinity for DMC with adsorption energy of -162.7kJ·mol^{-1} is the tightest DMC complex with coordination bond length of 1.94Å between the zinc metals and DMC. Consistently, Sn-FAU which have the lowest affinity for DMC with adsorption energy of -76.5kJ·mol^{-1} is the widen complex with coordination bond length of 2.43Å. Adsorption energy of DMC complexes is also found to correlate with the active complex mulliken charges, Zn-FAU having the smallest charge dispersion and Sn-FAU being the most polarized site (**Table 4.4**). Such patterns are not observed for the co-adsorption of DME and CO_2, suggesting that the adsorption energy is not only dependent on the interactions of DME and CO_2 with the metal but also on the actual interactions between each other. Na-FAU being the only site with a monovalent metal, important charges and geometry distinction are found for the DME CO_2 complex when compares to other structures. At first, table 3 shows that it is at the surface of Na-FAU that CO_2 present the tightest interactions with the metal (2.41Å) as well as the second closest interactions with DME (2.77Å) after Sn-FAU (2.74Å). More importantly, this close interaction of CO_2 with the sodium metal results in an important polarization of this highly inert reactant. Thus, in addition to close proximity between DME and CO_2, it also is at the surface of Na-FAU that the CO_2 carbon is the most electrophile with charge density of 0.87. Comparatively, the closest structure to Na-FAU in such regards is Cd-FAU, with charge density of 0.79 on the CO_2 carbon and 2.51Å between the metal and CO_2 molecule. This pattern is consistent along the five metal exchanged faujasite structure, as short is the CO_2 coordination bond, as high is the electrophilicity of the CO_2 carbon. Further comparison of the divalent metals sites also allows observing that tight complexes are favorable to DME carboxylation reaction while loosen complex are more likely to be preferable to DMC decarboxylation. Zn-FAU which is the tightest complex was found to have an equilibrium constant of 1.5 while Sn-FAU which presents the longest coordination bond was found to have an equilibrium constant of 18.2, both in favor of DMC decarboxylation.

4.3.4 Geometrical and charge population analysis of transition states

The transition structures between DMC, DME and CO_2 at the surface of the five metal exchanged faujasite sites is presented in **Figure 4.4**. The corresponding geometrical parameters and charge dispersion are given in **Table 4.5** and **4.6**. The atoms labeling of **Table 4.5** and **4.6** is given in the transition structure Zn-FAU of **Figure 4.4**. Despite an important dissimilarity of the thermodynamic and kinetic profile for DMC decarboxylation and DME carboxylation, transition state structure variation remained very subtle at the surface of the different sites, highlighting the metal nature importance on this reaction. It is found from **Table 4.5** and **4.6** that at the highest point of the reaction coordinates, metal variation induce structural and electronic deviation only on the reactants atoms which directly interacts with the metal. Effectively, the distance between the transiting methyl and its stabilizing oxygen's (**O2**, **O3** and **O4**) as well as their associated charges are consistent in all structure. Only Na-FAU show a slight structure deviation, at the surface of which the methyllium migrate with tighter interactions with the bicarbonate oxygen **O2**. Even if there is a slight geometrical difference relatively to the methyl transfer at the surface of Na-FAU, charges of the methyl and non-metal interacting oxygen's are quasi-identical within the five structures. Consequently, the differences on reaction activation energy and kinetic reside essentially only on the interactions of **O1** and **O2** with the metals (Figure 4).
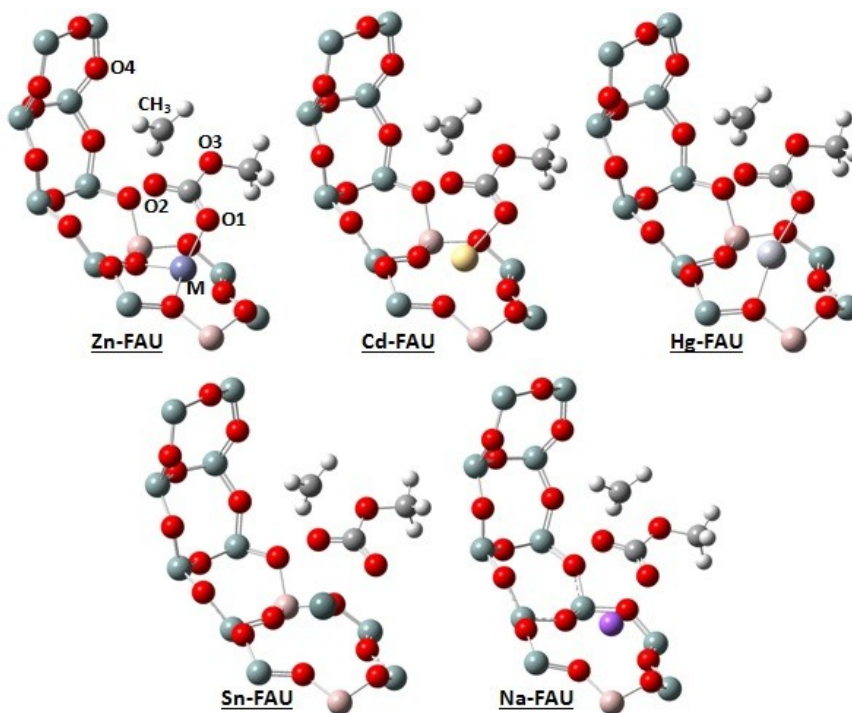
Figure 4.4: Transition structure between DMC and DME at the surface of Zn(II), Cd(II), Hg(II), Sn(II) and Na⁺ exchanged faujasite. Calculated using the M06(6-31g(d):SBKJC VDZ/PM6) method

Among the *IIB* metal exchanged faujasite, the reaction rates and charge of the metal in the transition structure is directly related, as high is the charge of the metal, as high is the reaction rate. Consistently, Na-FAU which shows the smallest charge density on the metal presents the lowest reaction rate. At the opposite, Sn-FAU which has the highest charge density on the metal also shows very low reaction rate and high activation energy compare to the other sites that contain a divalent metal. This exceptional thermodynamic and kinetic behavior of Sn-FAU is here explain not only by the site orbital structure difference, but also by a secondary interaction between the metal and **O2** (**Figure 4.4**). The distances between the metal and **O2** during the transition state appear to be directly related to the rate equilibrium constant between DMC and DME.

Table 4.5: Transition structures geometrical parameters[1]

Catalyst	M-O_1	M-O_2	CH_3-O_2	CH_3-O_3	CH_3-O_4
Zn-FAU	1.93	3.12	2.33	2.18	3.33
Cd-FAU	2.18	2.75	2.34	2.21	3.33
Hg-FAU	2.15	3.02	2.33	2.20	3.14
Sn-FAU	2.43	2.49	2.34	2.22	3.30
Na-FAU	2.26	3.38	2.25	2.10	3.18

[1] Distance in Angstrom (Å)

Table 4.6: Transition structure charge density dispersion[1]

Catalyst	M	O_1	O_2	CH_3	O_3	O_4
Zn-FAU	0.75	-0.56	-0.48	-0.25	-0.51	-0.62
Cd-FAU	0.94	-0.55	-0.51	-0.26	-0.51	-0.62
Hg-FAU	0.78	-0.56	-0.48	-0.26	-0.51	-0.63
Sn-FAU	1.04	-0.54	-0.57	-0.25	-0.51	-0.63
Na-FAU	0.36	-0.56	-0.55	-0.25	-0.51	-0.61

[1] Mulliken charge population

Na-FAU, the only structure at the surface of which DME carboxylation is found to be favorable over DMC decarboxylation, show the weakest interaction between the metal and **O2**. Consistently, Sn-FAU which were found to be the less favorable site for carboxylation, present the tightest interaction between the metal and **O2** (**Table 4.5**). This indicates that the availability and degree of freedom of carboxylate oxygen during the methyl transfer is a factor which has high influence on reaction equilibrium constant. A zeolite structure loaded with small and hard metal such as Na$^+$ interact tightly with a single oxygen of the carboxylate function, allowing the second oxygen to be fully involve in the reaction. At the opposite, a zeolite loaded with a large and soft metal such as Hg(II) and Cd(II) interacts more tightly with both of the carboxylate oxygen, thus limiting the carboxylate movement liberty and charge density which is necessary for accommodating the methyl transfer. According to the hard and soft classification of metals, Na$^+$ being hard, Zn(II) and Sn(II) being intermediate, Cd(II) and

Hg(II) being soft,[30] there is a clear correlation between metal hardness and reaction equilibrium constant. However, while Na^+ is favorable for carboxylation, Cd(II) and Hg(II) favorable to decarboxylation, it is still ambiguous for intermediate metals such as Zn(II) and Sn(II). On another hands, metal exchanged faujasite with a LUMO that consist of an empty s^0 orbital are definitively found to be more favorable to decarboxylation and carboxylation reaction than metal exchanged faujasite with a p^0 LUMO.

4.4 Conclusion

In summary, the activity of Na^+, Zn(II), Cd(II), Hg(II) and Sn(II) exchanged faujasite towards DMC decarboxylation and DME carboxylation was computationally evaluated. The LUMO of the materials respectively consist of an empty $3s^0$, $4s^0$, $5s^0$, $6s^0$ and $5p^0$ orbital. From this series, Na-FAU is the only structure which was found to favor DME carboxylation over DMC decarboxylation. However, Na-FAU is also the structure which presented the lowest reaction rate constant. Sn-FAU, which is the only structure in which the LUMO is not an empty s^0 orbital, is the structure which shows the lowest potential for DME carboxylation. Comparing the structures in which the metals have an empty s^0 coordinating orbital shows that reaction rate constant is directly related to the charge density of the metal, Cd-FAU having the highest charge density and reaction rate and Na-FAU having the lowest charge density and reaction rate. From the geometrical, charge density and orbital analysis of the active sites, intermediates and transition structures, three factors were identified as being determining on reaction equilibrium constant. First, metal exchanged faujasite with high energy LUMO is favorable to DME carboxylation while low energy LUMO is favorable to DMC decarboxylation. Second, sites which adsorb reactants tightly tend to be favorable to DME carboxylation while a site which makes loosen complex with reactants is favorable to DMC decarboxylation. The third factor concern carboxylate mode of adsorption during the transition state. A transition state in which one of the two carboxylate interact weakly with the metal will be favorable to DME carboxylation, while a transition state in which both of the carboxylate oxygen interact closely with the metal tend to be favorable to DMC decarboxylation. The Zn-FAU computational model being previously validated with experimental measurements, future

work will consist to experimentally validate trends observed in this work which will be used as the basic understanding for further catalyst design.

ACKNOWLEDGMENT

REFERENCES

1.   Sakakura, T.; Kohno, K., The synthesis of organic carbonates from carbon dioxide. *Chemical Communications* **2009,** *0* (11), 1312-1330.

2.   Wen, L.-b.; Xin, C.-Y.; Yang, S.-C., The effect of adding dimethyl carbonate (DMC) and ethanol to unleaded gasoline on exhaust emission. *Applied Energy* **2010,** *87* (1), 115-121.

3.   Rounce, P.; Tsolakis, A.; Leung, P.; York, A. P. E., A Comparison of Diesel and Biodiesel Emissions Using Dimethyl Carbonate as an Oxygenated Additive. *Energy & Fuels* **2010,** *24* (9), 4812-4819.

4.   Pacheco, M. A.; Marshall, C. L., Review of Dimethyl Carbonate (DMC) Manufacture and Its Characteristics as a Fuel Additive. *Energy & Fuels* **1997,** *11* (1), 2-29.

5.   Sakakura, T.; Choi, J.-C.; Yasuda, H., Transformation of Carbon Dioxide. *Chemical Reviews* **2007,** *107* (6), 2365-2387.

6.   Keller, N.; Rebmann, G.; Keller, V., Catalysts, mechanisms and industrial processes for the dimethylcarbonate synthesis. *Journal of Molecular Catalysis A: Chemical* **2010,** *317* (1–2), 1-18.

7.   Ono, Y., Catalysis in the production and reactions of dimethyl carbonate, an environmentally benign building block. *Applied Catalysis A: General* **1997,** *155* (2), 133-166.

8.   Honda, M.; Kuno, S.; Begum, N.; Fujimoto, K.-i.; Suzuki, K.; Nakagawa, Y.; Tomishige, K., Catalytic synthesis of dialkyl carbonate from low pressure CO2 and alcohols combined with acetonitrile hydration catalyzed by CeO2. *Applied Catalysis A: General* **2010,** *384* (1–2), 165-170.

9.   Santos, B. A. V.; Pereira, C. S. M.; Silva, V. M. T. M.; Loureiro, J. M.; Rodrigues, A. E., Kinetic study for the direct synthesis of dimethyl carbonate from methanol and CO2 over CeO2 at high pressure conditions. *Applied Catalysis A: General* **2013,** *455* (0), 219-226.

10.   Honda, M.; Suzuki, A.; Noorjahan, B.; Fujimoto, K.-i.; Suzuki, K.; Tomishige, K., Low pressure CO2 to dimethyl carbonate by the reaction with methanol promoted by acetonitrile hydration. *Chemical Communications* **2009,** *0* (30), 4596-4598.

11.   Honda, M.; Tamura, M.; Nakagawa, Y.; Sonehara, S.; Suzuki, K.; Fujimoto, K.-i.; Tomishige, K., Ceria-Catalyzed Conversion of Carbon Dioxide into Dimethyl Carbonate with 2-Cyanopyridine. *ChemSusChem* **2013,** *6* (8), 1341-1344.

12.   Sakakura, T.; Saito, Y.; Okano, M.; Choi, J.-C.; Sako, T., Selective Conversion of Carbon Dioxide to Dimethyl Carbonate by Molecular Catalysis. *The Journal of Organic Chemistry* **1998,** *63* (20), 7095-7096.

13.   Sakakura, T.; Choi, J.-C.; Saito, Y.; Masuda, T.; Sako, T.; Oriyama, T., Metal-Catalyzed Dimethyl Carbonate Synthesis from Carbon Dioxide and Acetals. *The Journal of Organic Chemistry* **1999,** *64* (12), 4506-4508.

14.   Sakakura, T.; Choi, J.-C.; Saito, Y.; Sako, T., Synthesis of dimethyl carbonate from carbon dioxide: catalysis and mechanism. *Polyhedron* **2000,** *19* (5), 573-576.

15.   Tomishige, K.; Kunimori, K., Catalytic and direct synthesis of dimethyl carbonate starting from carbon dioxide using CeO2-ZrO2 solid solution heterogeneous catalyst: effect of H2O removal from the reaction system. *Applied Catalysis A: General* **2002,** *237* (1–2), 103-109.

16.   Zhao, Y.; Truhlar, D., The M06 suite of density functionals for main group thermochemistry, thermochemical kinetics, noncovalent interactions, excited states, and transition elements: two new functionals and systematic testing of four M06-class functionals and 12 other functionals. *Theoretical Chemistry Accounts: Theory, Computation, and Modeling (Theoretica Chimica Acta)* **2008,** *120* (1), 215-241.

17.   Namuangruk, S.; Meeprasert, J.; Khemthong, P.; Faungnawakij, K., A Combined Experimental and Theoretical Study on the Hydrolysis of Dimethyl Ether over H-ZSM-5. *The Journal of Physical Chemistry C* **2011,** *115* (23), 11649-11656.

18.   Maihom, T.; Khongpracha, P.; Sirijaraensre, J.; Limtrakul, J., Mechanistic Studies on the Transformation of Ethanol into Ethene over Fe-ZSM-5 Zeolite. *ChemPhysChem* **2013,** *14* (1), 101-107.

19.   Gomes, J.; Zimmerman, P. M.; Head-Gordon, M.; Bell, A. T., Accurate Prediction of Hydrocarbon Interactions with Zeolites Utilizing Improved Exchange-Correlation Functionals and QM/MM Methods: Benchmark Calculations of Adsorption Enthalpies and Application to Ethene Methylation by Methanol. *The Journal of Physical Chemistry C* **2012,** *116* (29), 15406-15414.

20.   Maihom, T.; Boekfa, B.; Sirijaraensre, J.; Nanok, T.; Probst, M.; Limtrakul, J., Reaction Mechanisms of the Methylation of Ethene with Methanol and Dimethyl Ether over

H-ZSM-5: An ONIOM Study. *The Journal of Physical Chemistry C* **2009,** *113* (16), 6654-6662.

21.   Bobuatong, K.; Probst, M.; Limtrakul, J., Structures and Energetics of the Methylation of 2-Methylnaphthalene with Methanol over H-BEA Zeolite. *The Journal of Physical Chemistry C* **2010,** *114* (49), 21611-21617.

22.   Van Speybroeck, V.; Van der Mynsbrugge, J.; Vandichel, M.; Hemelsoet, K.; Lesthaeghe, D.; Ghysels, A.; Marin, G. B.; Waroquier, M., First Principle Kinetic Studies of Zeolite-Catalyzed Methylation Reactions. *Journal of the American Chemical Society* **2010,** *133* (4), 888-899.

23.   Toulhoat, H.; Lontsi Fomena, M.; de Bruin, T., Computational Study of the Effect of Confinement within Microporous Structures on the Activity and Selectivity of Metallocene Catalysts for Ethylene Oligomerization. *Journal of the American Chemical Society* **2011,** *133* (8), 2481-2491.

24.   Laflamme, P.; Porzio, F.; Ameduri, B.; Soldera, A., Characterization of the telomerization reaction path for vinylidene fluoride with CCl3 radicals. *Polymer Chemistry* **2012,** *3* (3), 652-657.

25.   Okamoto, Y.; Ogawa, M.; Maezawa, A.; Imanaka, T., Electronic structure of zeolites studied by X-Ray photoelectron spectroscopy. *Journal of Catalysis* **1988,** *112* (2), 427-436.

26.   Huang, M.; Adnot, A.; Kaliaguine, S., Characterization of basicity in alkaline cation faujasite zeolites—An XPS study using pyrrole as a probe molecule. *Journal of Catalysis* **1992,** *137* (2), 322-332.

27.   Xie, J.; Huang, M.; Kaliaguine, S., Characterization of basicity in alkali cation exchanged Faujasite zeolites: an XPS study using chloroform as a probe molecule. *Applied Surface Science* **1997,** *115* (2), 157-165.

28.   Selva, M.; Fabris, M.; Perosa, A., Decarboxylation of dialkyl carbonates to dialkyl ethers over alkali metal-exchanged faujasites. *Green Chemistry* **2011,** *13* (4), 863-872.

29.   Fu, Y.; Zhu, H.; Shen, J., Thermal decomposition of dimethoxymethane and dimethyl carbonate catalyzed by solid acids and bases. *Thermochimica Acta* **2005,** *434* (1–2), 88-92.

30.   Pearson, R. G., Hard and soft acids and bases, HSAB, part 1: Fundamental principles. *Journal of Chemical Education* **1968,** *45* (9), 581.

5. Conclusion

À la lumière de ce travail, l'insertion catalytique du CO_2 dans une fonction éther aliphatique produisant un di-alkyl carbonate aura été pour la première fois prouvée. Cette découverte résulte de l'extrapolation de la connaissance antérieure relative à la chimie des carbonates, soit qu'il y a insertion du CO_2 à basse température et relâchement du CO_2 à plus haute température. Ce type d'équilibre chimique dans lequel le CO_2 est impliqué avait effectivement préalablement été rapporté lors d'étude concernant les éthers cyclique et carbonates inorganiques, mais jamais avec un éther aliphatique.

C'est donc en étudiant la décarboxylation du DMC en DME et CO_2, plus spécifiquement la température à laquelle cette réaction débute, que les conditions dans lesquelles l'insertion du CO_2 dans le DME a été définie. Ainsi à 50°C, à la surface d'un catalyseur faujasite échangé au zinc, une conversion de 0.4% du DME en DMC a été obtenue en régime stationnaire dans un réacteur à lit fixe. Selon les données expérimentales, il a cependant été conclu qu'un trickle bed ou slurry reacteur serait plus approprié à cette réaction qu'un réacteur à lit fixe, dû a des limitations au niveau de la diffusion à la surface du catalyseur.

La résolution structurelle de l'état de transition entre le DMC et le DME a ensuite été étudiée en combinant des mesures thermodynamiques et cinétiques à des calculs théoriques. Il a été obtenu expérimentalement que l'énergie d'activation apparente entre le DMC et le DME soit de 66.7kJ·mol^{-1}. La structure de l'état de transition qui correspond à une telle énergie d'activation a donc été recherchée au sein d'intermédiaires réactionnels similaires à ceux connus pour le mécanisme d'hydratation du CO_2 par l'enzyme carbonique anhydrase. Il est ressorti de cette étude que le DMC est converti en DME suivant un chemin réactionnel entièrement concertée. L'adsorption du DMC à la surface de Zn-FAU, où l'oxygène carboxylate du DMC interagit avec le métal et un des méthyles avec un oxygène du support, résulte en un mode d'activation où un lien méthoxy est affaibli. La transition d'un méthyllium entre un oxygène carboxylate et méthoxy du DMC résulte de ce mode d'activation, produisant directement le DME et CO_2 en une seule étape. L'énergie de ce complexe activé a une valeur théorique de 68.7kJ·mol^{-1}, en excellent accord avec la valeur expérimentale de 66.7kJ·mol^{-1}.

Le mécanisme réactionnel et méthode de calcul développé lors de l'étude mécanistique ont ensuite été appliqués à l'évaluation théorique de plusieurs autres structures catalytiques. Cette application de la méthode de calcul a permis de définir l'influence du type de métaux échangé dans la faujasite sur la constante d'équilibre entre la carboxylation du DME et la décarboxylation du DMC. Ainsi, Zn-FAU, Cd-FAU, Hg-FAU, Sn-FAU et Na-FAU ont été théoriquement comparés. Cette étude a permis d'obtenir que plus l'énergie de l'orbitale LUMO du métal dans le site actif est élevée, plus la carboxylation du DME est favorisée. Il a également été observé qu'un état de transition compacte avec un métal qui interagit avec un seul oxygène carboxylate est également favorable à la carboxylation du DME par rapport à la décarboxylation du DMC. Ces résultats orientent donc vers la recherche de structure catalytique dont le métal actif est par exemple le béryllium, magnésium où le calcium.

Finalement, la carboxylation du DME aura été montrée comme étant une voie synthétique potentielle vers le DMC. Une solide compréhension fondamentale aura été apportée sur le mécanisme réactionnel ainsi que sur les propriétés désirables des structures catalytiques. Ce projet a été mené au sein d'un laboratoire de développement de procédés chimique, mais cette réaction n'a pas la maturité nécessaire pour être abordée à une telle échelle. Ainsi, avec les résultats ici obtenus, le futur de ce travail est destiné aux groupes qui travaillent au développement de catalyseurs à l'échelle d'un laboratoire.

Annexe 1 : Calcules de transferts de masse dans le réacteur

1. **Le nombre de Reynolds du flux gazeux au travers du lit réactionnel lors de la reaction de carboxylation du diméthyle ether est exprimé selon la relation suivante.**

$$Re_p = \frac{D_p V_x \rho}{(1-\varepsilon)\mu}$$

Où :

D_p = Diamètre sphérique équivalent des particules de catalyseur

(D_p = 6· Volume des particules / Aire des particules)

$$D_p = 6 \cdot \left(\frac{4/3 \cdot \pi \cdot (0.1cm)^3}{4 \cdot \pi \cdot (0.1cm)^2} \right) = 0.2\ cm$$

V_x = Vitesse superficielle (Flux volumétrique / Aire transversale du lit réactionnel)

Flux de CO_2 = 1500 cm^3 $_{gas}$·min^{-1}

Flux de DME = 127 cm^3 $_{gas}$·min^{-1}

Aire transversale : 2.85 cm^2

V_x = **570.9 cm·min^{-1}**

P = Densité du flux gazeux

Densité du DME = 2.3622 g·cm^3

Densité du CO_2 = 2.813 g·cm^3

$$\rho = 0.909 \cdot 2.813 + 0.0909 \cdot 2.3622 = 2.77\ g \cdot cm^{-3}$$

ε = Fraction vide du lit réactionnel

La forme des particules de catalyseur étant irrégulière, la fraction vide du lit réactionnel est estimée à partir de la moyenne des données connues pour les particules sphérique et cylindrique. Avec une grosseur de particules de catalyseur allant de 1.4 à 2.5 mm, et un diamètre de lit réactionnel de 19.05mm, la fraction vide du lit catalytique est estimée selon le ratio suivant.

$$D_p \Big/ D_f = \frac{(1.4 + 2.5)^{0.5}}{19.05} = 0.1$$

La fraction vide d'un lit avec un tel ratio est ε = 0.365 (0.35$_{cylindre}$ et 0.38$_{sphère}$)

Par ailleurs,

μ = est la viscosité dynamique du fluide

Dont :

Viscosité du CO_2 = $1.37 \cdot 10^{-4}$ g·cm^{-1}·s^{-1}

Viscosité du DME = $8.29 \cdot 10^{-5}$ g·cm^{-1}·s^{-1}

Ainsi,

$$\mathbf{\mu = 0.909 \cdot 1.37 \cdot 10^{-4} \, g \cdot cm^{-1} \cdot s^{-1} + 0.0909 \cdot 8.29 \cdot 10^{-5} \, g \cdot cm^{-1} \cdot s^{-1}}$$
$$\mathbf{= 1.32 \cdot 10^{-4} \, g \cdot cm^{-1} \cdot s^{-1} = 7.92 \cdot 10^{-3} \, g \cdot cm^{-1} \cdot min^{-1}}$$

Le nombre de Reynolds du flux au travers du lit catalytique est donc:

$$\mathbf{Re_p = \frac{0.2 \, cm \, x \, 570.9 \, cm \cdot min^{-1} \, x \, 2.77 \, g \cdot cm^{-3}}{(1 - 0.365)x \, 7.92 \cdot 10^{-3} \, g \cdot cm^{-1} \cdot min^{-1}} = 62\,878.44}$$

Puisque le nombre de Reynolds est supérieur à 2000, le flow au travers du réacteur lors de la carboxylation du diméthyle éther est entièrement turbulent.

2. Calcule de la chute de pression dans le lit catalytique lors de la carboxylation du diméthyle éther

$$\frac{\Delta P}{L} = 150 \cdot \frac{\mu \rho V (1 - \varepsilon)^2}{kg \rho D \varepsilon^3} + 1.75 \frac{(\rho V)^2 (1 - \varepsilon)}{kg \rho D \varepsilon^3}$$

ΔP = Chute de pression

L = Longueur du lit catalytique = 44 cm

μ = Viscosité du fluide réactionnel = $7.92 \cdot 10^{-3}$ g·cm^{-1}·min^{-1}

ρ = Densité du fluide réactionnel = 2.77 g·cm^{-3}

V = Vitesse linéaire superficielle du fluide réactionnel = 570.9 cm·min^{-1}

ε = Fraction vide du lit catalytique = 0.365

D = Diamètre effectif des particules de catalyseur = 0.2 cm

g = Constante gravitationnelle = 58 860 cm·min^{-1}

$$\frac{\Delta P}{L}$$
$$= 150$$
$$\cdot \frac{7.92 \cdot 10^{-3} \, g \cdot cm^{-1} \cdot min^{-1} \, x \, 2.77 \, g \cdot cm^{-3} \, x \, 570.9 \, cm \cdot min^{-1} (1 - 0.365)^2}{58 \, 860 \, cm \cdot min^{-1} \, x \, 2.77 \, g \cdot cm^{-3} \, x \, 0.2^2 \, cm \, x \, 0.365^3}$$
$$+ 1.75 \frac{(2.77 \, g \cdot cm^{-3} \, x \, 570.9 \, cm \cdot min^{-1})^2 (1 - 0.365)}{58 \, 860 \, cm \cdot min^{-1} \, x \, 2.77 \, g \cdot cm^{-3} \, x \, 0.2 \, cm \, x \, 0.365^3}$$
$$= 1777.87 \, g \cdot cm^{-3} \cdot min^{-1}$$

La longueur du lit réactionnel (L) étant 44 cm, la chute de pression est :

ΔP = 78226.4 g·cm^{-2}·min^{-1} = 78.23 kg·cm^{-2}·min^{-1}

La chute de pression en fonction du temps de passage est donc :

$\Delta P \cdot V$ = $4.466 \cdot 10^7$ kg·cm^{-1}·min^{-2} = 124 054.1 kg·m^{-1}·s^{-2}

Ce qui représente 124.05 kPa ou 18 PSI.

3. Phase du DMC lors des expériences de décarboxylation

Lors des expériences de décarboxylation du diméthyle carbonate, 0.02mL·min^{-1} (2.37·10^{-4}mol) a été pompé en continu au travers du lit catalytique et à pression atmosphérique en présence d'un flux d'azote de 1L·min^{-1} (0.165 mol).

La fraction molaire de l'azote dans le fluide réactionnel était donc de 0.9986, pour une fraction molaire de DMC de 0.00143.

La pression de vapeur du DMC est 0.342 PSI a 21.1°C

Donc la pression partielle du DMC dans le mélange gazeux est de 0.00143·14.696 PSI = 0.02 PSI

Les constant d'Antoine du DMC sont:

A = 6.4337

B = 1413.0

C = -44.25

La pression de vapeur du DMC dans le gaz est donc:

$$\log(\mathbf{p}) = \mathbf{6.4337} - \frac{\mathbf{1413.0}}{\mathbf{323K} - \mathbf{44.25}} = \mathbf{1.36}$$

P = 23.10 kPa

La fraction molaire du DMC dans le liquide au point de condensation de ce mélange est:

$$X_{DMC} = \frac{0.00143 \cdot 101.3 \, kPa}{23.10 \, kPa} = 0.0063$$

Puisque la fraction molaire du DMC dans le liquide au point de condensation est inférieure à 1 à 323K, cela signifie que 323K est une température supérieure au point de condensation du mélange. Conséquemment, le DMC est demeuré en phase gazeuse lors des expériences de décarboxylation qui ont tous été effectué à une température supérieure à 323K.

4. Évaluation de la vitesse de diffusion interne aux particules de catalyseur

Le module de Thiele peut être utilisé afin d'évaluer des limitations au niveau du transfert de masse entre les particules de catalyseur et le fluide réactionnel. Un module de Thiele élevé signifie que la réaction est limitée au niveau de la diffusion interne. Autrement, un faible module de Thiele signifie que la réaction est limitée cinétiquement ou au niveau de la diffusion de surface.

Le module de Thiele (ϕ) est exprimé tel que:

$$\phi = L_c \sqrt{\frac{k C_A^{n-1}}{D_e}}$$

Où:

L_c = longueur caractéristique des particules (6Vol/Surf)

k = constante de vitesse de la réaction

C_A = concentration des réactifs à la surface du catalyseur (généralement considérée identique au fluide réactionnel)

n = Ordre de la réaction

D = coefficient effectif de diffusion des particules de catalyseur.

Le coefficient effectif de diffusion s'exprime selon:

$$D_e = \frac{D \varepsilon_\tau \delta}{\tau}$$

Où:

D = Coefficient de diffusion dans les pores de réaction

$\boldsymbol{\epsilon_\tau}$ = Porosité disponible pour la diffusion des réactifs

$\boldsymbol{\delta}$ = Constructivité

$\boldsymbol{\tau}$ = Tortuosité

Puisque la constructivité et la tortuosité du catalyseur Faujasite échangé au zinc n'a pas été identifié, la définition des coefficients de diffusion interne de ce catalyseur n'est actuellement pas accessible. Par conséquent, un calcul précis du module de Thiele ne peut être obtenu.

La théorie de Smoluchowski est une alternative au module de Thiele afin d'évaluer si une réaction est limité au niveau cinétique ou de la diffusion. Cependant, cette théorie nécessite également la définition des coefficients de diffusion interne des catalyseurs.

5. Grosseur des pores de la faujasite et diametre du diméthyle carbonate et diméthyle éther

La faujasite est parmis les zeolites à grand pore. Le diamètre maximal d'une sphere pouvant être contenu dans la faujasite est de 11.24 Å, et le diamètre maximal des molécules pouvant diffuser à l'intérieur est de 7.35 Å. Le diamètre du diméthyle carbonate se situe entre 4 à 8 Å, alors que le diamètre du diméthyle éther peut aller de 2.5 à 5 Å, selon la conformation adoptée. Ainsi, le diméthyle éther et le diméthyle carbonate peuvent diffuser librement dans la faujasite. Cependant, la forme la plus étendue du diméthyle carbonate est à la limite de la grosseur des pores de diffusion de la faujasite.